Thermal conformance between metal-metal contacts under transient conditions – A study (The effect of TIMs, metal thermophysical properties, and the interfacial pressure)

Thesis

Submitted in partial fulfilment of the requirements for the degree of

DOCTOR OF PHILOSOPHY

by

RAMAKRISHNA DEVANAND P

DEPARTMENT OF METALLURGICAL AND MATERIALS ENGINEERING

NATIONAL INSTITUTE OF TECHNOLOGY KARNATAKA,

SURATHKAL, MANGALORE 575025

OCTOBER 2024

DECLARATION

by the Ph.D. Research Scholar

I hereby declare that the Research Thesis titled "**Thermal conformance between metal-metal contacts under transient conditions –A study (The effect of TIMs, metal thermophysical properties, and the interfacial pressure)**" which is being submitted to the **National Institute of Technology Karnataka, Surathkal** in partial fulfilment of the requirements for the award of the Degree of **Doctor of Philosophy** in **Metallurgical and Materials Engineering** is a bonafide report of the research work carried out by me. The material contained in this research thesis has not been submitted to any University or Institution for the award of any degree.

RAMAKRISHNA DEVANAND P

Register No. **165122MT16P01**

Department of Metallurgical and Materials Engineering

Place: NITK-Surathkal

Date:30/10/2024

CERTIFICATE

This is to certify that the Thesis titled "**Thermal conformance between metal-metal contacts under transient conditions –A study (The effect of TIMs, metal thermophysical properties, and the interfacial pressure)**" submitted by **Mr. RAMAKRISHNA DEVANAND P,** (Register Number: **165122MT16P01**) as the record of the research work carried out by him, is accepted as the Thesis submission in partial fulfilment of the requirements for the award of degree of **Doctor of Philosophy**.

30-10-2024

Prof K. Narayan Prabhu
Research Guide
(Signature with Date and Seal)

30/10/2024

Dr Kumkum Banerjee
Chairman, DRPC and HoD
Department of MME, NITK
(Signature with Date and Seal)

Chairman - DRPC
Dept. of Metallurgical and Materials Engineering
National Institute of Technology Karnataka, Surathkal
Post Srinivasnagar, Mangaluru - 575 025
Karnataka, India

ACKNOWLEDGEMENTS

First and foremost, I express my gratitude to my research advisor, Prof. K Narayan Prabhu. It has been a privilege to pursue my Ph.D. under his guidance and supervision. His immense knowledge, experience and passion in the field of heat transfer has been the sole motivation for me to pursue my research in the field. Apart from the enormous technical inputs, I am grateful for the painstaking effort put forth by him to remove the obstacles in the course of my work. Apart from guiding me in my doctoral research work, over the past few years Prof Prabhu has been the beacon that has guided me in various aspects of my life. He has a strong role to play in making me the person I am today. I shall always remain indebted to him.

I like to extend gratitude to my RPAC members: Dr. Ravishankar K S, Department of Metallurgical and Materials Engineering and Prof. Shrikantha S Rao, Department of Mechanical Engineering for their insightful comments and valuable suggestions during my research work.

I thank Dr Kumkum Banerjee, HoD, Metallurgical and Materials Engineering, NITK, Surathkal for her kind support and help. I also take this opportunity to thank former heads of the department, Prof Udaya Bhat K., Prof Jagannath Nayak, Prof Anandhan Srinivasan for their support and help. I also thank all faculty members of the Department who have educated and helped me in the course of my work.

I am deeply grateful to Dr. Pranesh Rao and Dr Augustine Samuels for their support and encouragement. I also thank Dr Swati Agarwala, Dr. Mrunali, Dr. Sudheer, Dr Vignesh, Dr. Sanjay, Mr. Kamala Nathan, and Mr. Hisham for their cooperation during the research work.

I thank Mrs. Sharmila, Mrs. Vinaya , Mr. Sundar and all non-teaching staff for facilitating and supporting me during my research. I also thank lab technicians of Department of Metallurgical and Materials Engineering namely Mr. Dinesh, Mr. Satish for their warm and gracious support.

I will always be grateful to NITK for providing me with necessary resources and providing me an opportunity to carry out my studies in the Department of Metallurgical and Materials Engineering.

I also thank the management, staff and my colleagues at Sahyadri College of Engineering and Management for their help and cooperation during this work.

I would like to express my deepest gratitude to my parents, wife and sister who have been supporting me throughout my research work. Finally, I thank all those who directly and indirectly helped me to complete the research work.

Ramakrishna Devanand P

ABSTRACT

A study of interfacial heat transfer between metal-metal contacts is essential in various engineering applications for designing thermal systems with increased efficiency. Interfacial heat transfer between metal-metal contacts under transient conditions is discussed in the present investigation. A novel technique based on solution to inverse heat conduction problem was adopted to estimate the interfacial heat flux transients between metal contacts. Thermal conformance parameters and a thermal conformance assessment parameter (TCAP) were proposed to assess conformance of metal-metal contacts. The metal-metal contacts with different combinations, such as Cu-Cu, Al-Al, Brass-Brass, Cu-Al, and Al-Cu, were subjected to varying degrees of interfacial pressure, and the heat flux transients were estimated using lumped heat capacitance and inverse heat conduction approaches. The effects of thermal interface materials (TIMs), thermophysical properties and surface roughness on the thermal conformance were also investigated. The study used polymer-based TIMs with thermal conductivity ranging from 0.193 W/m K to 7 W/m K. The interfacial pressure had a significant impact on heat transfer across the interface under bare conditions (without TIMs).

However, the effect of interfacial pressure on contact heat transfer is reduced with the application of TIMs of high thermal conductivity. The study also revealed that the effect of pressure was negligible on heat transfer beyond a limiting value of interfacial pressure. A smooth surface texture of the contacting materials resulted in enhanced heat transfer across the interface. The addition of multi-walled carbon nanotubes (MWCNT) in low conductive polymer-based TIMs on heat transfer was investigated. At low weight percentages, the heat flux transients increased marginally by about 6%. However, increasing the weight percentages of MWCNTs resulted in deterioration in heat flux owing to the agglomeration of MWCNTs. The study also found that the thermophysical properties of metals in contact affected the interfacial heat transfer with thermal conformance parameters increasing linearly with TCAP for all the combinations of metal-metal contacts except for the Cu-Cu combination, where interfacial pressure becomes dominant.

Further, 1-Methyl-2-pyrrolidone (NMP), a cleaning solvent generally used in the semiconductor industry, was applied on the source and sink surfaces to assess its effect on heat transfer at the interface. The use of NMP resulted in a significant increase in the thermal conformance at the interface. The increase in the thermal conformance on the

application of NMP was attributed to the (i) removal of oxide films on the source and sink surfaces and (ii) surface smoothening effect increasing the microscopic contact points and effectively reducing the mean gap width. The surface smoothening effect was validated by carrying out surface roughness measurements.

Keywords: Thermal conformance; metal-metal contacts; heat transfer; heat flux transients; interfacial pressure; thermal diffusivity; thermal effusivity; TIMs; thermal conformance parameters; thermal conformance assessment parameter (TCAP);1-Methyl-2-pyrrolidone; surface roughness

Contents

LIST OF FIGURES

LIST OF TABLES

ABBREVIATIONS

Al	Aluminium
AAO	Anodic aluminum oxide
BLT	Bond line thickness
CNT	Carbon nanotube
CTG	Commercial thermal grease
CVD	Chemical vapor deposition
Cu	Copper
DTG	Differential thermogravimetric
GNP	Graphite Nanoplatelet
IHCP	Inverse heat conduction problem
HTC	Heat Transfer coefficient
ITR	Interfacial thermal resistance
LMA	Low melt alloys
MP	Melting point
MWCNT	Multiwalled carbon nanotube
NL	No Load
NMP	N-Methyl-2-pyrrolidone
OLMA	Oxidized liquid metal alloy
PCM	Phase change materials
PDMS	Polydimethylsioxane
PECVD	Plasma Enhanced Chemical Vapor Deposition
PEG	Polyethylene glycol
PTFE	Polytetrafluroroethylene
SFE	Surface free energies
SG	Silicone grease
SST	Sink saturation temperature
STP	Silicone thermal putty
SS_t	Time taken for sink to reach saturation temperature

TCR	Thermal contact resistance
TCC	Thermal contact conductance
TC	Thermal conductivity
TCAP	Thermal conformance assessment parameter
TIM	Thermal interface material
TGA	Thermogravimetric analysis
VACNT	Vertically aligned carbon nanotube

Nomenclature

A	Cross sectional area of specimen (m^2)
C_p	Specific heat (J/kg K)
D	Diameter (m)
$\frac{dT}{dt}$	Cooling rate (°C/s)
h	Heat transfer coefficient (W/m^2K)
k	Thermal conductivity (W/m K)
L	Length (m)
t_g	Time for the source to reach target temperature (s)
ΔT	Temperature difference (°C)
ρ	Density (kg/m^3)
Θ	Dimensionless transient temperature
η	Dimensionless heat transferred
ϴ	Dimensionless temperature
q	Heat Flux (W/m^2)
R_T	Thermal contact resistance (cm^2 °C/W)
V	Volume of specimen (m^3)

Chapter 1 INTRODUCTION

The study of heat transfer across the solid interfaces is of significant importance in many engineering applications (Gao and Liu 2012). One such example is in the field of electronic devices, wherein heat needs to be transferred across processor-heat sink interface (Luo et al. 2001). Apart from microelectronics, the study of heat transfer at interfaces finds applications in the nuclear, space industry and cryogenics (Dai et al. 2018). Rapid miniaturization and massive scale integration especially in the field of microelectronics has resulted in generation of enormous amounts of heat that needs to be efficiently transferred from devices to ensure longer life cycles and enhanced performance (Sartre and Lallemand 2001) (Leong and Chung 2003). The efficient transfer of heat offers advantages such as achieving higher operating temperatures and prevents component failure. A device engineer has to, therefore, identify methods that would facilitate the efficient transfer of heat from the systems. Studies have found that, at a temperature range of 70°C to 80°C, every 1°C rise in temperature reduces the reliability of the equipment by over 10% (Zhao et al. 2019b).The existence of an interface between the heat source and the heat sink impedes the efficient transfer of heat.

High thermal conductive heat sinks are used to dissipate heat from the heat generating package (Leong and Chung 2004)(Xu and Chung 2000). Thus, there exists a structural interface between the heat generating package and the sink. Studies have shown that when two solids are brought in contact, the actual area of contact is very limited to a few discreate points and thus heat is constricted to flow though these points leading to thermal contact resistance and significant temperature drop at the interface (Snaith et al. 1984) (Gao and Liu 2012) (Qingyun and Weifang 2016). Hence, the presence of interface between the heat generating source and sink creates a bottleneck that limits the efficient heat transfer of heat (Ramakrishna Devananda P and K NarayanPrabhu 2019)(Yu et al. 2015). A conforming thermal contact between the heat source and the sink is highly essential for the efficient dissipation of heat (Hu and Chung 2011). A non-conforming contact interface as shown in Figure 1.1 leads to thermal contact resistance (TCR) which is the thermal resistance between two solids which are in contact(Zhang et al. 2014b). This resistance to heat flow at the interface is primarily

due to microscopic irregularities or unevenness of the surfaces in contact at the interface leading to voids and gaps which is the principal reason for TCR (Sarvar et al. 2006). These voids or gaps at the interface are filled with air/gaseous medium having a very low thermal conductivity and acts as a barrier to the heat transfer across the interface significantly (Gwinn and Webb 2002)(Roy et al. 2016) (Hansson et al. 2018). The inefficient heat transfer is also attributed to the thermal boundary resistance that arises as a result of the scattering of electrons and phonons caused by the abrupt changes in materials at the interface (Gwinn and Webb 2003) (Nagabandi et al. 2017). Thus, the interface is a natural barrier to the transfer of heat at contacts between two surfaces.

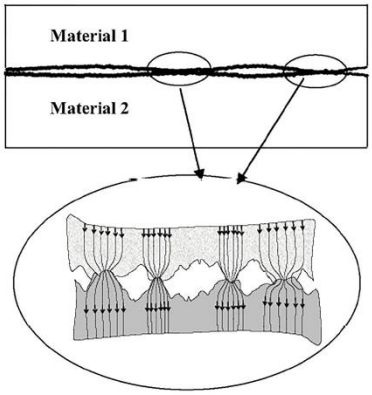

Figure 1.1 Waviness and roughness of two contacting surface (Sarvar et al. 2006)

Over the years, researchers have explored techniques that could be employed to reduce the interface impediments. Enhancement in heat transfer across the interface can be achieved increasing the contact area at the interface by applying contact pressure (Choi and Kim 2014). Increasing the contact pressure at the interface results in enhanced heat transfer, however load constrains curtail employing higher pressures in many practical applications (Gwinn and Webb 2003) (Hansson et al. 2018). Apart from pressure, the increase in surface finish of the contacting surface would also result in enhanced heat transfer, however, superior quality surface finishes would require expensive machining and polishing resulting in increased maintenance challenges(R.S Cook 1983).

One of the most widely used method to enhance heat transfer across the interface is by the application of Thermal interface materials (TIM) between the source and the cooling module. The TIMs acts as a thermal channel between heat generating source and heat sink and offers least thermal resistance path by filling the gap at the interface

and thereby enhancing the contact between the interfaces (Liu and Hu 2015) (Chu et al. 2019)(Hill and Strader 2006). Thus, the application of TIMs enhances the thermal conformance of the interface.

In many engineering applications it is important to quantify the amount of heat flow across the interface. Further it is also important to quantify the effectiveness of the application of TIMs at the interface. This can be accomplished by the measurement of TCR at the interface between the source and the sink and is an effective technique to assess the heat flow between them. The interfacial heat transfer is also quantified by thermal contact conductance (TCC) which is simply the reciprocal of TCR(Dai et al. 2018).

The steady-state approach is one of the techniques used in the estimation of TCR/TCC at the interfaces and has been extensively used in determining the performance of TIMs (Tariq and Asif 2016) (Roy et al. 2016). This approach of testing has been outlined in ASTM D5470 (Gwinn et al. 2002). The apparatus employing ASTM D5470 standard typically consists of two blocks forming an interface. The blocks are instrumented with temperature sensors. The TIMs that need to be tested are laced at the interface of the blocks. One of the blocks is heated and the temperature at different locations within the block and across the interface is measured by thermal sensors. Further, by using the Fourier heat conduction equation (equation 1.1) the heat flux can be computed within each block (Roy 2016).

$$Q = -kA(dT/dx) \tag{1.1}$$

Subsequently the contact resistance is computed by using equation 1.2

$$R = \triangle T / Q \tag{1.2}$$

where $\triangle T$ is the temperature drop across the interface, Q is average heat flux.

The steady-state technique is useful for characterizing a particular TIM under known interfacial conditions. However, it cannot accurately assess the actual heat flow between two materials that are separated by TIM under transient conditions. Under transient conditions of heat flow, one can define a dynamic thermal contact resistance

which can be calculated as the ratio of instantaneous heat flux to the temperature drop at the interface. The instantaneous heat flux is useful for modeling and simulation of heat transfer in microelectronics heating and cooling. Dynamic thermal contact resistance is not only a good parameter for comparison of various thermal interface materials but also a better estimator of contact conformity than that estimated under steady-state techniques. Further, there is a need for a better standard for assessment of the thermal performance of TIMs. The use of dynamic contact resistance instead of static contact resistance to determine the thermal performance of TIMs is a better way to quantify the thermal conformance of materials in contact separated by an interface material. However, a single value of TCR to quantify the heat transfer between two contacting surfaces is valid only under conditions of steady-state heat transfer and does not represent the transient conditions existing at the thermal interface. Further, dynamic thermal contact resistance takes into account the instantaneous heat transfer conditions at the thermal interface and is a better estimate of heat transfer between the two contacting surfaces, particularly in microelectronic applications.

1.2 Organization of the thesis

The thesis is organized into six Chapters. Chapter 1 gives the introduction to the field of thermal interfaces and TIMs. Chapter 2 presents a detailed review of the literature with subsequent sections of the chapter dwelling on scope and objectives of the research work. The experimental methodology employed in the present investigation are detailed in Chapter 3. Chapter 4 deals with the theoretical background of the present work. The results of the experiments carried out and a detailed discussion of the results are given in Chapter 5. Chapter 6 highlights the findings of the current research work

Chapter 2 LITERATURE SURVEY

2.1 Effect of interfacial pressure/load on heat transfer across the interface

There are several ways by which the interface resistance could be minimized. One such method is to increase the actual contact area-by applying high contact pressure (Choi and Kim 2014). The application of pressure at the interfaces reduces the contact resistance as shown in Figure 2.1.

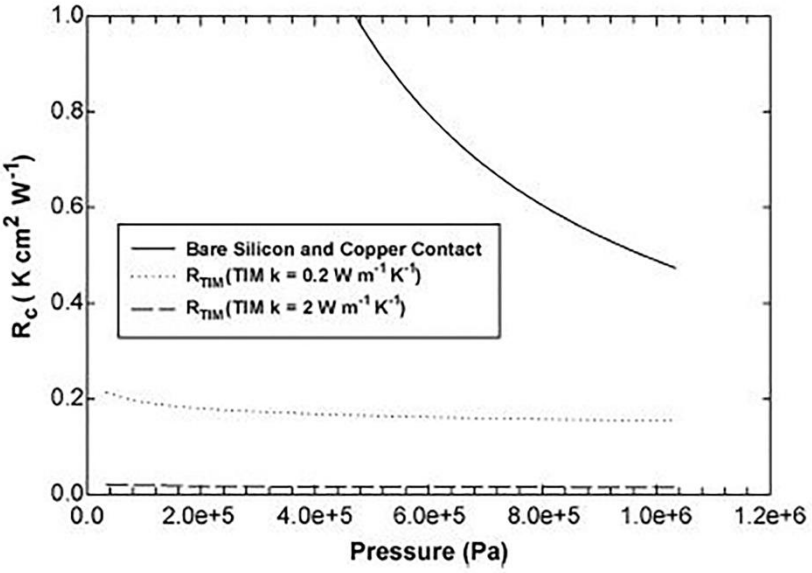

Figure 2.1 Thermal resistance without TIM and in presence of TIM (Prasher 2006)

(Stewart 1972) conducted an experimental study to determine TCR between various metals. The study found that the TCR decreased with the increase in the contact pressure and it was concluded that the apparent decrease in the TCR was due to the increase in the actual contact area. (Yovanovich et al. 1997) in their study on the aluminum-ceramic interface found the joint resistance decreases from 2.665×10^{-4} m^2 K/W to 1.903×10^{-4} m^2 K/W as the contact pressure increased from 0.007 to 0.35 MPa. (Abdullah, et al. 2017) studied the effect of pressure (0 to 868kPa) and roughness (2.63 to 40.69µm) on TCR. The study revealed that the application of higher contact pressure resulted in reduced contact resistance. (Xu et al. 2007) in their study on improving thermal contact found an increase in TCC between copper disks as the contact pressure increased. (Liu et al. 2010) reported the reduced values of TCR between brass contacts

with the increase in interfacial pressure. Similar trends of reduced TCR between aluminium alloy contacts upon increasing the pressure were reported by (Zhang et al. 2017). (Tariq and Asif 2016) assessed the TCC for copper, stainless steel, brass metallic interfaces and found that the TCC increased with the increase in contact pressure. (Narayana and Narayan 2014) in their study on TCR between similar and dissimilar materials also found that as the load increased, the TCR reduced. A similar trend in enhanced heat transfer with increased load was observed by (Ramakrishna Devananda P and K NarayanPrabhu 2019) for Cu-Cu interfaces. Thus, studies have shown that the increase in contact pressure results in decreased thermal contact resistance resulting in enhanced heat transfer across the interfaces. This trend of decrease in TCR is attributed to the increased contact area and elimination of air gap. However, the increase in contact pressure is not an ideal solution particularly in the electronic application as the application of higher load is unsuitable owing to the load constraints (Bahrami et al. 2005).

2.2 TIMs for thermal management of microelectronic packages

Heat transfer across the interface could also be enhanced by employing highly polished surfaces which would eliminate the surface roughness (Roy et al. 2016). The other techniques which could enhance heat transfer across the interface include treating contact surface by certain techniques like anodized CVD. The CVD technique is more effective. However, the implementation of it is complicated as it necessitates a vacuum environment (Sartre and Lallemand 2001). Further, these methods offer certain challenges that would either increase the cost of the entire system (Bahrami et al. 2005) or is not practically feasible.

One of the effective methods to reduce TCR is by placing a highly conductive TIM at the interface (Zhang et al. 2017) (Chung 2001). Figure 2.2 and 2.3 show the schematic representation of TIMs at the source-sink interface. TIMs eliminate the air gaps at the interfaces that are poor conductors of heat and thus reduce the TCR (Raza et al. 2015)(Saadah et al. 2017). The application of TIMs at the interface resulted in a reduction in the values of interface resistance as shown in Figure 2.1

.

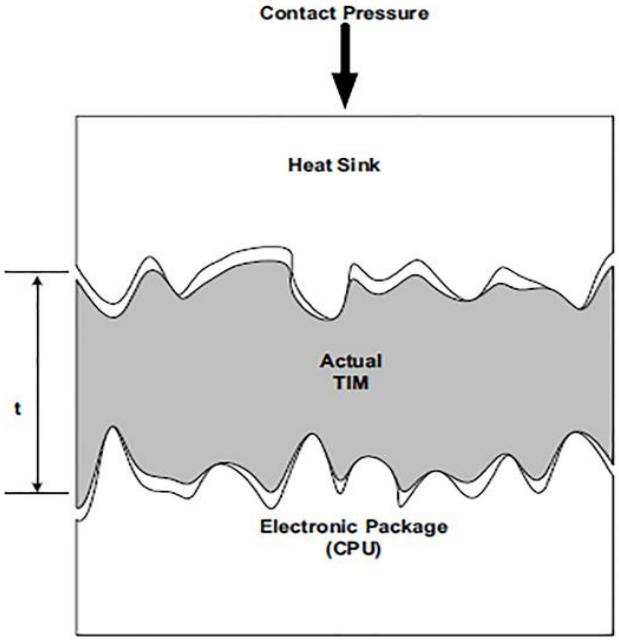

Figure 2.2 Real TIM inserted between an electronic package and a heat sink (Gwinn and Webb 2003)

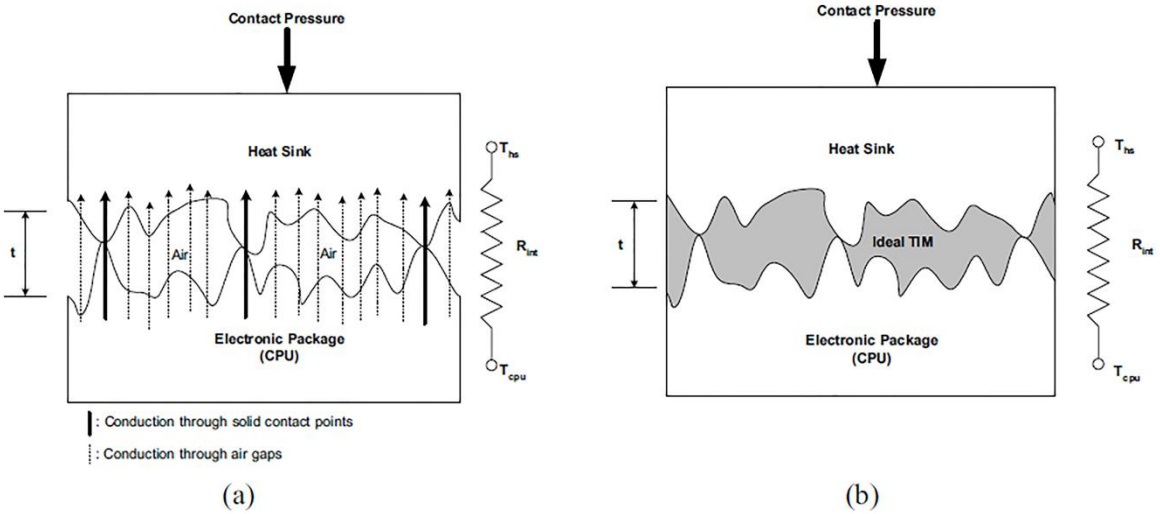

Figure 2. 3 (a) Interfaces with no thermal interface material b) Interfaces with the presence of an ideal TIM (Gwinn and Webb 2003)

The thermal performance of a TIM is a function of thermal conductivity and thermal resistance (Prasher et al. 2003) Thus,

The total effective thermal resistance (Prasher et al. 2003) is

$$R=R_{C1}+R_{C2}+ (BLT/k_{TIM}) \quad (2.1)$$

Where, BLT and k_{TIM} are the bond line thickness and thermal conductivity of the TIM respectively. R_{C1} is the interfacial resistance between the TIM and the heat sink. R_{C2} is the corresponding resistance between the TIM and the electronic package (Sarvar et al. 2006).

Hence, from the above equation, it is clear that TIM with high thermal conductivity and low BLT would be ideal for achieving lower thermal resistance (Sarvar et al. 2006) (Roy et al. 2016). However, the total effective thermal resistance also depends upon the contact resistance between TIM and Individual surfaces. The contact resistance in turn depends on factors such as clamping pressure, surface roughness, compressive modulus and flatness of the surface (Sarvar et al. 2006).

In addition to conformability and high thermal conductivity, the other factors that influence the selection of a TIM are minimal thickness, easy deformability, ease of manufacture, non-toxic, minimum weight, wide operating temperatures, resistance to chemicals, and dielectric strength, phase change temperature, optimum contact pressure, long term chemical stability, mechanical properties, viscosity, operating temperature, electrically conductivity and cost effectiveness (Sarvar et al. 2006) (Gwinn and Webb 2003) (Martin et al. 2007)(Chung 2001) (Yu 2012).

Over the years, thermal design engineers have used different classes of materials as TIMs. Table 1 shows the broad classification and typical commercially available TIMs. These could be broadly classified as thermal greases, Low melting alloys (LMA), metal foils, Phase change materials (PCM) and gels. In this section, an attempt is made to review the scientific progress that has been carried out in understanding the implications of using some of these TIMs in thermal management. Efforts have also been made to highlight the various factors that could affect the performance of these materials, the methods employed in characterization, and the recent advancements that have been accomplished in the field of TIMs.

Table 1 Broad classification and typical examples of TIMs

(Gwinn and Webb 2003)(Narayana and Narayan 2014)(Prasher 2006)(Fletcher 1990)(Gao and Liu 2012)(Ji et al. 2015)(Yang et al. 2014) (Huilong Yan 2019)(Sartre and Lallemand 2001) (Roy et al. 2015) (Roy et al. 2016)

Sl No	Thermal interface materials (TIM)	Typical examples/commercially available TIMs
1	Thermal grease/paste: Polymer (Silicone-based, PEG-based), sodium silicate based thermal greases	Artic silver, ShinEtsu G751, ShinEtsu G765, ShinEtsu G750, Berquist TIC 7500, G641,DC 340,P12,Eupec, Unial Rhodorsil, etc
2	LMA	Eutectic(Bi-Pb-Sn-In-Cd), Indium-Bismuth-Tin alloy (Ga-In), (Ga, In-Bi-Sn), (17Sn26In57Bi), (17Sn51In32Bi), (51 In, 32.5Bi, 16.5Sn), (100 Ga), (75.5Ga, 24.5In), ($Ga_{62.5}In_{21.5}Sn_{16}$), (GaIn10), ($GaIn_{20.5}Sn_{13.5}$)
3	Metallic foils	Copper, aluminum, lead, Gold, tin, indium
4	PCM	ThemaxHF-60110-BT, Chromeries T454, Bergquist HiFlow, Power Strate 60(AG), Orcus inc. FSF 52
5	Gels	Vinyl terminated silicone oil

2.3 Thermal grease/paste

Thermal greases also termed as thermal pastes (Skuriat et al. 2013) are generally polymer-based TIMs. The application of these polymer-based TIMs in the form of thick paste between the mating surfaces is found to have enhanced the heat transfer across the interface as it replaces the poor conductive air (Gwinn and Webb 2003). Thermal grease is synthesized by incorporating conductive particles like silver, zinc, carbon-based materials, aluminum oxide, etc to silicone oil or a hydrocarbon oil (Roy et al. 2016). Thus, it contains two principal components namely a polymer base/vehicle and a filler material.

The most commonly used polymer base is silicone owing to its superior thermal stability, wetting characteristics, high elasticity, low moisture uptake, ionic purity, and superior electrical properties (Becker et al. 2005) (Peterson 1990). Apart from silicone oil, PEG (Polyethylene glycol), and sodium silicates based thermal greases/pastes has been used. The filler material will be either metallic or ceramic (Sarvar et al. 2006)(Kusuma et al. 2019). Studies have also been conducted with carbon allotropes as filler materials. Some of the important parameters that have to be considered while selecting a filler materials are its thermal conductivity, coefficient of thermal expansion, geometry and concentration in the mixture (Lewis et al. 2020). Based on fillers applied, thermal greases can be classified into three categories namely metal-based, ceramic-based, and carbon-based (Otiaba et al. 2011)(Mallik et al. 2011). Metal-based thermal grease based on metals uses metals like silver (Ag), aluminum (Al), copper (Cu), etc whereas ceramic-based greases use ceramic fillers like alumina, AlN, SiC, ZnO, beryllium oxide, etc. In the case of carbon-based thermal greases, CNTs, Graphene, few layered graphene sheets (FLG), graphite nanoplatelets, carbon black dispersions, are used (Raza and Westwood 2019). The advantages of carbon-based fillers especially the likes of CNT and graphene is attributed to their high thermal conductivity that ranges from about 3000W/m K to 6000 W/mK (Otiaba et al. 2011) (Wang et al. 2014).

Before 1990 thermal grease was primarily used as interface materials to address TCR problems (Veilleux 1968). A detailed review of these studies was published by Fletcher (Fletcher 1990). The review paper compiled the studies that involved the usage of thermal grease (mostly silicone-based) and other materials such as metallic foils,

composite and cement, etc for obtaining thermal solutions. The paper highlighted the effect of various parameters such as surface finish, the thickness of the grease, contact pressure, the effect of additives on viscosity, material property, etc on contact resistance. (Prasher 2006) published a review paper that focused on various physical models that could be used in analyzing polymer-based TIMs. The typical thermophysical values of greases are given in a research paper by (Gwinn and Webb 2003). The paper records the thermophysical properties of various commercially available greases such as Arctic Silver, ShinEtsu G751, ShinEtsu G750, ShinEtsu G765, Berquist TIC 7500 with resistance values ranging from 0.018×10^{-4} m^2 K/W to 0.387×10^{-4} m^2K/W. The typical thermal conductivity values of these thermal greases range from 2.89 W/mK to values greater than 7.5 W/mK. The paper published by (Chung 2001) has also recorded the values of thermophysical properties of many types of greases based on both silicone and sodium silicate greases. Majority of the studies that are associated with thermal grease is aimed at enhancing thermal conductivity, estimation of TCR/ TCC, and the parameter that affect it. Studies have also been focused on understanding the reliability of greases at operating temperatures.

(Chiu et al. 1997) investigated grease type interface material in Plastic Pin Grid Array (PPGA) application. The study concluded that the selection of TIMs must not be based only on bulk thermal conductivity. Apart from bulk thermal conductivity, the contact resistance also needs to be considered. (Yovanovich et al. 1997) in their attempt to calculate the joint thermal resistances between aluminum-ceramic interfaces used silicone grease as TIM. The study was conducted by subjecting the interfaces to a pressure range of 0.007 and 0.35MPa. For interfaces with silicone greases, the calculated joint resistance was in the range of 0.335×10^{-4} m^2 K/W to 0.213 m^2 K/W. Similarly, for the case of bare interfaces with the above-mentioned pressure range, the joint resistance was recorded to be in the range of 2.665×10^{-4} m^2 K/W to 1.90310^{-4} m^2 K/W. Thus, the magnitude of joint resistance values was lower in the case of interfaces with TIM (silicone grease) as compared to bare interfaces. The study also noted that the joint resistance could be reduced to values lower than 0.065×10^{-4} m^2 K/W if the gaps at the interfaces were filled with ceramic particle doped grease. Sartre et al [3] conducted experiments based on steady state approach to determine TCR when

silicone-based greases were used as TIMs. These were applied at the copper- aluminum interface. Among them, the application of one of the greases G641 (General Electric) yielded TCR of 1.46×10^{-4} m^2K/W. However, for bare junctions, the TCR value was 6.67×10^{-4} m^2K/W. The study also investigated various metallic foils, silicone foils, and PCM coated foils. It was found that among various interstitial materials, greases were most promising. Further, the performance of PCM coated foils was comparable with that of greases. The effect of various parameters like heat transfer rate, bolt torque, and grease thickness was studied. It was found that among the parameters bolt torque is the highest influential parameter.

(Skuriat et al. 2013) calculated thermal resistance using Ag thermal grease (thermal stability range: -57°C to 252°C) from Circuitworks® as TIM for Copper stack samples. The thermal resistance values were determined based on steady state test method. The study found that the thermal resistance of Cu stacks with Ag thermal grease was significantly lower when compared to Cu stacks without Ag thermal grease. The study also focused on the effect of aging time and found that the Ag thermal grease to be not durable for continuous operation at 170°C. This is attributed to the fact that all the polymer base burns out during isothermal aging resulting in decreased contact between Ag particles and Cu. The effect of pressure on thermal resistance was studied. The study revealed that the thermal resistance of the Cu stacks reduced as the pressure increased owing to the reduced contact resistance. Furthermore, the study was also conducted with Sn-3.5Ag, Sn foil (25µm) as TIMs. Among the TIMs employed, Ag-based thermal grease produced superior results with the lowest thermal resistance values.

(Leong and Chung 2003) studied thermal pastes based on organic vehicles namely PEG and butyl ether along with ethyl cellulose. These thermal pastes were prepared by dissolving ethyl cellulose, carbon black, and other conductive fillers. In their study, the thermal pastes were applied between copper disks, and the TCC was measured by using the laser flash method. The thickness of the thermal paste was about 25µm and the copper thermal paste sandwich was subjected to pressure at 0.46, 0.69, and 0.92MPa. Ethyl cellulose and carbon black were added to the organic vehicles at different proportions and were tested. For thermal pastes based on PEG, the highest TCC of 3×10^5 W/m^2 °C was recorded when ethyl cellulose and carbon black were added at 3

vol% and 1.25 vol% respectively. Similarly, for thermal pastes based on butyl ether, the highest TCC of 28×10^4 W/m^2 °C was recorded when ethyl cellulose and carbon black were added at 40 vol% and 0.2 vol% respectively. Their study also revealed that more than the thermal conductivity, conformability, and spreadability play a significant role in determining the performance of TIMs.

Apart from silicone oil and other polymer-based thermal pastes, sodium silicate based thermal pastes have been studied. When compared to the polymer-based pastes, sodium silicate based TIMs yielded better TCC when used across conductors and also facilitated application of lower contact pressure (Yunsheng Xu, Xiangcheng Luo 2000). The superiority in thermal performance of sodium silicate is attributed to the lower viscosity and there by conforming to the topography of the surfaces between which it has been applied (Chung 2001)

(Kusuma et al. 2019) studied sodium silicate based thermal grease TIMs for CPU applications. In their study Zinc oxide (ZnO) was used as filler materials with concentrations of 16, 18, and 20wt%. The thermal resistance of sodium silicate TIMs with ZnO filler concentration of 16 wt% was 0.0123 °C/W. Thus, the reported value of thermal resistance was significantly lower when compared to the resistance values of thermal grease that are available in the market

The use of thermal greases as TIM provides several vital advantages. Thermal grease provides a very thin thermal joint (Sarvar et al. 2006) and could be screen printed to specific thickness on heat sinks (Nagabandi et al. 2017). The ability to have a thin thermal joint would result in very low thermal resistance as it would reduce BLT to a significant level. Thermal greases have been found to have excellent flowability at the interfaces which would fill the cavities that were previously filled by air(Roy et al. 2016) and thereby decreasing the contact thermal resistance. Further, thermal grease requires no post dispensing (Due and Robinson 2013). In addition to these stated advantages, the other advantages include reduced manufacturing cycles (Gowda et al. 2005), significantly low cost when compared to other types of TIMs, and the requirement of lower pressure to fill the interstitial gaps (Otiaba et al. 2011). Thermal grease as TIM is best suited for applications which operate at a relatively lower

temperature as well as applications which employ lower loading and requires low power cycling(Viswanath et al. 2000).

The loading of the thermal greases with filler conductive material is another important critical factor that affects the performance of the thermal greases. The thermal conductivity of the thermal grease increases as the loading of filler material increases (Becker et al. 2005), which in turn would make them eligible for carrying out effective heat transfer and thereby validating their use as potential TIMs. The typical thermal conductivity values of thermal greases lie in the range of 0.45-5 W/m K (Otiaba et al. 2011). Further, there have been reports of thermal greases with a thermal conductivity greater than 7.5 W/mK (Nagabandi et al. 2017). Further, attempts have been made to enhance the thermal performance of greases by the addition of nanoparticles

The thermal resistance offered by thermal greases typically lies in the range of 0.1×10^{-4} m^2 K/W to 1×10^{-4} m^2 K/W (Roy et al. 2015). Studies have shown that the voids in TIMs severely affect the heat transfer across the interface. These voids that are found in TIMs are formed due to outgassing or due to inadequate volume resulting in reduction in performance, reliability and strength of TIMs (Chiu et al. 1997)(Gowda et al. 2005) (Gowda et al. 2004) found that the voids have got a direct bearing on the thermal performance of TIM. In their study, they found that as the percentage of voiding increased, thermal resistance values increased. TIMs were placed between a silicon die and aluminum heat spreader at a pressure of 0.07 MPa. In their study, three different TIMs adhesive systems namely, unfilled silicone (TIM-1), alumina filled silicone (TIM-2) and an alumina filled epoxy (TIM-3) were used. The in situ thermal resistance for the void-free sample in the case of TIM-1 is 232×10^{-6} m^2 K/W. However, TIM-2 and TIM-3 recorded a thermal resistance of 45×10^{-6} m^2K/W. The experimental results showed a rise in thermal resistance value as the voiding percentage increased.

The effect of voiding was also studied by (Chiu et al. 1997). Figure 2.4 shows the effect of grease voids on the thermal interface resistance. The study was conducted by using finite element model. The study revealed that the thermal resistance is significantly affected by center voiding, whereas it is less sensitive to peripheral voiding. The overall thermal resistance value in the case of 30% centre voiding came out to be 0.23°C/W.

However, the value of interface resistance in the case of 30% peripheral voiding resulted in almost no change. Further, they also investigated the role of the thickness of grease on the thermal resistance and concluded that the increase in the thickness of grease increases the thermal resistance for both the conditions of center voiding and peripheral voiding

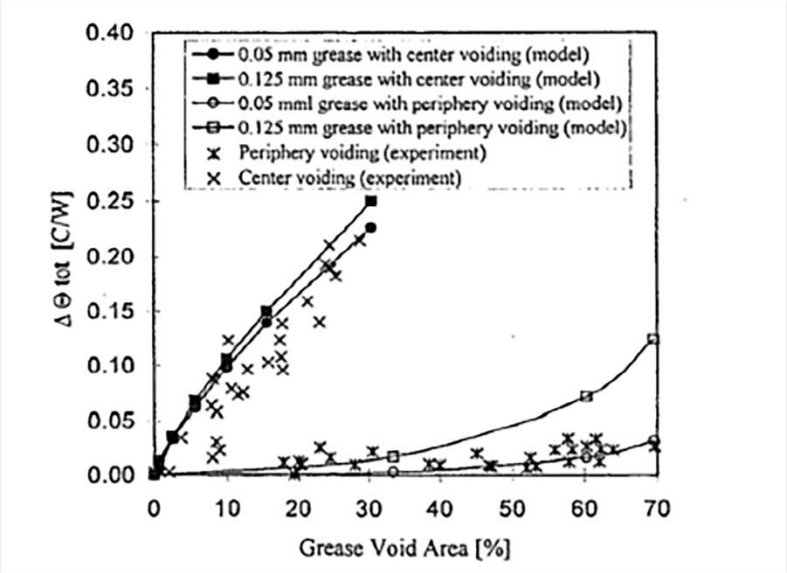

Figure 2.4 Impact of voiding area on thermal interface resistance (Chiu et al 1997)

Thermal greases have some of the disadvantages which hinder their usage. Apart from being messy, the application of thermal greases is considered untidy(Snaith et al. 1984) and removal of the thermal greases is a challenge. Grease dry out and pumped-out are other problems associated with usage of thermal grease as TIMs (Gwinn and Webb 2003). The temperature of operation plays a significant role in TIM's performance of and it has been found that the thermal performance deteriorated with temperature and time (Chen et al. 2013). Further, with power cycling, it has been seen that expansion and contraction lead to a pump out phenomenon and resulted in thermal degradation (Viswanath et al. 2000). Thermal greases are also found to be ineffective in applications wherein long contact must be maintained (Fletcher 1990).

2.4 Metal based /Low Melting Alloys (LMA)/ Solders

One of the inherent characteristics of the metal is its high thermal conductivity (Yu et al. 2012). Hence, metals form a perfect fit as TIM owing to high thermal conductivity values. The enhanced interfacial heat transfer can be achieved by having an all-metal thermal path between the heat source and heat sink.

The bulk of the work in the field of TIMs is focused on enhancing heat transfer at the interfaces that occur in the electronic package; particularly computers. In the case of computers, the operating temperatures are typically below 100°C and hence the metal-based TIMs ideally need to be in a liquid state in the operating temperature zones(Ma and Liu 2007). Hence metals or metal alloys with low melting temperatures need to be identified. With the use of Low meting alloys (LMAs), the TCR is significantly reduced as it flows into the surface cavities while being in a liquid state below the operating temperature of the equipment attached (Sarvar et al. 2006). Metal such as Gallium, mercury, indium, Tin etc could be used as TIMs. (Roy et al. 2016)(Ma and Liu 2007) (Hill and Strader 2006) (Hamdan et al. 2011).

High thermal conductivity and excellent wettability make low melting alloys (LMAs) or sometimes referred to as LMTI (Liquid metal thermal interface); an excellent choice as TIM (Sarvar et al. 2006). Apart from being high thermal conductive some of the other advantages of LMAs include reworkability, excellent wetting characteristics requiring no curing cycle, and ease of handling. Further, LMAs could be well implemented as a TIM in the case of materials having a different coefficients of thermal expansion(Macris et al. 2004).

To reduce TCR, (Cook et al. 1984) introduced a novel approach of using low melting alloys (LMAs) at the metal-metal interstice and were successful in reducing the TCR to a significant level. Subsequently other researchers (Gwinn and Webb 2003) (Hill and Strader 2006) (Hamdan et al. 2011) studied LMA TIMs and reported significant reduction in thermal resistance with LMAs as TIMs.

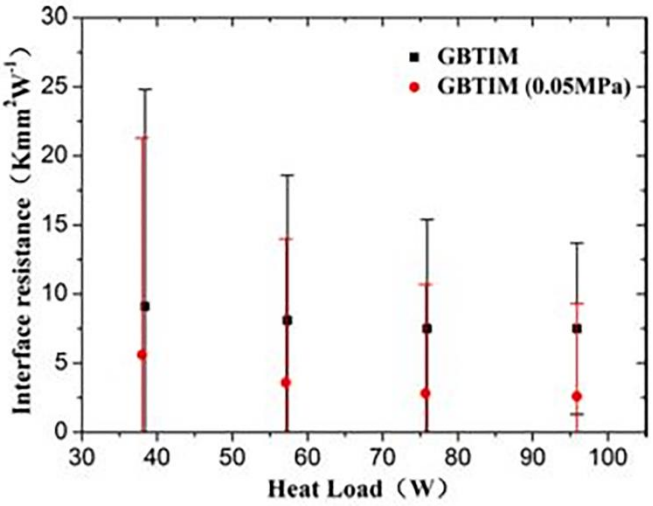

Figure 2.5 Thermal interface resistance with heat load (Gao and Liu 2012)

(Gao and Liu 2012) studied Gallium based thermal interface materials (GBTIM). The thermal resistance was found by applying GBTIM between copper blocks under steady state conditions. The study found that, when compared to thermal grease, the thermal resistance values with the application of GBTIM were significantly lower. This reduction in thermal resistance values was attributed to better wettability of GBTIM. Further, it was also observed that as the pressure is increased, GBTIM offers increased performance. As shown in Figure 2.5, it was found that as the heat load increases the thermal resistance of GBTIM decreased from 9.1×10^{-6} m^2 K/W to 7.5×10^{-6} m^2 K/W. The decrease in thermal resistance was also found in the case of pressure being applied to GBTIM. The value of thermal resistance decreased from 5.6×10^{-6} m^2 K/W to 2.6×10^{-6} m^2 K/W when the pressure of 0.05 MPa was applied. The thermal resistance values were minimal when the heat load was above 75W. This was attributed to the fact that fluidity of GBTIM increased the mobility under higher heat flux resulting in filling up voids which reduced the thermal resistance values.

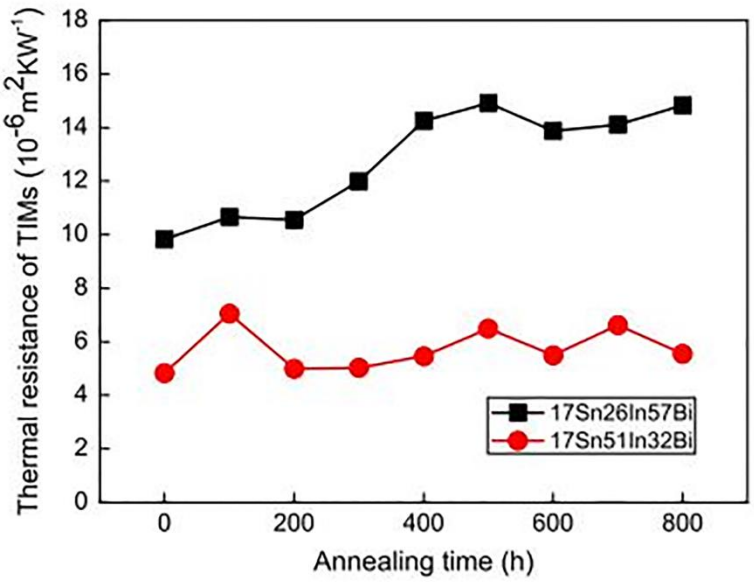

Figure 2.6 Changes in thermal resistance after aging for different times (Yang et al 2014)

(Yang et al. 2014) studied the thermal performance of LMTAs viz. 17Sn26In57Bi and17Sn51In32Bi between copper plates. The study used laser flash method to determine thermal resistance of LMTA TIMs and found that LMTA TIMs degrade during the heating process. Figure 2.6 shows the variation of thermal resistance with annealing time. The findings revealed that the thermal resistance change in the case of 17Sn51In32Bi was insignificant during 800h of aging with the thermal resistance value increasing from 4.83×10^{-6} m^2K/W to 5.55×10^{-6} m^2K/W, thus recording an increase of 15%. Whereas in the case of 17Sn26In57Bi there was an increment of 51% in the value of thermal resistance from 9.83×10^{-6} m^2K/W to 14.83×10^{-6} m^2K/W. It was found that the interfacial reactions between molten LMTA TIMs and copper were the main reasons for the deteriorating thermal performance. Further, they concluded that the precipitation of intermetallics that are brittle leads to crack initiation resulting in its expansion and thus causing a rise in the value of thermal resistance of TIM.

(Roy et al. 2015) studied the performance of LMA TIMs containing In, Ga, Sn, Bi as a function of applied pressure. The thermal performance of TIMs was generated using ASTM D5470 tester. They investigated three alloys namely alloy 19(51 In, 32.5Bi,

16.5Sn), alloy 14(100 Ga), and alloy 60 (75.5Ga, 24.5In). The results revealed that the interfacial resistance is independent of applied pressure because LMAs are non-viscous and hence higher pressures need not be employed to fill the irregularities. The experiments were conducted with different substrate-alloy combinations, and the study revealed that depending on the specimen preparation, the lowest thermal resistance was 0.005×10^{-4} m^2K/W and the highest was 0.065×10^{-4} m^2 K/W. Further, they also studied the performance of these TIMs by subjecting it to thermal cycling from -40°C to 80 °C. In their study, an alloy 19 (51 In, 32.5Bi,16.5Sn) in the form of a sheet and molten form were applied on copper discs and subjected to thermal cycling. The study revealed that the thermal resistance of the alloy in the sheet form saw an increase of about 115% after 500 cycles owing to improper wetting of the alloy at the interface. However, for the alloy in molten form, the degradation was negligible as the alloy wets the interface and thereby surviving for a larger number of cycles. Thus, wetting of alloy is of significant importance as it determines the reliability of LMAs. Further, the study also revealed that post alloy melting the interface temperature has no significant effect on the performance of the LMAs.

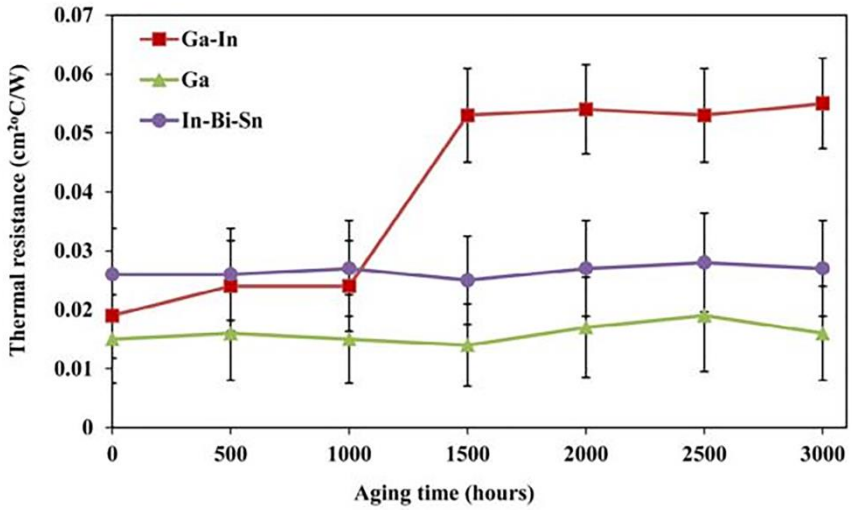

Figure 2.7 Isothermal aging performance of Ga-In, Ga and In-Bi-Sn alloys between Cu and Ni surfaces at 130°C (Roy et al 2016)

(Roy et al. 2016) studied the thermal performance by subjecting three alloys viz., Ga-In, Ga, In-Bi-Sn to accelerated thermal aging at a temperature of 130°C. The

experiment was carried out by employing a pressure of 20 psi by placing the alloys at the interface of Cu and nickel surfaces. All three alloys performed well, with very low thermal resistance. The alloys were subjected to thermal aging for up to 3000 hours as shown in the Figure 2.7 (Roy et al. 2016). The study noted that there were no significant changes in thermal resistance value after 1500 hours and that the superior performance of the three alloys was attributed to the enhanced wetting of alloys at the substrates. It was also observed that the resulting intermetallics formed did not contribute to increasing the thermal resistance. Further, the thermal performance was studied by subjecting the assembly to thermal cycling and the temperature was made to fluctuate between -40°C to 80°C. It was observed that thermal degradation occurred earlier in the case of thermal cycling than in the case of aging. The degradation was the result of subjecting the thermal joint to expansion and contraction during thermal cycling which causes the onset of degradation early.

(Li et al. 2017b) investigated the use of LMA based thermal paste as TIM. The experiments were carried out based on laser flash technique. The LMA that was proposed was eutectic $Ga_{62.5}In_{21.5}Sn_{16}$ alloy. LMAs were sandwiched between specially designed copper plates. Three variants were used that include LMA, OLMA (Oxidized liquid metal alloy) and OLMA mixed with copper particles of 9µm (5% Wt). The thermal conductivities of these TIMs were 44.48, 13.55, and 24.34 W $m^{-1}K^{-1}$respectively.The corresponding thermal resistance was 4.044×10^{-6} m^2 K/W, 5.638×10^{-6} m^2 K/W, and 4.075×10^{-6} m^2 K/W respectively. The study also found that, for, OLMA mixed with copper particles, as the percentage of copper particles increased from 5% to 10%, the thermal conductivity value increased from 24.34 $Wm^{-1}K^{-1}$ to 29.09 $Wm^{-1}K^{-1}$. Further, as the percentage of copper particles increased, the value of TCR reduced from 4.075×10^{-6} m^2K/W to 3.37×10^{-6} m^2K/W.

(Ji et al. 2015) used vertically aligned CNTs with LMA as a bonding material in their study on TIMs. The study showed that employing VACNT film as TIM resulted in increased performance with regards to the heat transfer at the contacts. Further, LMAs were also used as the bonding material. The study found that the plasma treatment of contacts enhanced the contact area of LMAs. The study used a laser flash method to

measure thermal resistance and revealed a decrease of 31% in the thermal resistance values between copper silicon contacts after the application of VACNT films.

(Ji et al. 2020) studied the use of Gallium based $Ga_{62.5}\,In_{21.5}\,Sn_{16}$ (MP 10.7°C) as TIM between aluminum substrates and used laser flash method to measure thermal performance. The substrates were coated with AAO (anodic aluminum oxide) film to reduce the reaction between Al and Ga based substrates. The thermal parameters such as thermal conductivity, thermal diffusivity, and thermal contact resistance were measured by the laser flash method. For comparison, dry Al-Al contacts and Al contacts with TG 250 (Thermal grease) as TIM were tested. The thermal contact resistance values were over 0.001 m^2K/W at all pressure ranges for dry Al contacts owing to the presence of air gaps at the interface. For all the three types of contacts, the thermal resistance reduced significantly as the pressure increased at the initial ranges and reached to near-constant values as the pressure increased. For contacts with TG 250 as TIM, at 0.05MPa the TCR was about 2.79604×10^{-4} m^2K/W which reduced to about 99% for contacts with Ga based TIM with the value of TCR recorded as low as 3.575×10^{-6} m^2 K/W at 0.05MPa. As the pressure was increased to above 1 MPa the TCR was about 2.5×10^{-6} m^2 K/W for gallium-based contacts. Thus, the application of GBLMA resulted in enhance heat transfer across interfaces.

(Chu et al. 2019) studied the use of LMTA with a confined seal as TIMs. This novel design of using LMTA with an annular seal was proposed so as reduced the problems such as overflow and dislocation problems that were associated with the use of LMTAs as TIMs. The study was conducted under steady state conditions. In their study, they also used solid-state TIMs such as Indium, copper, lead, and Tin TIMs. Among the solid-state TIMs Indium outperformed other solid TIMs. Further, In the case of Indium foil as TIMs, with the increase in pressure, the thermal contact resistance was reduced to 0.112×10^{-4} m^2K/W to 0.078×10^{-4} m^2K/W at pressures of 130 kPa to 550 kPa owing to low Young's modulus and high thermal conductivity of Indium. Also, with the loading and unloading of contact pressure, hysteresis was observed. The use of LMTA further reduced the thermal contact resistance to 0.0332×10^{-4} m^2K/W. However, problems such as overflow and dislocation remained. Hence to mitigate the problems of overflow and dislocation a novel design of using an annular seal was proposed. The

thermal contact resistance was recorded to be 0.0388×10^{-4} m^2 K/W in the case of an indium seal. The application of 100 thermal cycles resulted in thermal contact resistance to fluctuate between 0.039×10^{-4} m^2K/W to 0.044×10^{-4} m^2 K/ W under the heating load of 100W and 50W.

To enhance interfacial heat transfer, (Liu et al. 2018) proposed a composite TIM. This new composite was synthesized by combining gallium based liquid metal and PDMS (Polydimethylsioxane) with AlN powder (ALTG- AlN liquid metal thermal grease). The thermal contact resistance was obtained by analyzing transient temperature response curve. In the study, the performance of ALTG was compared with Liquid metal/PDMS (LMTG), GLTG (Graphene liquid metal Thermal grease), and X23-7762 (commercially available thermal grease). The study revealed that ALTG showed superior thermal performance when compared to liquid metal/PDMS composites (LMTG), X23-7762, and GLTG with thermal conductivity of 5.014 W/mK. The contact resistance for ALTG was recorded to be 15×10^{-6} m^2 K/W which was also lower when compared to LMTG (18×10^{-6} m^2 K/W), X23-7762 (27×10^{-6} m^2 K/W) and GLTG (16×10^{-6} m^2 K/W). Further, when compared to the liquid metal TIMs, the ALTG showed reduced fluidity thus mitigating the problem of spillage.

Furthermore, (Bai et al. 2005) studied the measurement of solder/copper interfacial thermal resistance wherein the feasibility of employing flash technique was demonstrated in measuring interfacial thermal resistance. The results showed that the interfacial thermal resistance (ITR) was found to be in the range of 0.011×10^{-4} m^2 K/W to 0.033×10^{-4} m^2 K/W. For interfacial thermal resistance in the case of solder, copper alloy is attributed to the mismatch of crystal structure in addition to elastic moduli differences at the interfaces. In addition to this, poor wetting also results in significant value of ITR.

(Zhang et al. 2014c) applied Sn-Bi solder paste between copper plates. The study used laser flash method to measure the thermal resistance of Sn-Bi solder paste. The experiments revealed that, for a defect-free thin Sn-Bi TIM layer, the thermal resistance of fewer than 5×10^{-6} m^2 K/W was recorded. Further, the TCR between copper alloy and Sn-Bi was found to be 0.576×10^{-6} m^2 K/W showing Sn-Bi solder paste to be a

promising TIM. Also, it was observed that thermal cycling resulted in a decrease in thermal resistance of Sn-Bi TIM.

(Van Heerden et al. 2004) studied the thermal behavior of Si-Cu Interface which was reactively soldered. Reactive soldering is a technique that employs a nanostructured reactive multilayered foil as a heat source. The soldering is carried out initially by metalizing Si with Au. Further, a 37Pb-63Sn eutectic solder foil is placed over followed by placing a Nano foil. Furthermore, the joint is accomplished by placing a Cu sink which is pre-wet by the Pb-Sn solder. The bond is formed as a compressive force is applied and as the reaction in the foil is initiated the heat which gets liberated melts the solder resulting in bond formation. The study revealed that there was no significant degradation even after 1000 cycles in the temperature range of 25°C to 125°C with a mere 1.7% change in thermal resistance. The conventional soldered joint showed similar results wherein the thermal resistance change was about 4.4%.

(Hansson et al. 2017) characterized carbon fiber solder composite TIM using transient laser flash technique. The TIM was fabricated by infiltrating molten (Sn95.5 Ag3.8 Cu0.7) into heated carbon fiber at a pressure of 20 MPa in a vacuum filled cavity and was followed by cooling the composite to room temperature. The addition of carbon fiber greatly increases the handling characteristics. The fabricated TIM was placed between Cu plates which were coated with 5µm Ni diffusion barrier and 100 nm Au finish that prevented oxidation. The experiments were conducted at a pressure of 200kPa.The TIM composite shows an excellent performance with a reported thermal resistance lesser than 2×10^{-6} m^2K/W at 43 µm BLT. Further, the degree of voiding is significantly low and was confirmed by SEM analysis of the cross section of TIM. The reduced voiding resulted in enhanced performance of the system.

(Carlberg et al. 2009) proposed a novel nanostructured polymer-metal composite film as TIM. The polymer matrix was fabricated by the electrospinning method and subsequently, the LMTA was infiltrated into the porous polymer network. The resulting TIM composite film was tested for its thermal performance by using ASTM D5470 technique. In the pressure range of 200-800 kPa the TIM exhibited thermal resistance as low as 8.5×10^{-6} m^2 K/W at 70µm bond line thickness and corresponds to thermal

conductivity as high as 8 W/mK.

(Gao et al. 2017) studied the use of Gallium based binary alloy (GBTIM- GaIn10) and Gallium based Ternary alloy (GTTIM- $GaIn_{20.5}Sn_{13.5}$) with about 40µm thickness as TIMs. The TCR was measured by self-designed apparatus under steady-state conditions with heat loads of 60W, 80W and 100W.The study found that the thermal resistance values were not significantly affected by varying the heat load. Further, for the heat load of 100W, thermal resistances of 7.8×10^{-6} m^2 K/W and 4.3×10^{-6} m^2 K/W were recorded for GTTIM and GBTIM respectively. The experimental studies also found that the TCR could be reduced to as low as 2.2×10^{-6} m^2K/W for the case GBTIM when the contact pressure was about 0.05MPa. This indicates that a small order of pressure would sufficient to fill the air gaps at the interface resulting in enhanced heat transfer. The study also focused on understanding the wettability of the Gallium alloys that were used as TIMs in the present study and found that increasing the amounts of gallium oxide (Ga_2O_3) in gallium alloys enhances the wettability but results in reduced thermal conductivity owing to the low thermal conductivity of Gallium oxide. However, the thermal conductivity values of Gallium based alloys are still higher than the commercially available thermal grease. The highest thermal conductivity of GBTIM was recorded to be 19.2 W/m K.

(Huilong Yan 2019) studied the interfacial heat transfer of polished Cu plates with buffer layers deposited on it. The LMA alloy of $Ga_{62.5}$ $In_{21.5}$ Sn_{16}(MP= 10.6°C) was sandwiched between coated Cu plates. The buffer layers of Ag, Ti, W, Cu, Mo of thickness 60 nm were deposited using DC magnetron sputtering on copper discs. The contact angles of water and diiodomethane were determined by the drop shape analyzer (KRUSS). The surface free energies (SFE) were calculated by Owens-Wendt-Rabel-Kaelble equation. The study used a laser flash analyzer to determine thermal properties. The study found that the coatings have a significant impact on the contact angle and was found that the contact angle decreased with an increase in SFE. The study also revealed that SFE of the buffer layer significantly impacted on the properties such as wettability, thermal diffusivity, and thermal contact resistance. The high value of SFE of buffer layers enhanced the thermal transfer resulting in decreased TCR.

(Swamy and Satyanarayan 2019a) conducted the study on thermal performance of brass and Sn coated brass TIMs. In their study, ASTM D 5470 method was used to assess the thermal performance. The study showed that the use of Sn coated brass TIMs resulted in lower thermal contact resistance when compared to bare brass TIMs. Thus, coated brass showed superior performance as TIMs. Further, the study also revealed that the contact resistance of interface materials reduced with increase in load and surface finish.

(Narayana and Narayan 2014) studied the effect of load and Interface Materials on TCR between similar and dissimilar materials. The study involved the use of copperfoil, aluminium foil, lead, and Sn-9Zn lead-free solder as TIMs. These TIMs were placed between similar/ dissimilar materials of copper, brass, aluminum and 304 stainless steel.In their study, the effect of load on the thermal resistance was studied. It was found that as the load increased, the peak heat flux shifted to lower times, thus as the pressure was increased, the TCR reduced early resulting in the enhanced heat transfer. The study was also conducted to understand the variation in TCR for low thermal conductivity stainless steel and high thermal conductivity copper as hot source materials against various other materials as cold sink materials have high thermal conductivity. The study revealed that thermal contact resistance becomes a dominant factor when both the source and sink are of high thermal conductivity. The study revealed that Sn-9Zn showed better performancewhen compared to other materials owing to the conformance to the contacting surface at higher temperatures.A reduction of 67% in thermal contact resistance was recorded when Sn-9Zn was used as TIM for the Al –Cu interface. Thestatistical significance of various parameters was determined by the use of Analysis of variance (ANOVA) technique. It was found among various factors such as materials in contact, load, and interface materials, the load has got significant contribution when compared to the other factors in determining the contact resistance.

The formation of intermetallics is one of the major concerns in the application of LMAs as TIM (Yang et al. 2014). Dewetting, dripout, migration, oxidation and corrosion related problems are the other challenges faced in using LMAs as TIMs (Macris et al. 2004). The formation of voids and their growth is a major challenge while using solders as TIM since they reduce the heat transfer across the interface to a significant level.

(Hu et al. 2004) studied the effect of the void like inclusions in a eutectic alloy of 52In48Sn which is used as a TIM between a silicon chip and a copper plate. In their study, the temperature field was characterized using through-wafer infrared microscopy. The study revealed the presence of hot spots with a temperature of about 15°C higher than the average die temperature at the locations corresponding to void/void like inclusions that were present in the eutectic layer that was used as TIM between the silicon die and copper plate. This non-uniformity in temperature distribution reduces the degree of heat transfer between the thermal contacts. However, polymers are preferred over solders as the implementation of solders involves considerations of cost and complexity.

2.5 Phase change materials (PCM)

PCMs are essentially a mixture of high conductive materials suspended in base materials and offer thermal resistance in the range of 0.3×10^{-4} m^2 K/W to 0.7×10^{-4} m^2 K/W (Otiaba et al. 2011). The base materials could be refined paraffin, a polymer, or a copolymer that acts similar to thermal greases due to the reduction in viscosity upon reaching operating temperatures of typically 50°C-60°C (Gwinn and Webb 2003)(Rauch 2000). Several advantages like easy to handle, no cure, no dry-out problems make them an ideal candidate for TIMs. However, PCMs are characterized by lower values of thermal conductivity that varied between of 0.17 and 0.35 W/m K(Goli et al. 2014)

(Liu and Chung 2006a) studied the effectiveness of wax incorporated with hexagonal boron nitride as a phase change TIMs. The study concentrated on the role played by factors that include temperature, boron Nitride content, and pressure on the thermal contact conductance. The Boron Nitride was added to the wax at different proportions of 0, 5, 10, 15and 20 wt%. The thermal interface material formed after the mixing of Boron Nitride with wax was applied between the copper disks. The TCC was measured using laser flash method. The study revealed that increasing the Boron Nitride content increased thermal conductance. The increase was seen up to 6.2 vol.%, however, a further increase in the volume percent of 8.6 saw a decrease in thermal contact conductance owing to the increase in viscosity that decreased the conformability of the thermal interface material between the copper discs. The thermal contact conductance

decreased as the temperature of the interface material was increased from 22 °C to 48 °C owing to the expansion of wax, however, with the increase in temperature from 48°C to 55°C the thermal contact conductance saw an increase in value as the interface material melted resulting in increased conformability of the interface material between the mating surfaces. Further, increasing the pressure increases the value of thermal conductance as it reduces the voids between the copper discs in addition to the reduction in thickness by the virtue of pressure. The use of boron nitride in the wax as thermal interface material saw the highest conductance of $18\times10^4 W/m^2$ at a vol.% of 4.2 at a temperature of 55 °C for pressure of 0.3MPa. An increase in pressure above 0.3 MPa resulted in no significant change in the contact conductance.

(Grujicic et al. 2005) et al studied the effect of TCR in thermal performance of CPU/heat sink assembly. In their study, they used phase change material (Thermaflow^{TM} T766, k=0.3W/mk) and acrylic/silicone-based tapes (Thermattach$^{®}$T414 tapes filled with kapton, k= 0.7W/mK) as TIMs. The study revealed that the deformation of micro contacts aided by increased pressure, lowered microhardness, and the application of these TIMs results in reduced thermal contact resistance resulting in reduced temperature being experienced by the CPU. The temperature experienced by CPU in the case of the application of PCM and acrylic/silicone tapes is 330.92 K and 390.91 K respectively.

(Zhao et al. 2019a) studied the effect of surface roughness, Interfacial temperature, and pressure on interface thermal resistance of TIMs. In their study different variants of TIMs including thermal pads, PCM, LMPA (Low melting point alloys), and carbon-based TIMs were studied. The study found that, for pressure below 0.3MPa, the interfacial thermal resistance (ITR) decreases as the pressure increases. Beyond 0.3MPa The ITR does not follow similar trends. The study found that for PCMs, the performance has got no influence on the surface roughness. Further, the ITR of PCM decreases as the temperature increases.

2.6 Thermally conductive elastomers and Gels

Elastomeric pads consist of elastomers typically filled with thermally conductive ceramic particles and finds extensive use as TIM in low power devices (Viswanath et

al. 2000). These pads with typical thickness of 0.25 mm offer advantages like, ease of handling, high stability, high operating temperatures, overall reduced cost (Mallik et al. 2011) (DeSorgo 1996) . Elastomeric pads are characterized by lower thermal conductivity and require high pressures to achieve lower contact resistance (Mallik et al. 2011). However, (Uetani et al. 2014) fabricated elastomeric TIMs with a thermal conductivity of 23.3W/mK. The study involved the use of electrostatic flocking technique to fabricate vertical aligned high density carbon fibers and involved filling the interstitial spaces with elastomeric materials. Some of the other recent study with respect to elastomeric TIMs includes the works of (Bhanushali et al. 2017) The study reported copper nanowire filler elastomer TIM with thermal conductivity of 3.1±0.2 W/mK. Further, (Zhang et al. 2019) fabricated elastomer – type TIM with silicone rubber matrix and graphene aerogel nanofiller. The study reported a thermal conductivity of 1.26 W/mK at a graphene aerogel loading of 0.50 wt%.

Gels are a class of TIMs that are developed in order to address the limitations offered by other classes of TIMs such as thermal grease, elastomeric pads etc (Prasher and Matayabas 2004). Gels contain silicone, crosslinker, and thermally conductive particles as principal components (Otiaba et al. 2011). Gels exhibit properties similar to that of thermal grease before cure and are characterized by high thermal conductivity, low surface energy and good conformance resulting in reduced thermal contact resistance (Matayabas Jr 2005). They are also characterized by low modulus which enables them to withstand thermo-mechanical stress without undergoing interfacial delamination (Otiaba et al. 2011). (Prasher and Matayabas 2004) studied contact resistance of cured Gel polymeric TIM. They proposed a semi-analytical model which shows that the contact resistance in the case of a cured gel is a function of applied pressure, the thermal conductivity of TIM, roughness of the substrate, and shear modulus of TIMs. The study laid design guidelines for reliable gel TIMs based on the parameters $G^{'}$(storage shear modulus), $G^{''}$ (loss shear modulus) and showed that to avoid pump out which is a common problem associated with grease, $G^{'}$ should be greater than $G^{''}$.

(Chano et al. 2017) in their study showed that it is possible to independently optimize the thermal conductivity of silicone gel TIM with required proprieties like compliance and minimized contact resistance by replacing cross linker with a chain extender. Thus,

it is possible to engineer higher performing Gel TIMs with better knowledge or understanding of the rheology.

2.7 Effect of addition of nanoparticles to TIMs on TCR/TCC

Recent studies have shown that apart from microfilters, nanofillers also have a profound impact on the performance of TIMs. A variety of nanostructures has been used as fillers for TIMs resulting in enhanced performance. The majority of the work involving nano-based TIMs has focused on enhancing TC. TC has a direct role in the performance characteristics of TIMs as higher TC contributes significantly results in heat transfer (Yujun et al. 2014). TIMs having high TC are generally used as interface materials since they provide good heat-conducting paths resulting in enhanced performance. Poor TC values of TIM fail to achieve higher rates of heat conduction required for the proper functioning of advanced systems. Hence this requires the development of TIMs having exceptionally high TC. Apart from TC, studies by (Zhang et al. 2014a) has also shown that TCR also depends on filler property, microstructural characterization, and surface morphology.

The ability to enhance TCC has made CNTs to achieve much attention in the recent past (Cola et al. 2007). CNTs are widely used as a filler material for TIMs due to high values of thermal conductivity at room temperature. The thermal conductivity varies from about 3000-3500 W/m K which makes them an excellent filler material (Shahil and Balandin 2012). In addition to the excellent thermal properties, CNTs have been reported to have exceptional optical, electrical, vibrational, and mechanical properties (Yujun et al. 2014)(Lin et al. 2010)(Cola et al. 2009) (Xu et al. 2006) . With regards to the thermal performance, CNTs can sustain temperatures as high as 200-300°C at oxygenic environments and could go up to 900°C in vacuum (Tong et al. 2007). The addition of CNTs as a filler material greatly enhances the TC of the TIMs. Further, CNTs are mechanically compliant (McNamara et al. 2015) and thus enabling them to conform to asperities resulting in increased contact area (Hao et al. 2017). Further, CNTs could be grown on metal substrates thus eliminating challenges such as pump out and voiding which are major concerns that limit the use of thermal grease and other liquid TIMs (Haight et al. 2016).

(Chen et al. 2013) studied the TCC of thermal grease which was added with functionalized CNTs. They investigated the performance of thermal grease which are dispersed with pristine CNTs and with that of functionalized CNTs viz. carboxylated CNTs and amino-functionalized CNTs. The study used the modified ASTM D5470-06 standard to measure TCC. The study found that the thermal impedance of carboxylated CNTs is significantly lower than thermal grease which is dispersed with pristine CNTs and amino-functionalized CNTs. Carboxylated thermal grease result in better performance owing to fine dispersion of CNTs in the polymer matrix. The study reported that with an addition of 2 wt.% carboxylated CNT, a thermal impedance as low as 0.18×10^{-4} m^2 K/W could be achieved. Furthermore, the study also found that with the addition of pristine CNTs at weight proportions of less than 1% to silicone grease the thermal impedance increased slightly. However, if the addition is beyond 1 wt. % the thermal impedance increases sharply. Further, with the addition of CNTs-COOH to silicone grease, the thermal impedance decreases and drops to 0.18×10^{-4} m^2 K/W at 2 wt%. The results further indicated that the addition of CNTs-COOH above 2wt% increases the thermal impedance. In the case of grease with CNTs-NH_2, the thermal impedance remained nearly unchanged up to 0.5 wt%. However, the addition of CNTs-NH_2 to about 1 wt%, the value of thermal impedance increased to 0.57×10^{-4} m^2 K/W which further increased to 2.75×10^{-4} m^2 K/W at 2 wt%.

(Xu et al. 2007) studied the use of single-walled CNT as filler material on PEG-based thermal paste. The paste was sandwiched between copper plates with transient laser flash method being used to measure TCC. The incorporation of CNTs saw the thermal conductance value rise to 20×10^4 W m^{-2} K^{-1} at a vol% of 0.6 as shown in the Figure 2.8. Further, the increase of CNT content above 1.8 vol % resulted in the drop in the conductance owing to conformability loss. In their study, the TIM was sandwiched between two copper discs. The surfaces of discs were polished mechanically by 0.05µm alumina particles. The pressures of 0.46, 0.69, and 0.92 MPa were applied to the sandwich. The study revealed that nanotube performed better than hexagonal Boron Nitride, However, carbon black outperformed nanotubes and recorded a conductance value of 30×10^4 W m^{-2} K^{-1}.

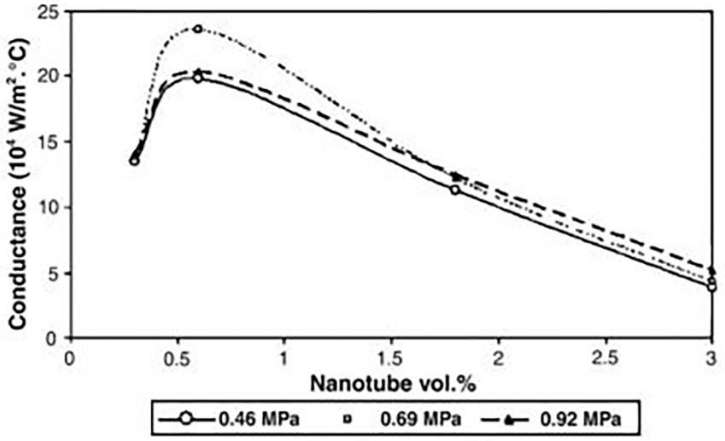

Figure 2.8 Variation in the value of conductance for different nanotube vol% at three different pressure (Xu et al 2007)

(Xu and Fisher 2006) studied the TCR of Cu-Si interfaces. A reference calorific setup based on axial one-dimensional steady state heat conduction was used to measure TCR of the interface at different conditions. CNT arrays were grown on the silicon surface by plasma enhanced chemical vapor deposition (PECVD). Apart from CNTs, the effect of placing Indium sheets and PCM were also studied. In addition to these, the combination of indium and PCMs with CNTs were also tested. The thermal resistance for Cu-Si interfaces as well as Cu-CNT-Si interfaces decreased with the increase in pressure as shown in Figure 2.9.

The deployment of CNT arrays resulted in a minimum thermal resistance of 19.8×10^{-6} m^2K/W at a pressure of 0.45 MPa. Further, the combination of CNTs with indium and PCMs were also studied. It was found that there was a slight reduction in the thermal resistance value of the composite upon the introduction of CNTs to the Cu-In-Si. However, the reduction in thermal resistance was significant in the case of PCM-.CNT composite. The thermal resistance value was 5.2×10^{-6} m^2K/W in the case of PCM-CNT array composite.

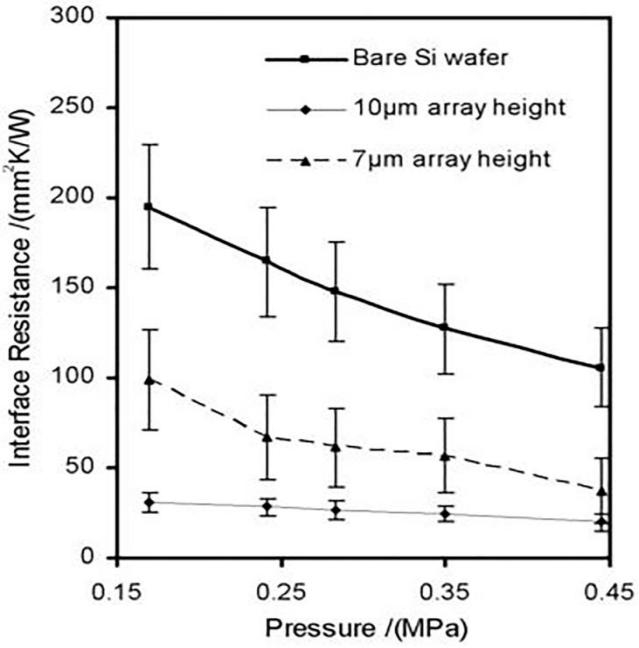

Figure 2.9 Thermal resistance as a function of pressure for Cu-Si and Cu-CNT-Si interfaces (Xu and Fisher 2006)

(Cola et al. 2007) synthesized CNT array on either side of a metal foil which could be used as an effective TIM. This method eliminated the necessity of exposing thermally sensitive materials to temperatures that are required for CNT growth. In their study, a CNT/foil TIM was fabricated and was placed at the interface. The study found that the thermal resistance of approximately 10×10^{-6} m^2 K/W was obtained at moderate pressures. The CNT/foil provides high conformability and reduces the effect of surface roughness. The deformation of CNT/foil results in increased CNT contact spots which in turn resulted in reduced thermal resistance. Further, they opined that the performance of the aforesaid TIM depends on several factors that include CNT density, diameter, length, foil material, and thickness and whose effects need to be further probed.

(Fabris et al. 2011) studied the effect of CNT addition to TIMs. In their study, two variants of TIMs were tested. CNTs were added to commercially available TIM (Arctic silver®) and silicone oil. The experimentation was conducted as per ASTM D4570-06 standard. In the case of CNT- Arctic silver (CNT-AS), the addition of CNTs resulted in increased thermal resistance which led to the deterioration in the thermal

performance. The reason behind the reduced performance is due to the increase in thickness which will also lead to the difficulty in spreading. However, the introduction of CNTs into silicone oil resulted in improved performance vis a vis CNT- AS. The increase in pressure resulted in a decrease in thermal resistance for CNT-silicone oil. The CNT-Silicone oil and also exhibited high compliance.

(Taphouse et al. 2014) used Pyrenylpropyl Phosphonic acid as a surface modifier to reduce the thermal resistance of CNT contacts. A reduction of thermal resistance of over 9 fold was reported. For dry contacts, the thermal resistance values at 7 kPa and 138 kPa were $(40 \pm 20)\times10^{-6}$ m^2 KW^{-1} and $(20 \pm 6)\times10^{-6}$ m^2 KW^{-1} respectively. The decrease in thermal resistance with an increase in the pressure is ascribed to the fact that the increase in pressure compressed the CNTs thus increasing the heat conduction area. Furthermore, the thermal resistance value in the case of samples that were coupled with the PyprPA modifier was $(4.6\pm0.5)\times10^{-6}$ m^2 K W^{-1}at 7kPa and $(4.9\pm0.5)\times10^{-6}$ m^2 K W^{-1} at 138 kPa. The study revealed that the effect of pressure in the case of coupled samples was insignificant thus revealing the fact that the area of contact remained the same. Further, the value of electrical resistance also reduced over to a similar magnitude.

(Pei et al. 2018) used PSTTR (phase-sensitive transient thermo reflectance technique) to determine the thermal conductance between the copper surface and CNT arrays. The experiments were conducted at different loading conditions. The study revealed that the entanglement of the upper surface of CNT arrays impairs the contact with the surface and could be improved by increasing the pressure. The study also revealed that the $h_{Cu\text{-}CNT}$(contact thermal conductance of Cu-CNT arrays) increases as the applied load increases up to 0.15MPa following which the $h_{Cu\text{-}CNT}$ levels off. Thus, the contact pressure of 0.15MPa is an optimum pressure for the electronic equipment for the CNTs used. However, it was also noted that the optimum pressure is also the function of the height and the density of CNT arrays used. Further, roughness of the target material also plays a vital role and the effect of contact pressure with different roughness needs considerable attention.

(Peacock et al. 2016) studied solder-CNT composite TIM. The composite TIM was fabricated by using VACNT. The CNT arrays were grown on a silicon surface by employing the CVD process. The grown CNTs were transferred to the Cu surface and were soldered to the copper surface by using bismuth/Tin/Silver solder. The tests were conducted by employing pressure of 20 psi and 50 psi and the thermal resistance was measured using a standard ASTM D 5470. The study reported thermal resistance value of 0.458×10^{-4} m^2K/W and 0.425×10^{-4} m^2K/W at a pressure of 20 psi and 50 psi respectively. This method offers several advantages that include the elimination of thermal resistance at the free end of CNTs by soldering both the ends to the substrates and thereby increasing the joint life. It also eliminates the problems associated with high-temperature requirements as CNT arrays would be grown on substrates that are ideal to grow and subsequently transferred to the substrates as per the requirements of particular applications. Zhang et al., (Zhang et al. 2014a) studied the thermal contact resistance of epoxy composite incorporated with nanocopper particles and MWCNTs. They reported the minimum TCR of 11.5×10^{-4} m^2 K/W for the case of composite filed with 70% nano copper

(Zhao et al. 2019b) studied the suitability of Ga based TIMs. Liquid gallium whose melting temperature is 28°C is mixed with CNTs to form heat conduction pads. The thermal conductivity of Ga based thermal pad is 14.2 W/mK which is much larger when compared to Thermal silicone pads whose thermal conductivity is about 5W/mK. The introduction of Ga based CNT TIMs enhanced the heat extracting capabilities to a much greater extent when compared to commercially available silicone thermal pads.

Apart from CNTs, Graphene and FLG (few layer graphene) have also been used as filler materials in the synthesis of TIMs. These are characterized by high intrinsic thermal conductivity and low Kapitza resistance (Zhong et al. 2013) (Tang et al. 2015) (Liu and Hu 2015) (Dmitriev and Valeev 2017). Their excellent compatibility particularly with polymer matrices makes graphene an excellent filler material (Mahadevan et al. 2019). Apart from these advantages, graphene is stable at high temperatures. Figure 2.10 shows TGA (Thermogravimetric analysis) and DTG (Differential thermogravimetic) curves. The curves indicate that the graphene films are stable even up to temperatures as high as 900 °C making it suitable for high-temperature

applications (Zhang et al. 2018). The use of FLG offers several additional advantages. Apart from being highly thermal conductive, FLGs are flexible, degrade to a lesser degree and the larger cross section area of it results in higher heat fluxes when compared to single layer graphene (Kargar et al. 2018) (Renteria et al. 2015). Further, it is worth noting that in TIMs the term graphene fillers are generally referred to the mixture of graphene single layer and FLG flakes (Lewis et al. 2020).

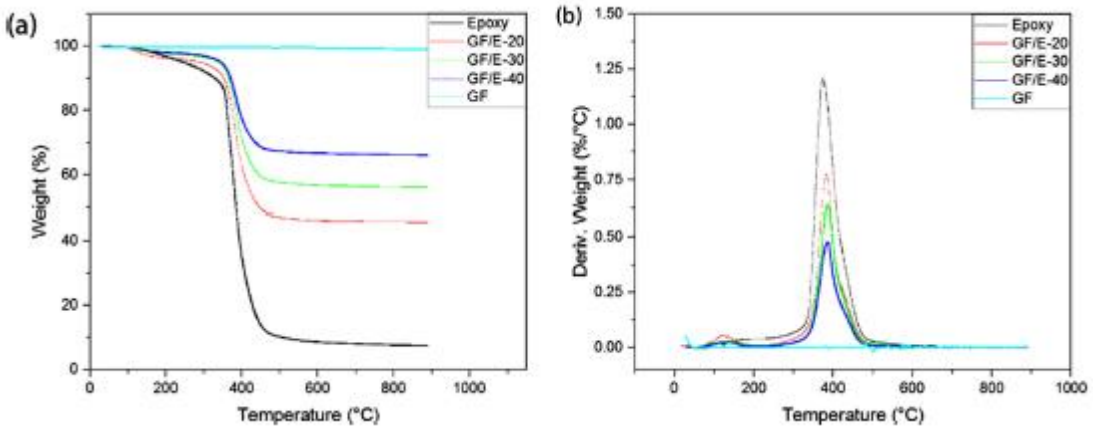

Figure 2.10 TGA and DTG curves of materials used (GF: Graphene films, Epoxy, GF/E: graphene film epoxy composites (Zhang et al 2018)

TIMs with graphite nanoplatelets as filler materials. In their study four layers of graphene, with a thickness of 4nm was used as filler which raised the thermal conductivity by over 3000%. The performance of graphite nanoplatelet (GNP) as a filler was greater than the conventional fillers which require high proportions of loading. Further, the thermal conductivity of GNP-800 epoxy material is found to increase with the increasing temperature ensuring efficient heat transfer even at elevated temperatures. The increase of thermal conductivity with temperature makes it a potential TIMs as it ensures efficient heat transfer in computers wherein the use of TIMs is pertinent for heat removal.

(Tang et al. 2015) studied the influence of the addition of graphene on epoxy-based TIMs. The graphene was prepared by using methods namely CVD and chemical reduction process and was termed as three-dimensional graphene networks (3DGNs) and reduced graphene oxide (RGO) respectively. The 3DGNs and RGO fillers were added to the epoxy resin to improve the thermal property of the resultant TIM. Further,

natural graphite powder (NG) was also used as a filler material to enable comparison between the TIMs. The study revealed that the addition of graphene enhanced the thermal conductivity of the matrix (epoxy) and increased with the increased load fraction. The increase in the thermal conductivity is greater in the case of 3DGNs-epoxy and showed superior thermal performance when compared to RGO- epoxy, and NG-epoxy. The increase in the value of thermal conductivity of the composite is attributed to the high intrinsic value of graphene as well as to the low thermal boundary resistance. Further, the resulting TIMs showed higher values of K even at higher temperatures indicating its excellent thermal stability. The mechanical testing revealed that the addition of graphene did not affect the mechanical properties of the resulting TIMs. It was concluded that the 3DGNs assisted epoxy TIMs could be used as potential TIM.

(Zhang et al. 2018) fabricated vertical and horizontal aligned graphene film epoxy composites as heat-dissipating materials. The addition of graphene-enhanced heat transfer capabilities of the composite. The study revealed that vertically aligned graphene composites exhibited enhanced performance when compared to their horizontal counterparts. The thermal conductivity of horizontal graphene film/epoxy composite at 44 vol. % of graphene was recorded to be 0.81W m^{-1} K^{-1}. However, the value of thermal conductivity of vertical graphene film epoxy composite was 384.9W/ mK. The orientation of graphene, therefore, plays a vital role in the increased value of thermal conductivity. The study revealed that the application of vertical Graphene film /epoxy composite to LED can bring a temperature drop of about 15°C when compared to horizontal Graphene film /epoxy composite thus making vertical Graphene film /epoxy composite a potential material for heat management

(Shahil and Balandin 2012) found that the addition of graphene and multi layered graphene (MLG) resulted in the increased the cross-plane thermal conductivity of graphene based polymers by 2300% at a loading factor of 10%. Figure 2.11 shows the enhancement factor of measured thermal conductivity as a function of filler volume loading fraction.

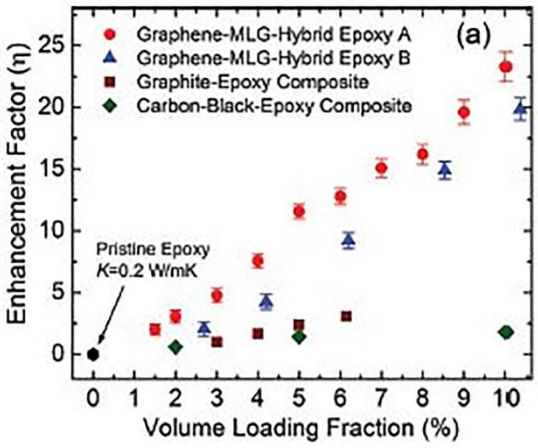

Figure 2.11 Enhancement of thermal conductivity in graphene-MLG nanocomposite epoxy TIMs (Shahil and Balandin 2012)

The study revealed that the addition of graphene and multi-layer graphene enhances the performance of such TIMs when compared to CNT based TIMs owing to the aspect ratio of graphene. In addition to the aspect ratio, a low Kapitza resistance between graphene and the polymer matrix also plays a vital role in the enhanced performance of graphene-based TIMs.

(Naghibi et al. 2020) studied the use of non-curing TIMs for advanced electronics. In their study they synthesized TIMs based on thermal grease with graphene and few layer graphene (FLG) flakes as fillers. The study found that unlike curing TIMs, the thermal conductivity of non-curing TIMs showed a sub linear dependence on filler loading. The thermal conductivity showed an initial rise with the filler loading, However, as the filler loading increased, the thermal conductivity plateaued. This was due to the tradeoff between the enhancement of thermal conductivity and decrease in thermal conductance due to the increase thermal resistance between filler-filler and filler matrix interfaces. Further, the synthesized thermal paste was benchmarked against the commercial paste. The study revealed that the synthesized thermal paste outperformed the commercial TIMs.

(Yu et al. 2014) studied graphene-based silicone oil which is a potential TIM material. They found that for reduced graphene oxide silicon grease (RGO-SO) at 1% vol. fraction, the thermal conductivity increased. Further, an increase in loading resulted in

higher viscosity causing reduced mobility and thus proving it to be ineffective at higher loading. They also investigated the thermal performance of graphene nanoplatelets (GNP) silicone oil and found that at lower loading, the GNP-SO was slightly inferior in comparison with RGO SO. At higher loading, however, the GNP–SO performed well when compared to RGO SO. Thus, the study revealed that the methodology of the synthesis of the filler also plays a vital role in performance characteristics.

(Yu et al. 2015) studied the synergistic effect of graphene and alumina in enhancing the thermal conductivity of silicone oil-based thermal grease. The study revealed that the addition of graphene to a silicone-based thermal grease filled with hybrid size alumina particles increased thermal conductivity to a significant level by the virtue of combined advantages of both graphene and alumina particles. The thermal conductivity of the resulting novel grease was recorded to be 3.45 W/m K. Further, the resulting novel grease saw an increase of 2553% in the value of thermal conductivity when compared to the silicone base. Apart from the fraction of fillers the particle size of the filler also plays a vital role as smaller particles result in a thin joint and thereby reducing the thermal resistance(Becker et al. 2005).Further, they found that with different sizes of particles mixed, the viscosity was found to be lower.

(Cui et al. 2015) studied the thermal properties of graphene/hot melt pressure sensitive adhesive (GHMPSA). The study revealed that with the increase in graphene content, the thermal conductivity of the composite increases. Further, the value of hardness also saw an increase with the increase in graphene content. In their study, the graphene-based composite TIM was applied between Al surfaces. The study was conducted by using the above-mentioned composite with different graphene weight percentages. Figure 2.12 shows the variation of thermal contact resistance with weight percentage of graphene. The TCR was measured under steady state conditions. The least value of thermal contact resistance was found when 6 wt% GHMPSA was used. The value of TCR stood at 30×10^{-6} m^2 K/W when compared to 660×10^{-6} m^2 K/W when no TIM was used. Further, with the increase in the weight percentage of graphene beyond 6 wt%, the TCR increased because increased filler content leads to increased agglomeration leading to increased internal interface resistance.

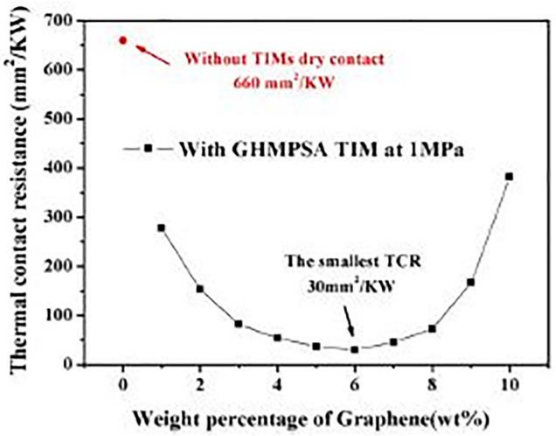

Figure 2.12 Thermal contact resistance after using GHMPSA TIMs as a function of weight percentage of graphene (Cui et al 2015)

The study also revealed that the increase in temperature had a positive outcome as it reduced the thermal contact resistance. This was ascribed to the fact that, at the higher temperature, the TIM liquefied increasing the contact with the surface.

(Li et al. 2017a) produced a series of reduced graphene oxide/ thermoplastic polyurethane (RGO/TPU) composites as a potential TIM for high power devices. The composite with a segregated structure exhibited excellent thermal conductivity and was prepared by hot pressing. The (RGO/TPU) was prepared by coating RGO on TPU by dip-coating TPU in an aqueous solution of graphene oxide in different concentrations. The above process greatly enhanced the thermal conductivity of TPU. The maximum thermal conductivity was recorded to be 0.8 W/m K at 1.04 wt%. The aforesaid composite was used as TIM between a heat source and heat sink. The study found that the heat dissipation capacity of the composite is much higher when compared to TPU. Further, they also found that with an increase in RGO content the ability of heat dissipation of the composite increases. The RGO/TPU composite also showed good reliability during thermal cycling, thus indicating that the suitability of RGO/TPU as a potential TIM.

(Park et al. 2015) studied the feasibility of few-layer graphene (FLG) composite TIMs (FLGTs) that have been developed by interlayer catalytic exfoliation. The studies reveal that the thermal resistance between FLG and copper at 5 vol % and 10 vol % at 330 K

is recorded to be $(3.2\pm1.7)\times10^{-6}$ m^2 K/W and $(4.3\pm 1.4)\times10^{-6}$ m^2 K/W respectively. R_{TIM} of two TIM samples having 45 µm thick 10% FLGTs and 49 µm thick 15 % FLGTs was measured at a temperature of 330 K. The pressure was varied from 0.14 MPa to 1MPa. It was found that there were no appreciable changes in the R_{TIM} values for the samples as the pressure was varied. Further, the study revealed that the increase in FLG concentration leads to the increase in FLGT's glass transition temperature by about 50K, thus making the FLGTs more stable thermally as properties often deteriorate beyond glass transition temperature. Furthermore, the study reveals that subjecting the FLGTs under thermal cycling causes no significant changes in R_{TIM}.

(Zandén et al. 2014) fabricated a solder matrix nano polymer composite (SMNPC) that could be used as an alternative to polymer-based and solder based TIMs. The SMNPC was fabricated by electrospinning nanofibre polyamide network. The polyamide network was then coated by Ag nanoparticles and was further infiltrated with Sn95.5-Ag3.8-Cu0.7 alloy matrix. The composite was sandwiched between two copper squares (coated with electroless nickel immersion gold- ENIG) having 1mm thickness. The thermal resistance of SMNPC was measured to be below 1 K mm^2/W indicating that the thermal resistance values of SMPC were similar to that of Sn-Ag-Cu alloy without fibers. Further, the SMNPC is seen to be reliable for longer times thus making it as a potential alternative to solder and polymer-based TIMs. The reliability tests were conducted by subjecting the SMPCs to thermal cycling (-40 to 115°C) at 2 cycles per hour. The thermal resistance values were not affected significantly even after 1000 cycles. This may be attributed to the fact that the formation of intermetallics is very low. Thus, SMNPCs TIMs could be alternate interface materials to indium and polymer materials.

(Loeblein et al. 2017) studied the use of three-dimensional foams (3D Boron nitride and 3D graphene) as TIMs. The 3D foams have thermal conductivities in the range of 62-86W/mK. The thermogravimetric analysis (TGA) study revealed that the 3D graphene can withstand a temperature of about 700°C whereas 3D Boron nitride can withstand temperature as high as 900°C. The stability of 3D foams at these high temperatures proves that 3D foams could be successively used at important applications including electronic, military automotive, and other commercial purposes. Further, 3D

foams have reported a thermal resistance as low as 0.197$KW^{-1}$and may be attributed to the fact that 3D foams offer high surface conformity. Apart from high cross-plane thermal conductivity, the 3D foams have excellent surface conformity that makes the 3D foam a potential thermal interface material.

(Luo et al. 2014) studied the thermal resistance of novel BN-In TIM composite. The TCR between the composite and copper plates was measured by using flash instrument. As shown in Figure 2.13, the study revealed that the thermal resistance increases with the bond line thickness when the TIM was sandwiched between copper plates.

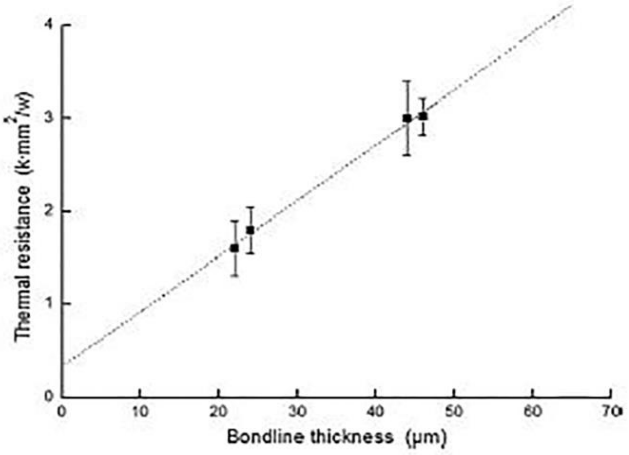

Figure 2.13 Thermal resistance of BN nanofibre indium composite TIMs sandwiched between copper at various bondline thickness (Luo et al 2014)

The study reported a TCR of 0.2 K mm^2/W. Hence, favorable high thermal conductivity values in addition to low TCR make BN–indium composite extremely useful in the electronic industry as it will help in efficient dissipation of heat thus improving operational lifetime and reliability of electronic components.

Studies have revealed that the use of nanowires had a positive impact owing to its high aspect ratio. (Wang et al. 2014) found that the implementation of copper nanowires at an ultra-low loading of 0.9 vol% as a filler material resulted in thermal conductivity of 2.46 W/m K. This amounts to an increase in thermal conductivity of about 1350% when compared to plain matrix thus making nanowires excellent fillers for high-performance interface materials. In their study, the CuNW - Polyacrylate which was synthesized by solution mix processing was tested for its thermal conductivity at different filling

fractions It was found that the increase in vol % of CuNWs increased thermal conductivity as shown in Figure 2.14.

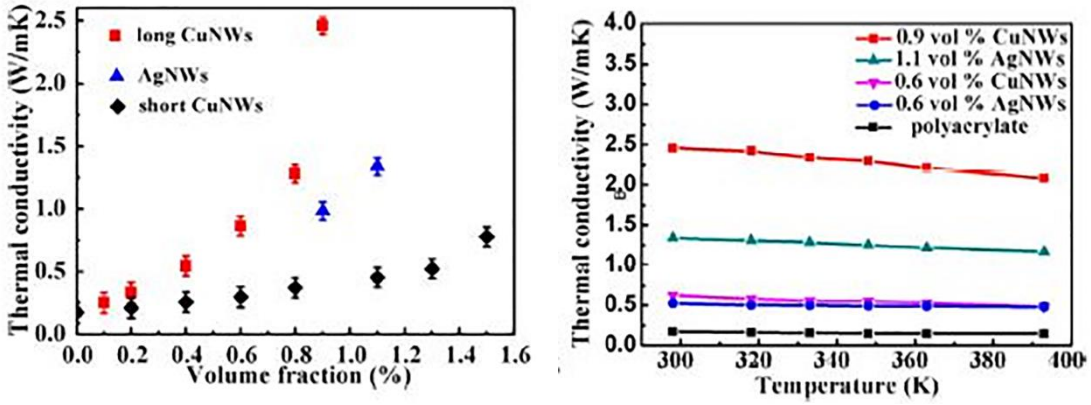

a **b**

Figure 2.14 a) Experimental thermal conductivity of metal nanowire-polyacrylate composites with different volume fraction at 298K. b) Thermal conductivity of metal nanowire–polyacrylate composite as a function of temperature. (Wang et al 2014)

2.8 Development of recyclable TIMs with high cooling performance and reliability

The performance of TIMs deteriorates with usage resulting in increased temperatures at the junction causing potential failures of electronic devices (Due and Robinson 2013)(Goel et al. 2008). Thus, it is pertinent to study the stability and reliability of TIMs for its effective use. Several researchers have carried out reliability tests with TIMs. A comprehensive review of the various stress tests and techniques that are used to characterize and determine the reliability of TIMs is discussed by (Due and Robinson 2013) (Goel et al. 2008) and could be studied by tests such as elevated temperature stress test, high-temperature storage tests, thermal cycling, power cycling, TGA, DSC, etc . Among the TIMs, thermal greases have more reliability issues as polymers in these TIMs degrade at higher temperatures over a longer duration of time (Gowda et al. 2005)(Prasher and Matayabas 2004) . (Skuriat et al. 2013) studied TIMs for high-temperature power electronics. The study carried the reliability studies of Ag thermal grease, Sn-3.5Ag solder joints, and Sn foil between Cu disks. It was reported that the Ag thermal grease was stable within the temperature of -57°C to 252°C. However, the TIM was not durable at a temperature of 170°C (isothermal aging) for a long duration

of time owing to the burn out of the polymer-based matrix. (Prasher and Matayabas 2004) extended the studies of reliability based on rheology. Apart from thermal greases, the reliability of LMAs has also been studied. (Roy et al. 2016) studied the reliability of LMAs on isothermal aging (130°C) and thermal cycling (-40°C to 80°C). The study found that the LMAs were reliable to a significant degree and exhibited superior performance up to 3000 hours of aging and 1500 cycles. (Hill and Strader 2006) proposed design solutions to enhance the reliability of Cu-LMA TIMs. The study found that oversizing copper-LMA TIMs, operating below the melting point and the use of gaskets resulting in a seal around the TIMs are some of the ways to enhance reliability. The former solutions result in a reduction of oxidation of TIMs thus enhancing reliability while the latter solution results in the containment of TIMs. (Yang et al. 2014) conducted the performance studies of LMTA alloys as TIM. Two alloys, namely, 17Sn26In57Bi and17Sn51In32Bi were placed between Cu samples. The results indicated that the thermal performance degraded with aging owing to the interfacial reactions between the Cu sample and LMTA. The reliability of TIMs depends on factors such as, type of TIMs, the duration, and the temperature to which it is exposed. Thus, an in-depth analysis of the reliability of the TIM is an important step to recognize a potential TIM. Further, studies must focus more on analyzing the thermal performance of TIMs for its entire operation cycle. With advances in miniaturization and the adoption of niche technologies like 5G the heat generation in electronic circuitry would increase manifold thus throwing a significant challenge to device engineers (Swamy and Satyanarayan 2019b). The heat thus generated needs to be efficiently dissipated so as to ensure maximum performance and reliability (Raza et al. 2018). The heat generated could be efficiently removed by the use of TIMs. However, a potential TIM needs to cater to the demands of the devices that incorporate this newer technology and thus increase the efficacy of the devices. A significant amount of research in the field of nanomaterials in recent years has paved the way for synthesizing TIMs that have improved capabilities to reduce the operating temperatures to lower levels. However, with growing concerns about electronic waste and the increased use of nanomaterials, there is an immediate need to develop sustainable, economic, and environmentally friendly TIMs. Attempts have been made by (Zahid et al. 2018) in this regard and were able to synthesize TIM based on regenerated cellulose and graphene

nanoplatlets. The resulting TIMs possessed In-plane thermal conductivity of 800W/m K. More attempts need to be done to design environmentally friendly, recyclable bio-TIMs. It is also very much relevant in the present times to synthesize TIMs with better recyclability as it would significantly reduce the pricing and make electronic devices less expensive and more affordable to the electronics manufacturing industry. Table 2 and Table 3 highlights the TCR and TCC respectively of different TIMs.

2.9 Summary

Minimizing the contact resistance at the interface in microelectronic packages remains a core challenge to engineers aiming at achieving enhanced heat transfer. The application of pressure significantly reduces the thermal resistance at the contact between two materials. The method is not practicable, particularly in the microelectronics packaging industry. For these applications, the use of TIMs at the interface is beneficial as it results in achieving superior thermal performance. Over the past three decades, a lot of efforts have been made in designing TIMs that facilitate the easy dissipation of heat across the interfaces. With advancements in science and technology, thermal management has become more challenging. Thus, engineered TIMs become indispensable to cater to challenging demands. Initial research was focused on replacing low conductivity air at the interface by higher thermal conductive polymer-based TIMs. Further advancements in this field have led to the creation of additional classes of thermal interface materials (TIMs), including liquid metal alloys (LMAs), phase change materials (PCM), and more recently, TIMs impregnated with nanoparticles

Table 2 TCR of various TIMs

Sl No	TIM	Thermal Contact Resistance	Applied between/on	Reference
1	Mercury Droplets	0.253×10^{-6} m^2K/W	Silicon die	(Hamdan et al. 2011)
2	Sn-Bi Paste	0.576×10^{-6} m^2K/W	Copper	(Zhang et al. 2014c)
3	Arctic Silver	1.8×10^{-6} m^2 K/W	CPU Applications	(Gwinn and Webb 2003)
4	Polymer LMA composite	8.5×10^{-6} m^2 K/W @800kPa	Heat-flux meters (Al)	(Carlberg et al. 2009)
5	Gallium based TIMs	2.6×10^{-6} m^2 K/W @0.05MPa	Copper	(Gao and Liu 2012)
6	Eutectic Pb-Sn	2×10^{-6} m^2 K/W	Copper	(Bai et al. 2005)
7	17Sn51In32Bi	$4.83\times10^{-6}m^2K/W$	Copper	(Yang et al. 2014)
8	Dry contact of CNT Array	19.8×10^{-6} m^2 K/W @ 0.445 MPa	Cu-CNT-Si	(Xu and Fisher 2006)

Table 3 TCC of various TIMs

Sl No	TIM	Thermal contact conductance	Applied between/on	Reference
1	Wax filled with hexagonal boron nitride	18×10^4 W/m^2 °C @ 55°C,0.30 MPa	Copper	(Liu and Chung 2006b)
2	Wax filled with hexagonal boron nitride	16×10^4 W/m^2 °C @ 55°C,0.18MPa	Copper	(Liu and Chung 2006b)
3	Wax filled with hexagonal boron nitride	5×10^4 W/m^2 °C @ 55°C, without pressure	Copper	(Liu and Chung 2006b)
4	PEG	11×10^4W/m^2°C @0.46MPa	Copper	(Chung 2001)
5	Sodium silicate	14.1×10^4W/m^2°C @0.46MPa	Copper	(Chung 2001)
6	Silicone	3.08×10^4 W/m^2 °C 0.46MPa	Copper	(Chung 2001)

2.10 Scope

The trends of reduction in size of devices and enhanced power densities, particularly in the field of microelectronics have made thermal management a critical issue for design engineers (Gwinn and Webb 2003) (Hansson et al. 2016) . Efficient management of thermal issues is fundamental as it would be necessary to maintain the device operating temperature within the specific limits. The increased power densities would require better dissipation of heat from the heat source to the heat sink as it would affect the device performance and reliability. It has been found that the reliability of integrated circuits has got significant impact on the operating temperatures. Efficient management of thermal issues would result in lower operating temperature which would result in reduced gate delay and higher processing speeds (Viswanath et al. 2000) . One of the main challenges in efficient heat dissipation is the presence of interface between the heat source and heat sink. The interface results in inefficient transfer leading to higher operating temperatures. The effects of interface could be minimized by introducing a TIM. The present investigation aims at the understanding the role of thermal interface on heat flow between metal-metal contacts and the assessment of the effect of TIM, interfacial pressure and thermophysical properties of contacting materials on contact heat transfer.

Majority of the work, in the field of TIMs are carried under steady state conditions. The suitability of TIMs under transient conditions is seldom studied. Tests that employ transient approach are expensive and are difficult to conduct but offer advantages that include shorter test duration and helps in estimating time varying heat flux and other heat parameters and further, in majority of applications, the characteristics of heat flow at the onset of process determine the effectiveness of heat transfer (Kumar and Tariq). Hence it is of foremost importance to understand the process of heat transfer under time varying conditions. In the present work, an equipment has been designed with an objective of quantitatively estimating thermal performance parameters for interfaces in transient conditions. The analysis has been carried out by employing the inverse heat conduction problem (IHCP). IHCP is a powerful technique to estimate the dynamic TCR at the interfaces with and without TIM. The method estimates the boundary conditions from knowledge of thermal history at inner locations very close to the interface of both the materials in contact. The application of the inverse technique is more appropriate in cases where heat sinks are thicker leading to appreciable magnitudes of temperature gradients within the heat sinks (Prabhu and Ashish 2002). A significant amount of literature is available on mathematical details of the solution to IHCP (Beck 1970)(Burggraf 1964) (Prabhu and Ashish 2002) (Stolz 1960). The present study focuses on assessment of transient contact heat transfer with and without TIMs under various interfacial pressure conditions at the metal-metal interface.

2.11 Objectives

The following are the objectives of the current research work

1. To assess the transient heat transfer at the interface between similar and dissimilar specimens with and without TIMs.
2. To propose thermal conformance parameters under transient conditions to quantify the heat flow between metal-metal contacts
3. To study the effect of thermophysical properties of the materials in contact, TIMs of varying thermal conductivity and interfacial pressure on interfacial heat transfer and thermal conformance.

Chapter 3 Experimental Methodology

3.1 Instrumentation

The experiments were conducted by placing the TIM at the interface between two cylindrical specimens. The schematic diagram of the setup is shown in the Figure 3.1 and was designed to estimate heat flux transients. The specimens were placed on a PTFE holder which in turn was placed over the load cell (Epoch Instruments and controls Pvt. Ltd, Model No: LZYB, Capacity: 0-200kg). The load cell was used to measure the load that was applied on to the specimens. The load cell is mounted on a flat plate and is connected to a microcontroller based digital indicator (Epoch Instruments and controls Pvt. Ltd, Model No: SM-12, Excitation voltage 5 VDC (±1%)). The accuracy of the load indicator was ± 0.01% of the full scale with the minimum bridge resistance of 85Ω. The interfacial pressure was applied by placing plates of known weights on the top of the upper specimen. The set up consist of four pillars that facilitate the placement of plates over specimens at appropriate alignment. The experiments were conducted for two sets of cylindrical specimens of copper. In each set, the upper specimen with the heater acted as heat source and the lower specimen was heat sink. The heating was accomplished by a mica strip heater which was attached to the upper specimen. The mica strip heater was connected to a temperature regulator which allowed the user to regulate or set the temperatures to a preset value The source and sink were instrumented with a mineral insulted sheathed K-type thermocouple of 1mm diameter. The thermocouples were instrumented by drilling holes in to the specimens at the appropriate locations through EDM technique. The source was heated to a temperature of 75 ± 2°C and the corresponding changes in temperature in the lower specimen were recorded. The specimens were insulated with PTFE tape and cerawool material so as to minimize heat transfer in the radial direction thus enabling one dimensional heat transfer. The acquisition of the variation of temperature with time was accomplished by using a data logger (National Instruments 9213) which was connected to thermocouples using compensating cables. The data logger was in turn interfaced to a computer.

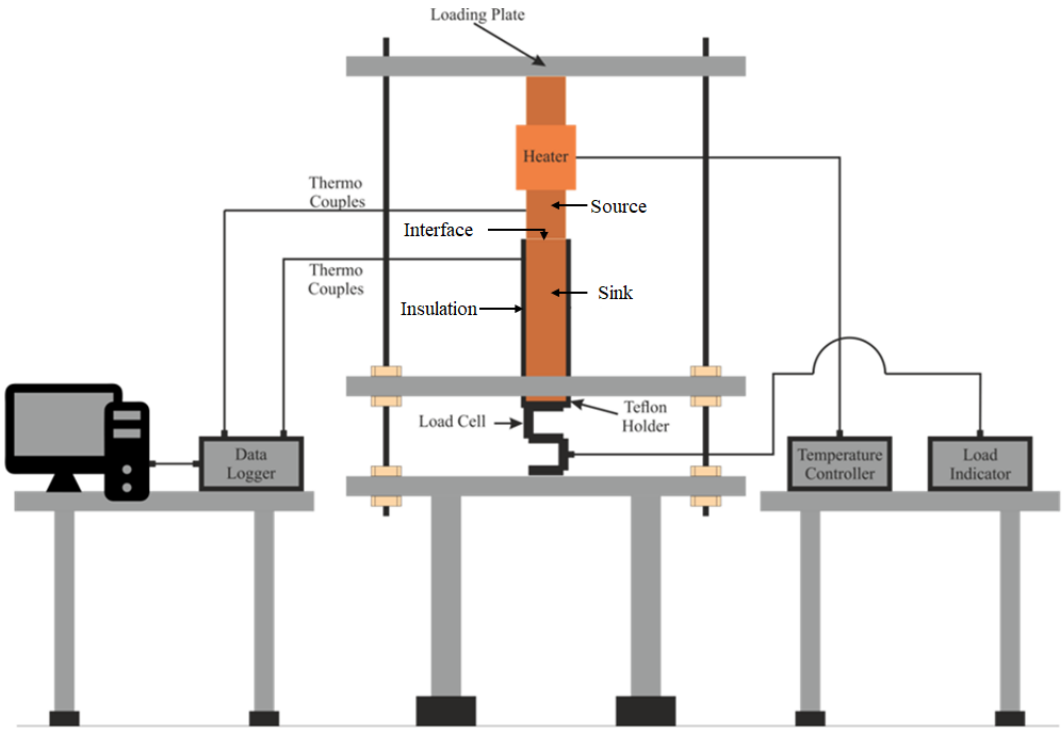

Figure 3.1 Schematic representation of experimental setup

3.2 Materials

The heat transfer studies for metal-metal contacts were studied for Cu-Cu interfaces with L/D (length/diameter) ratio of 1 and 5. In case of L/D =1, the experiments were extended to various other combinations such as Al-Al, Brass-Brass, Cu-Al, Al-Cu. The schematic diagrams of the specimens with L/D=1 and L/D=5 is shown in Figure 3.2 and 3.3 respectively. The thermophysical properties of the various metals used in the study has been tabulated in the Table 4.

Table 4 Thermophysical properties of Copper, Aluminium and Brass(Poirier and Geiger 2016)

Material	**Thermophysical properties**		
	ρ (kg/m^3)	**C_p (J/kg K)**	**k (W/m K)**
Copper	8920	380	398
Aluminum	2698	900	237
Brass	8400	390	127

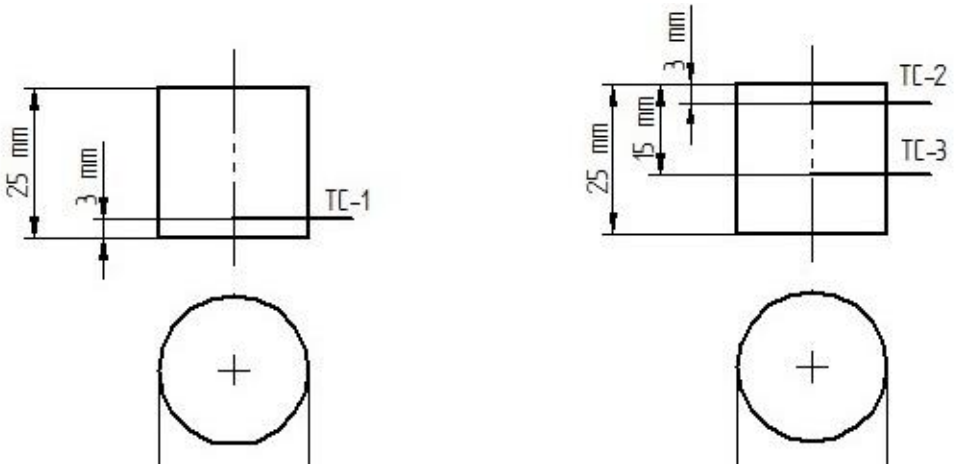

Figure 3.2 Dimensions of specimens with L/D of 1. TC-1, TC-2 and TC-3 represent thermocouple locations a) dimensions of source b) dimensions of sink

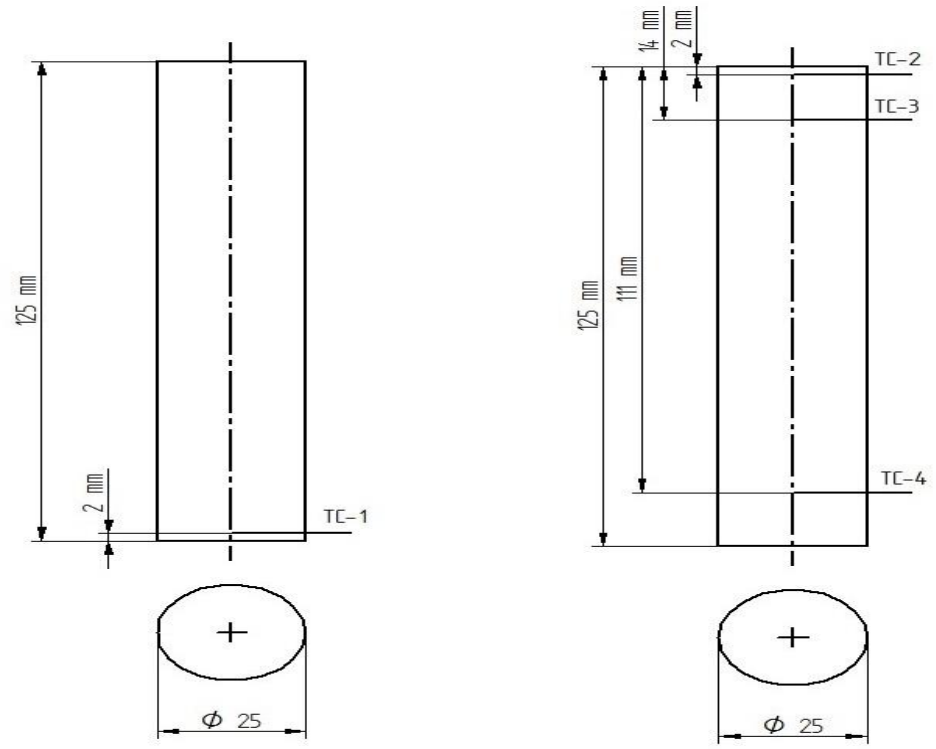

Figure 3.3 Dimensions of specimens with L/D of 5. TC-1, TC-2, TC-3 and TC-4 represent thermocouple locations a) dimensions of source b) dimensions of sink

In the case of specimens with L/D ratio of 1, the source was instrumented with the thermocouples at 3mm and 6mm, whereas the sink was instrumented with thermocouples at 3mm and 15mm. The temperature data was acquired at every 0.1 second using data logger. For specimens with L/D ratio of 5 (ø25×125mm), the source was instrumented with thermocouples at 2mm and 50mm from the interface whereas the sink was instrumented with thermocouples at 2mm,14mm and 111mm from the interface. Figure 3.4 shows the images of specimen (source and sink materials) used in the present investigation. The surface roughness of the specimens (source/sink) were measured using Taylor Hobsons surface roughness tester (model: FORM TALYSURF 50)

3.1.1 TIMs used in the present investigations

Commercially available silicone grease (Metroarc 211 compound from Wacker Metroark Chemicals Pvt. Ltd Kolkata), thermal grease (HALNZIYE, Shenzen) and silicone thermal putty (RS Components & Controls (I) Ltd) was used as TIM. The thermal conductivity of the various TIMs used in the study has been tabulated in the Table 5

Table 5 Thermal conductivity of TIMs

Sl No	TIM	Thermal Conductivity k (W/mK)
1	Silicone Grease (SG)	0.193
2	Thermal Grease (CTG)	1.93
3	Silicone thermal putty (STP)	7

The effect of MWCNT addition on TIMs was studied by adding MWCNT on to the silicone grease. The as-received MWCNT (diameter 10nm-25nm, Length 300-500nm, Chengdu Organic Chemical Co Ltd, Chinese Academy of Science, China) was dispersed in silicone grease and was mixed for about 15 minutes. The MWCNTs were added at a weight concentration of 0.1 and 1%. The selection of low weight

concentration was based on the fact that, large aspect ratio of CNTs makes it possible to achieve percolation at lower concentration (Hansson et al. 2018). The experiments were conducted at different loading of no load (NL), 20kPa, 40kPa, 100kPa, 200kPa. The study used suitability of 1-Methyl-2-pyrrolidone/NMP (Tokyo Chemical Industries Co Ltd) as interfacial solvent for metal-metal contacts.

(a)

(b)

(c)

Figure 3.4 Images of the specimens used during experiments (a) Cu, (b) Al and (c) Brass

Chapter 4 Theoretical Background

The Lumped heat capacitance method assumes negligible temperature gradients and the temperature are considered to be uniform within the specimen materials.

Thus,

$$q = \rho C_p (V/A)\frac{dT}{dt} \qquad (4.1)$$

where, q is the heat flux, C_p is the specific heat, V is the volume of the specimen, A is the cross-sectional area, $\frac{dT}{dt}$ is the cooling rate.

However, the application of the lumped heat capacitance method was limited to initial experiments. As the calculated Biot number was greater than 0.1, inverse heat conduction approach was used in order to estimate the heat flux transients in the case of interfaces with L/D=1. The inverse heat conduction approach was also used in the case of interfaces with L/D=5. The Inverse heat conduction approach utilizes the knowledge of interior temperature history to determine the unknown boundary conditions like heat flux, surface temperature and other interfacial heat parameters [Prabhu and Ashish 2002, Stolz 1960]

The heat flux transients were estimated by using Beck's nonlinear estimation technique [Beck 1970]. Since, the heat transfer along the radial direction was negligible; the problem was modelled to be a case of one-dimensional heat conduction. The one-dimensional heat conduction equation is as follows,

$$\frac{\partial}{\partial x}\left(k\frac{\partial T}{\partial x}\right) = \rho C_P \left(\frac{\partial T}{\partial t}\right) \qquad (4.2)$$

The above equation was solved by considering following boundary conditions

$k\frac{\partial T}{\partial x}\Big|_{X=0} = q$ (where X is the distance from the interface)

$k\frac{\partial T}{\partial x}\Big|_{X=L} = 0$

T (X, 0) = 25°C (Initial condition)

Inverse algorithm requires minimization of objective function f(q). The objective function f(q) is defined as the summation of square of difference between measured temperature and the calculated temperature. Thus, the heat flux (q) at the unknown boundary (X=0) was estimated by minimizing equation 4.3.

$$f(q) = \sum_{i=1}^{n} \sum_{j=1}^{m+1} (T(L_i, t + (j-1) \triangle t) - Y_i)^2 \qquad (4.3)$$

Where, n is the number of thermocouples location (n=3), m is the total number of future time steps (m=4), Similarly, Y_i represents measured temperature at the i^{th} location, T represents calculated temperature, L_i is the thermocouple location, t is time, $\triangle t$ is time step increment, The temperature data was taken at every 1 second, hence $\triangle t$=1s.

The temperature increment at i^{th} thermocouple location and j-1^{th} future time step was calculated for an increment of 1% of $q^{l-1}(t)$. Further, the heat flux increment $\triangle q^l(t)$ for minimizing objective function was calculated as shown in equation 4.4.

$$\triangle q^l(t) = \frac{\sum_{i=1}^{n} \sum_{j=1}^{m+1} (T^{l-1}(L_i, t+(j-1)\triangle t) - Y_i) \varphi_{i,j}^{l-1}}{\sum_{i=1}^{n} \sum_{j=1}^{m+1} (\varphi_{i,j}^{l-1})^2} \qquad (4.4)$$

In the above equation $\varphi_{i,j}$ is sensitivity coefficient. The sensitivity coefficient signifies the effect on estimated temperature resulting due to small changes in the heat flux (q). The above equation (4.4) is obtained by equating the first derivative of equation 4.3 to zero and subsequently combining the Taylor's series of expansion of temperature dependent heat flux. The heat flux q is calculated as shown in the equation 4.5 by using the value of $\triangle q^l$ obtained from equation 4.4

$$q^l(t) = q^{l-1}(t) + \triangle q\,(t) \qquad (4.5)$$

The objective function is optimized at each time step by iteratively calculating heat flux using equation 4.4-4.5**.** The convergence limit for terminating the iterative algorithm was obtained when $[(\triangle q^l(t)/q^l(t))] < 10^{-6}$ (4.6)

Chapter 5 Results and Discussion

5.1 Effect of interfacial pressure and TIM on heat transfer on Cu-Cu metal contacts with L/D ratio of 1.

5.1.1 Results

Experiments were conducted to study the effects of interfacial pressure and the TIMs for Cu-Cu interfaces with L/D =1. The upper specimen is termed as the source while the lower specimens was termed as the sink. As the temperature of the upper specimen is increased from room temperature to 75°C, the heat gets transferred to the sink resulting in increased temperature of the sink. The sink temperatures were measured at 3mm and 6mm below the interface. The surface roughness of the specimens was 165.6±63.4 nm. Figure 5.1 shows the typical temperature-time curves of the source and sink as the source gets heated from room temperature to 75°C under no load (NL) conditions. Figures 5.2-5.4 show the variation in temperature with time for Cu-Cu bare interfaces under 40kPa, 100kPa and 200kPa interfacial pressure respectively. Figure 5.5 and 5.6 show the variation of temperature and time for Cu-Cu interfaces with silicone grease thermal interface material (SG TIM) under no load condition and 200 kPa interfacial pressure. The figures depicting the variation of temperature and time for other combinations with SG TIM under 40kPa, 100kPa are given in Appendix A. Figure 5.7 and 5.8 shows the variation in SS_t (time to reach sink saturation temperature) and SST (sink saturation temperature) for bare Cu-Cu interfaces and for Cu-Cu interfaces with SG TIM respectively. In the plots depicting Temperature vs Time, T1 represents temperature of the source at 3mm from the interface. T2 and T3 represent sink temperatures at 3mm and 6mm from the interface.

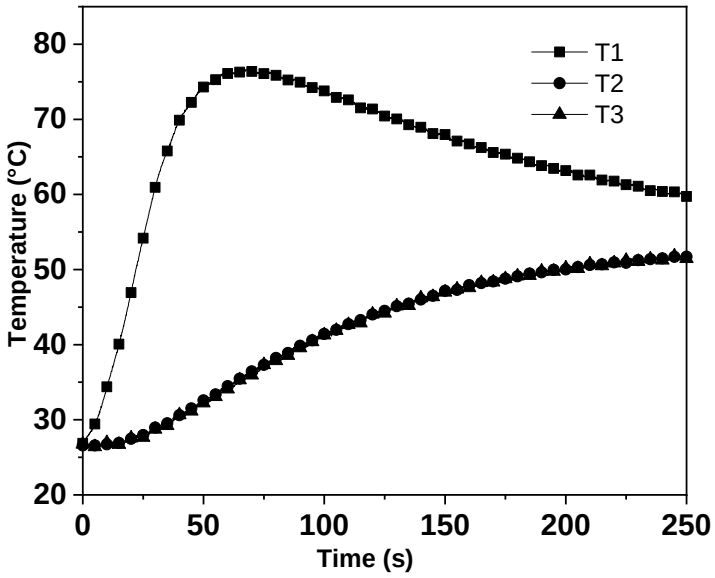

Figure 5.1 Variation of temperature with time for Cu-Cu interfaces under no load conditions

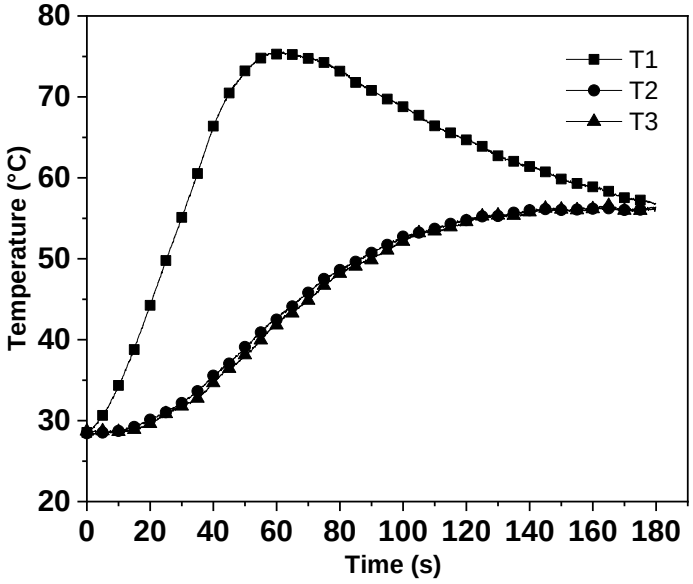

Figure 5.2 Variation of temperature with time for Cu-Cu bare interfaces under 40kPa interfacial pressure

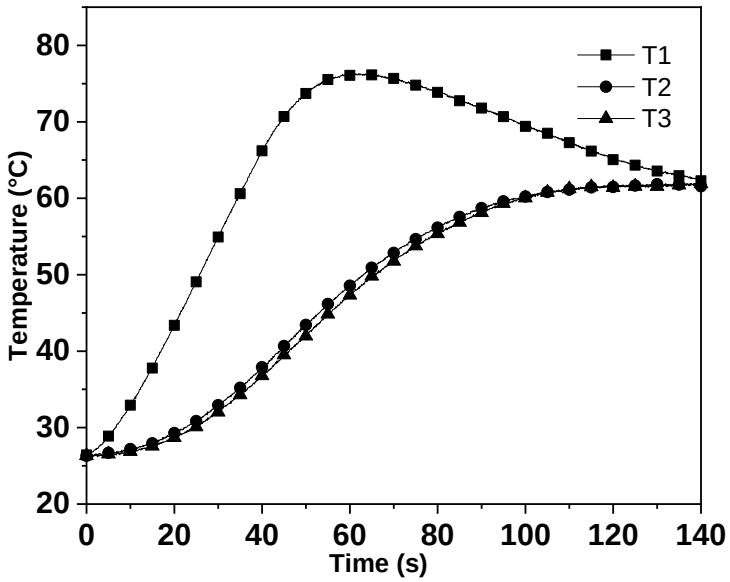

Figure 5.3 Variation of temperature with time for Cu-Cu bare interfaces under 100kPa interfacial pressure

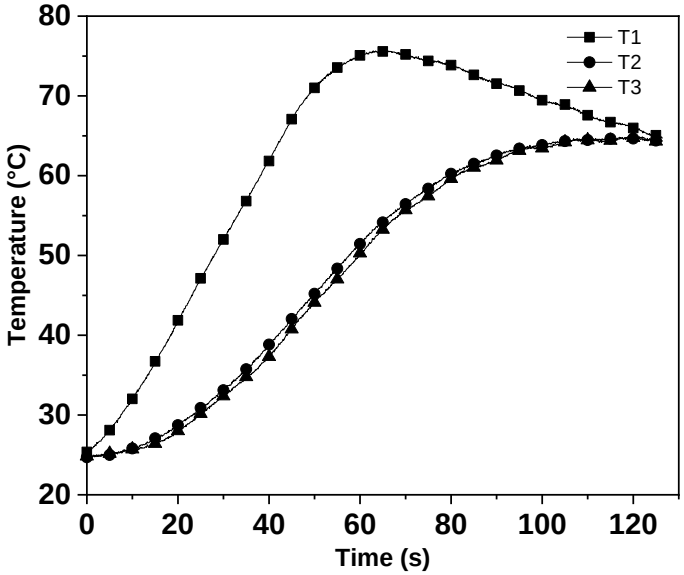

Figure 5.4 Variation of temperature with time for Cu-Cu bare interfaces under 200kPa interfacial pressure

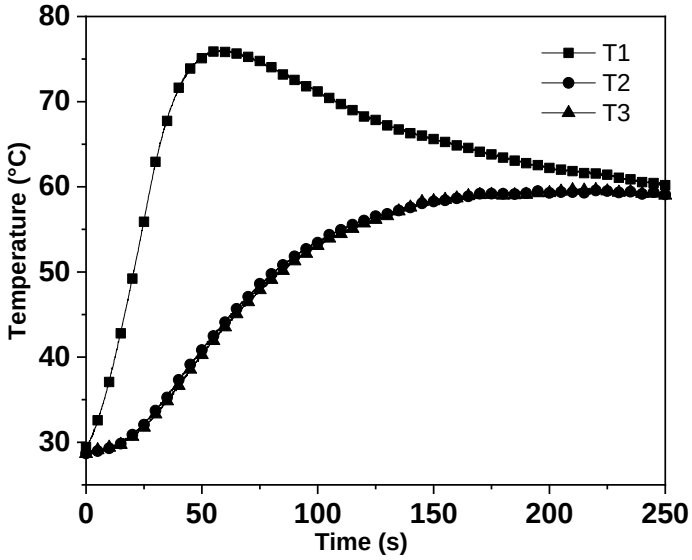

Figure 5.5 Variation of temperature with time for Cu-Cu interfaces, interfacial conditions: SG TIM, no load

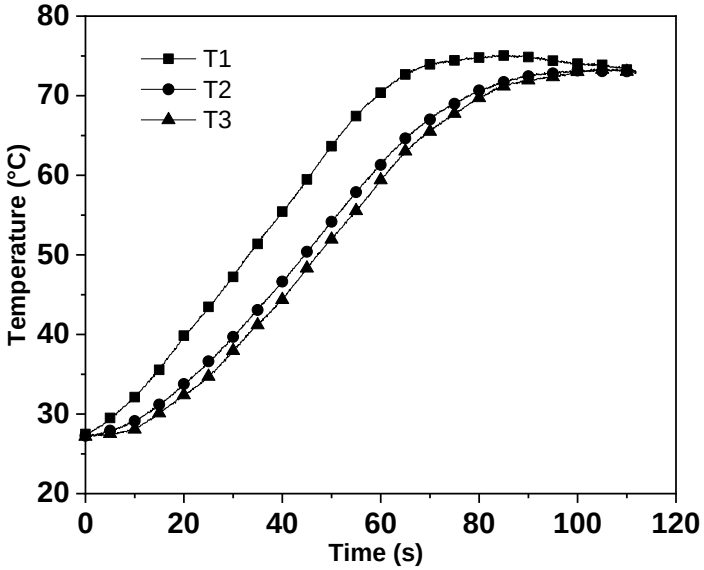

Figure 5.6 Variation of temperature with time for Cu-Cu interfaces, interfacial conditions: SG TIM, 200 kPa

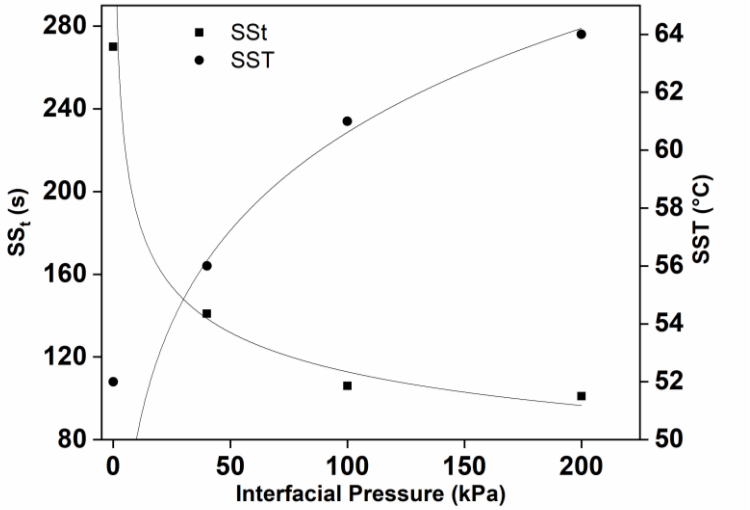

Figure 5.7 Variation of SS_t and SST with interfacial pressure for Cu-Cu bare interfaces

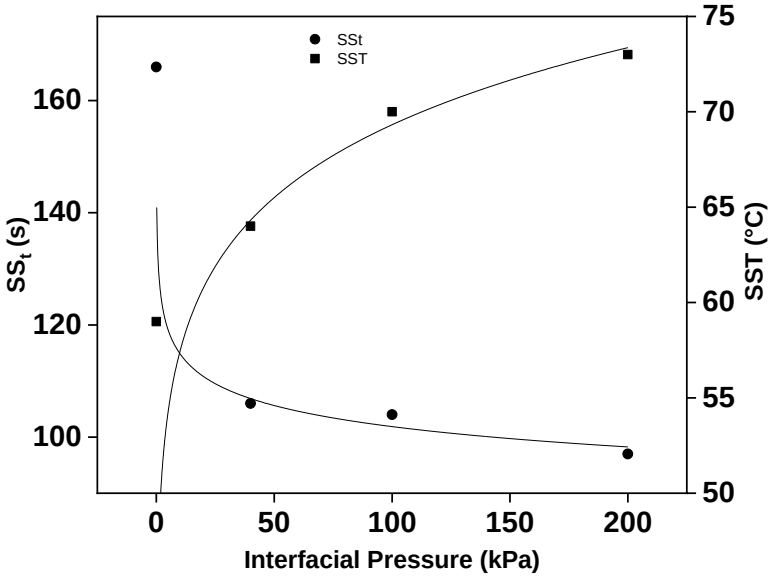

Figure 5.8 Variation of SSt and SST with interfacial pressure for Cu-Cu interfaces with SG TIM

5.1.2 Discussion

Figures 5.9 and 5.10 show the variation of estimated heat flux with time in case of bare Cu-Cu interfaces and for Cu-Cu interfaces with silicone grease as TIM (SG TIM). The heat flux was estimated by using lumped capacitance method.

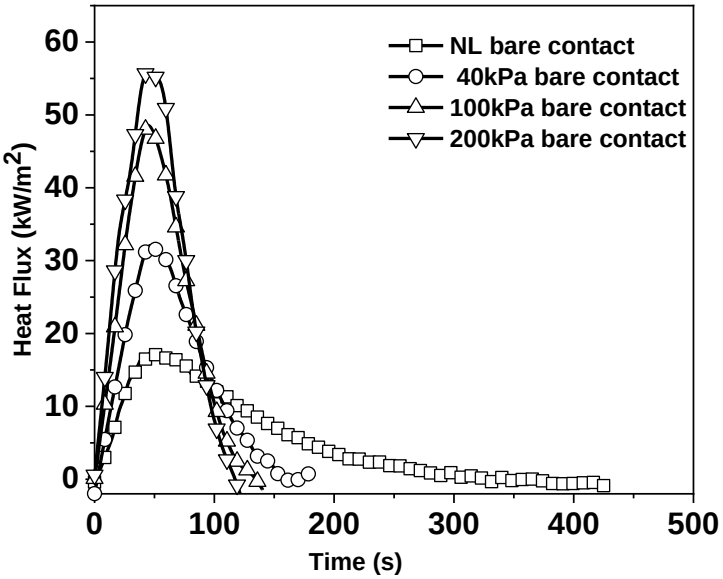

Figure 5.9 Effect of interfacial pressure on heat flux for Cu-Cu bare interfaces

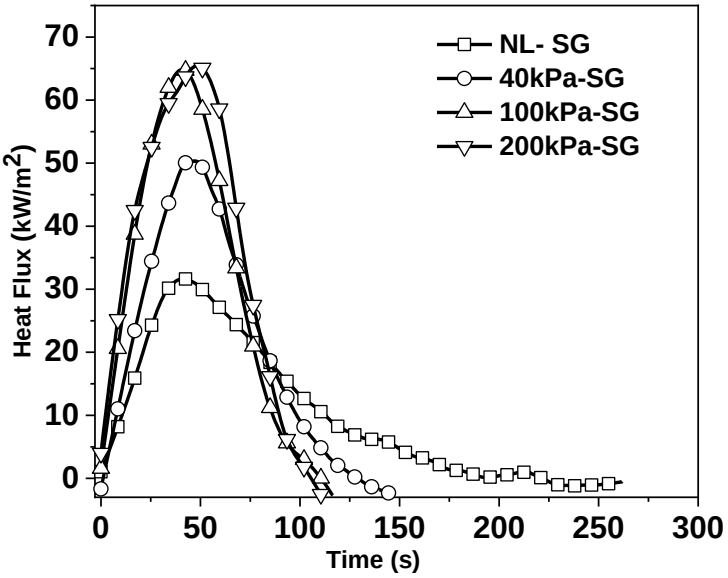

Figure 5.10 Effect of interfacial pressure on heat flux for Cu-Cu interfaces with SG TIM

Figure 5.11 shows the comparison of heat flux with time for Cu-Cu interfaces with and without TIMs.

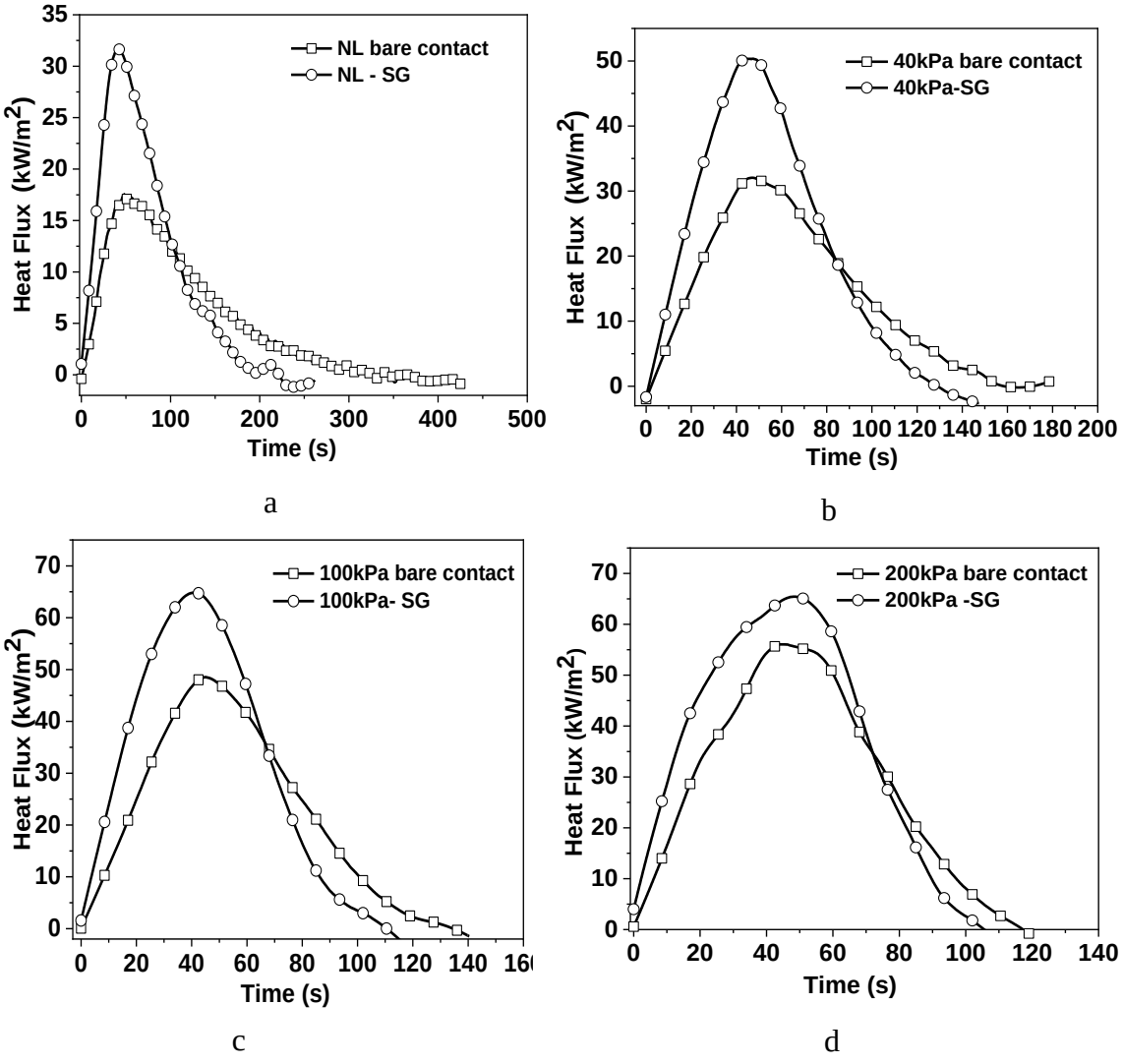

Figure 5.11 Variation of heat flux with time for Cu-Cu interfaces (bare and for interfaces with SG TIM) a) No load b) 40 kPa c) 100 kPa d) 200 kPa interfacial pressure.

In case of bare Cu-Cu bare interfaces as shown in figure 5.9, the peak heat flux increases with the increase in interfacial pressure. In the present investigation the peak heat flux under the no load condition was about 17.52kW/m^2. The increase in the interfacial pressure to 40 kPa resulted in the increase in peak heat flux substantially to a value of 32.04kW/m^2. Further, increase in interfacial pressure from 40kPa to 100kPa resulted in the rise of peak heat flux value to 48.53kW/m^2. This is due to the fact that as the interfacial pressure increases, the interfacial contact condition improves leading to enhanced heat transfer. The peak heat flux showed an increasing trend even as the interfacial pressure was increased to 200kPa. This trend of increase in peak heat flux with the increase in interfacial pressure was also reported by (Kumar and Tariq 2017) in their studies for stainless steel contacts. The peak heat flux for 200kPa interfacial pressure condition was estimated to be 56.06 kW/m^2.

The application of higher interfacial pressure for enhancing contact heat transfer is not an ideal solution particularly for the applications involving miniaturization. Hence, a more ideal approach is to introduce a TIM between two surfaces at contact. Thus, silicone grease was chosen as TIM because of its excellent wettability, stability and lower modulus. For interfaces with silicone grease as TIM, the peak heat flux values for loading conditions of no load, 40 kPa, 100 kPa and 200 kPa were found to be 31.71, 50.35, 64.86 and 65.43kW/m^2 respectively. Figure 5.11 shows the comparison of peak heat flux values obtained for bare interfaces and for the interfaces with silicone grease TIM. In each of the interfacial loading condition the application of silicone grease as TIM resulted in an appreciable increase in peak heat flux. The application of TIM at the interface results in the replacement of air which is a poor conductor of heat. In addition to the higher thermal conductivity of silicone grease, excellent wettability, decrease in viscosity with increased temperature and lower modulus aid in enhanced heat transfer as the TIM flows in to the voids that exist at the interface.

In addition to peak heat flux, the area under the heat flux transients was determined. This gives integral heat flow and is a quantitative measure of the heat flow into the sink**.**

The integral flow was calculated by using the following equation

$$Q = \int_0^t q \, dt \tag{5.1}$$

Where Q is the integral heat flow, q is the heat flux, t is the time.

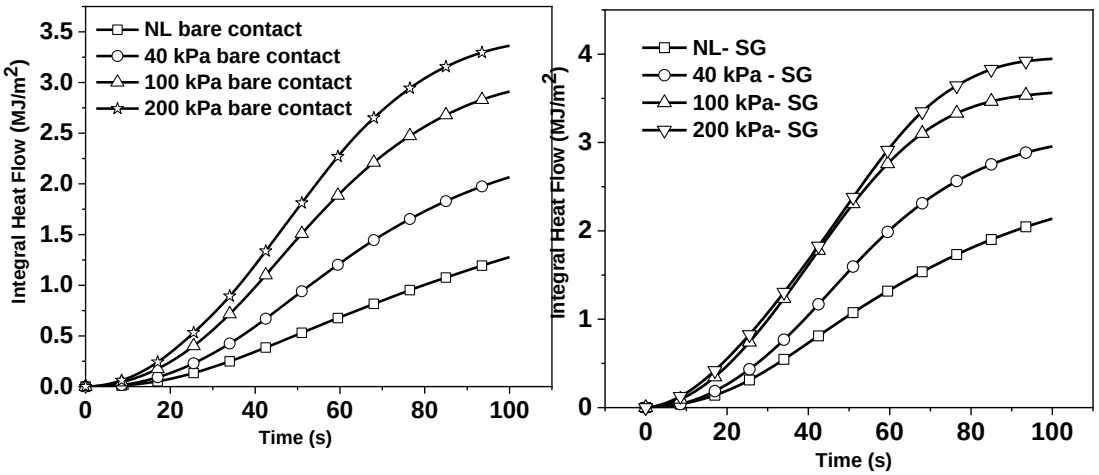

a b

Figure 5.12 Variation of Integral heat flow with time for Cu-Cu a) bare interface b) interface with SG TIM

Figure 5.12 show the variation in integral heat flow with time at different interfacial loading conditions for both bare interface and for interfaces with silicone grease as TIM. For the purpose of comparison, the integral curve for the first 100 seconds was plotted**.**

It was observed that the area under curve increases as the interfacial pressure is increased. The increase in the area under curve indicates that, at higher interfacial pressures the heat transferred to the lower specimen increases. Thus, higher interfacial pressures result in better conformance of the interfaces owing to the increase in the contact area. However, it is observed that for bare interfaces as the interfacial pressure increases, the percentage increase in heat flow across the interface decreases. The percentage increase in heat flow as the interfacial pressure is increased from no load condition to 40kPa and further from 40kPa to 100kPa was about 62% and 40% respectively. Further, the percentage increase in heat flow as the interfacial pressure was increased from 100kPa to 200kPa was only about 15.46%. This is attributed the fact that there is no much scope in increasing the contact area as the application of 100kPa interfacial pressure would have brought significant deformation leading to a

better thermal contact at the interface. Figure 5.12 b shows the variation in integral heat flow when SG was used as TIM. The application of SG as TIM results in enhancement of heat across the specimen. From the graph and from the integral flow data that has been shown in the Table 6, it is evident that, under transient conditions, the application of silicone grease TIM increases heat flow across the interface. The percentage rise in heat flow was as high as 67% under no load condition and at higher interfacial pressure of 200kPa the increase was about 17.46%.

Table 6 Values of peak heat flux and integral heat flow for Cu-Cu interface

Sl No	TIM/interface condition	Interfacial pressure (kPa)	Peak heat flux (kW/m^2)	Integral flow (MJ/m^2)
1	bare contact	NL	17.52	1.27
2	bare contact	40	32.04	2.07
3	bare contact	100	48.53	2.91
4	bare contact	200	56.06	3.36
5	SG TIM	NL	31.71	2.13
6	SG TIM	40	50.35	2.95
7	SG TIM	100	64.86	3.56
8	SG TIM	200	65.43	3.94

Experiments showed that for bare contacts, increasing the interfacial pressure from no load condition to 200 kPa resulted in a rise of 164% in the integral heat flow value, whereas in the case of interfaces with SG, an increase in the interfacial pressure from no load to 200kPa resulted in 84.97% rise in the value. This indicates that the effect of interfacial pressure on thermal contact resistance is significant when there is no use of TIM. In the presence of TIM, the effect of interfacial pressure on heat transfer is less significant.

In order to characterize heat transfer across the interface, a dimensionless transient temperature was defined.

The dimensionless transient temperature was found as follows

$$\Theta = (T_{max}-T_2) / (T_{max}-T_i) \text{ where} \qquad (5.2)$$

Θ is the dimensionless transient temperature, T_2 is the temperature at 3mm below the interface in the lower specimen, T_{max} is the temperature to which the upper body is heated, T_i is the initial temperature.

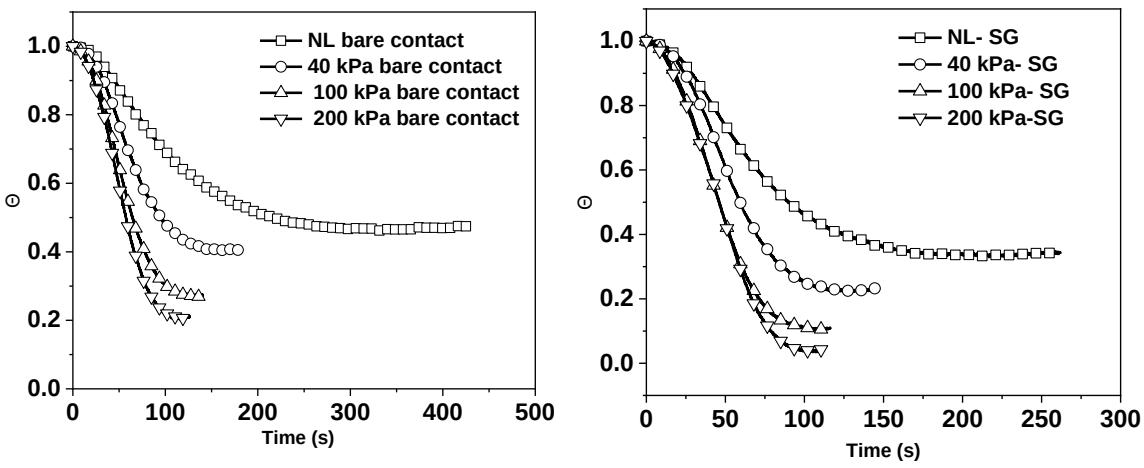

a b

Figure 5.13 Variation in dimensionless temperature (Θ) with time for Cu-Cu interfaces a) bare contacts b) interfaces with SG TIM

The dimensionless transient temperature gives a qualitative account of the rate at which heat is extracted from the heat source to the heat sink. Figure 5.13 clearly shows that for Cu-Cu interfaces, as the interfacial pressure increases the heat absorbed also increases. In the case of bare contacts, the time taken by heat sink to reach 50% of the maximum temperature is about 200s under no load condition. Upon applying SG the corresponding time taken reduces to about 100s. When the interfacial pressure is increased to 200kPa in the case of bare interfaces, the time taken for the heat sink to reach 50% of the maximum temperature is about 80s. The application of silicone grease for interfaces subjected to 200 kPa interfacial pressure, the time taken to reach 50% the maximum temperature reduces to about 50s. Thus, the study reveals that subjecting the interfaces to higher interfacial pressure and the application of silicone grease as TIM results in faster extraction of heat. The faster transfer is attributed to the fact that as the interfacial pressure increases the number of contact point theoretically increases which results in greater establishment of link between upper body and lower body resulting in lower degree of air barrier. The lower degree of air barrier would result in faster

propagation of heat across the interface. Further, the application of silicone grease as TIM would result in the source and sink material to be more contiguous physically, resulting in faster propagation of heat**.**

5.2 Effect addition of MWCNT in heat transfer across the metal-metal interface

5.2.1 Results

Experiments were carried out to study the effect of the addition of MWCNTs to the TIM on contact heat transfer for Cu-Cu interfaces with L/D=1. Figures 5.14 and 5.15 show the variation of temperature with time for Cu-Cu interfaces with 0.1 wt% MWCNT SG TIM under no load and 200kPa interfacial pressure respectively. Figure 5.16 and 5.17 shows the variation of temperature with time for Cu-Cu interfaces with 1 wt% MWCNT SG TIM under no load and 200kPa interfacial pressure respectively. Figure 5.18 and 5.19 show the variation in SS_t and SST for Cu-Cu interfaces with 0.1 wt% and 1 wt % MWCNT SG TIM respectively.

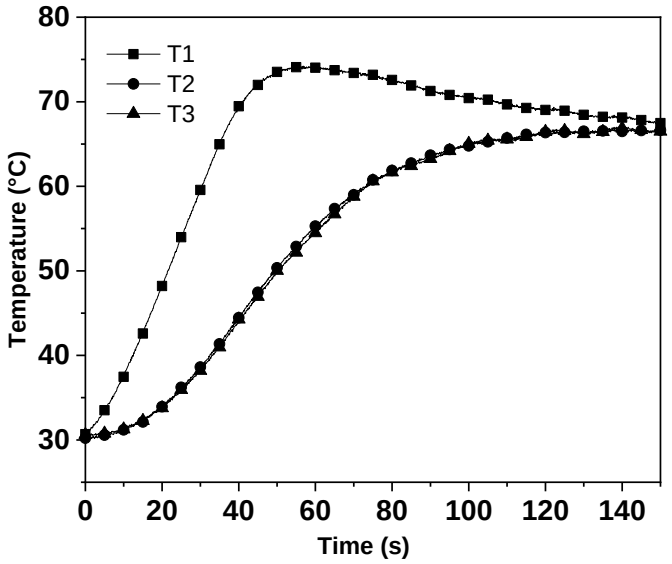

Figure 5.14 Variation of temperature with time for Cu-Cu interfaces, interfacial conditions: 0.1 wt% MWCNT- SG TIM, no load

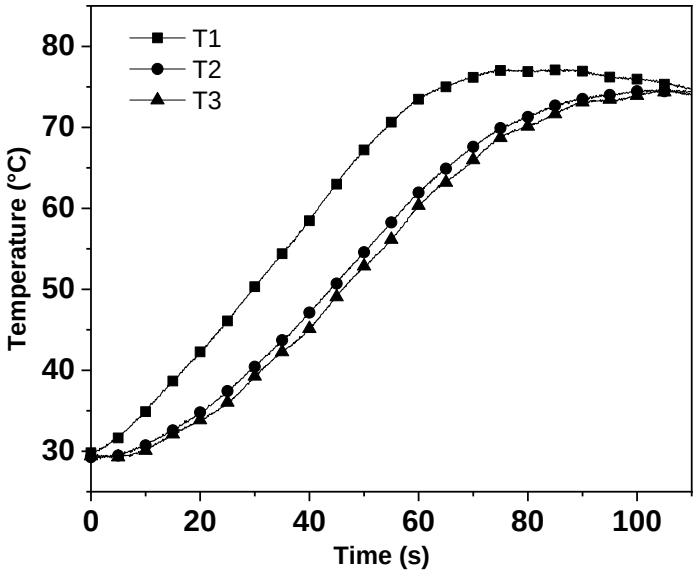

Figure 5.15 Variation of temperature with time for Cu-Cu interfaces, interfacial conditions: 0.1 wt% MWCNT- SG TIM and 200 kPa

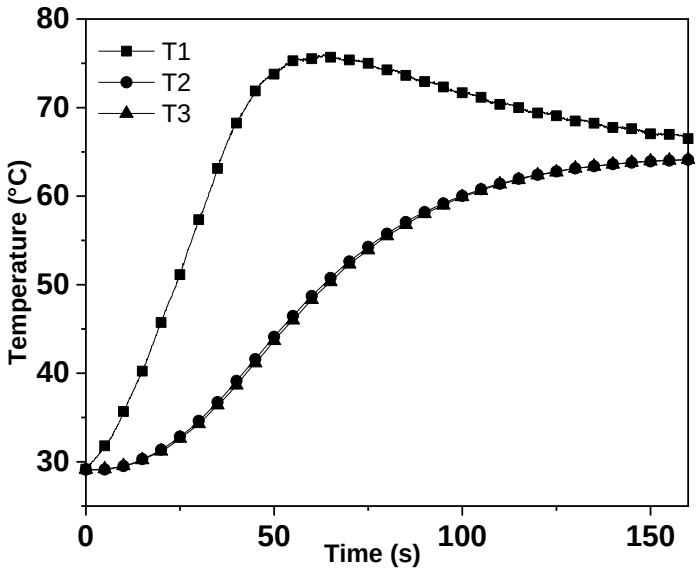

Figure 5.16 Variation of temperature with time for Cu-Cu interfaces, interfacial conditions: 1 wt% MWCNT- SG TIM, no load

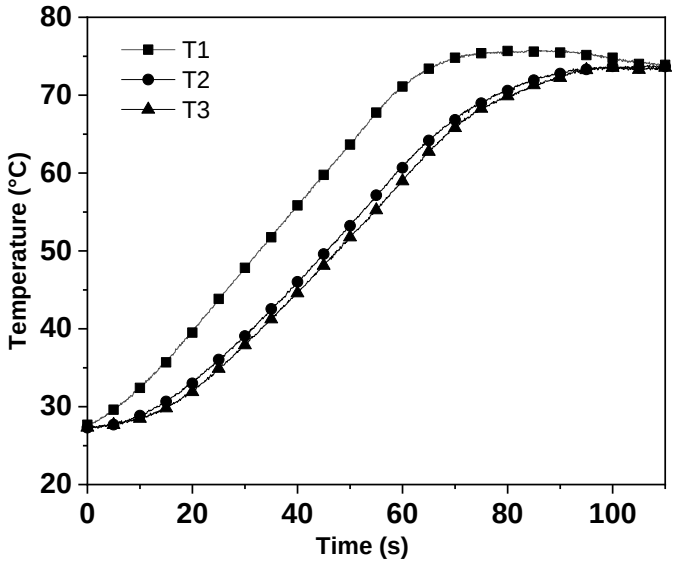

Figure 5.17 Variation of temperature with time for Cu-Cu interfaces, interfacial condition: 1 wt% MWCNT -SG TIM and 200kPa

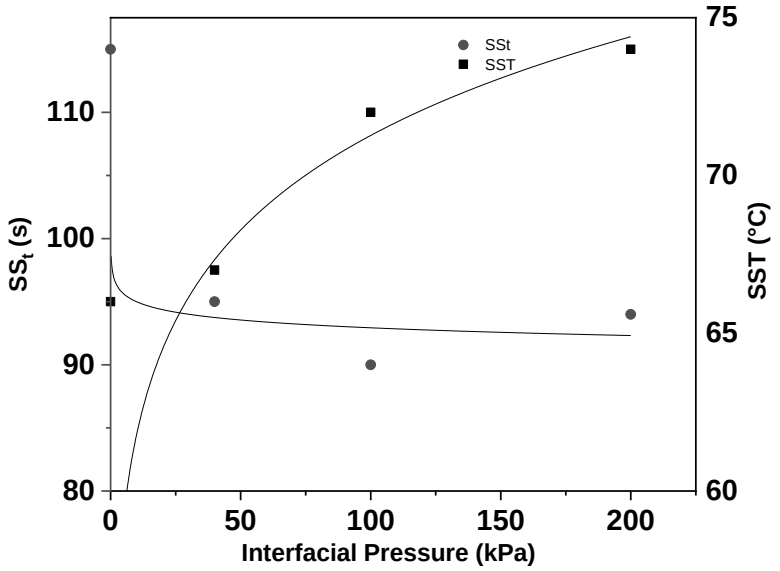

Figure 5.18 Variation of SS_t and SST with interfacial pressure for Cu-Cu interfaces with 0.1 % MWCNT SG TIM

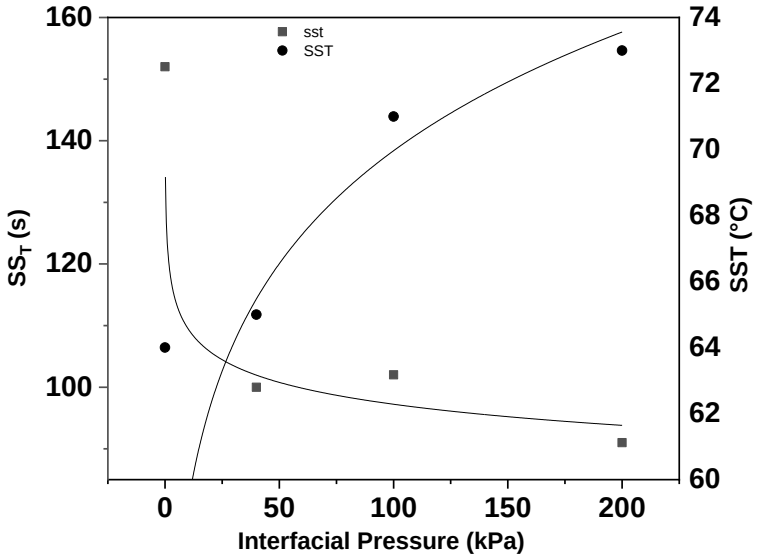

Figure 5.19 Variation of SS_t and SST with interfacial pressure for Cu-Cu interfaces with 1 % MWCNT SG TIM

5.2.2 Discussion

Figures 5.20 - 5.23 show the interfacial heat flux transients when SG and MWCNT-Silicone grease was used as TIM for Cu-Cu interface with L/D ratio of 1 under no load, 40kPa, 100kPa and 200kPa interfacial pressure respectively.

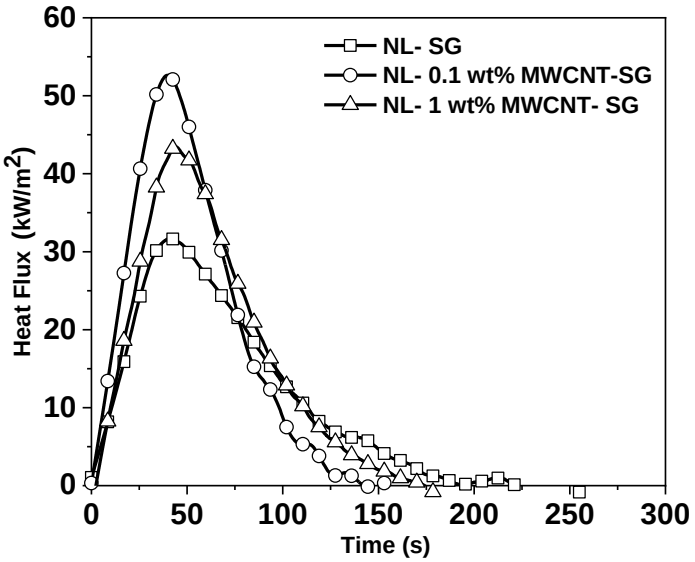

Figure 5.20 Variation of heat flux with time for Cu-Cu interfaces, interfacial conditions: SG TIM , MWCNT-SG TIM, no load conditions

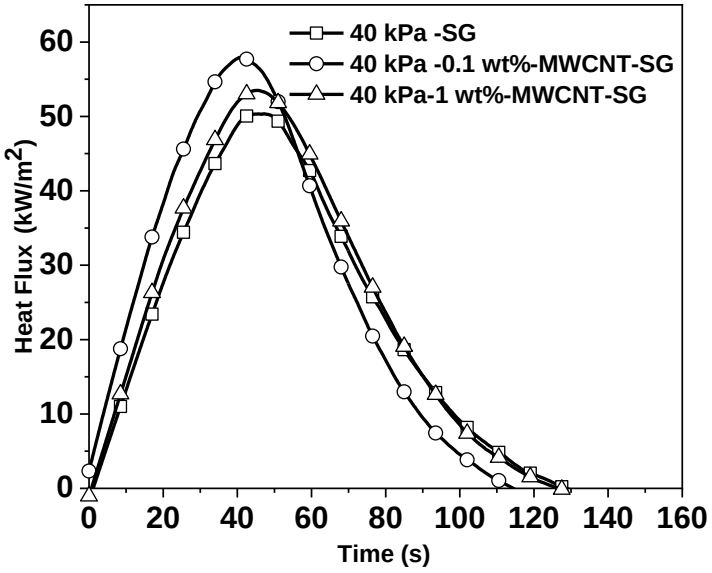

Figure 5.21 Variation of heat flux with time for Cu-Cu interfaces, interfacial conditions: SG, 0.1wt% MWCNT-SG, 1 wt% MWCNT-SG as TIMs and 40kPa

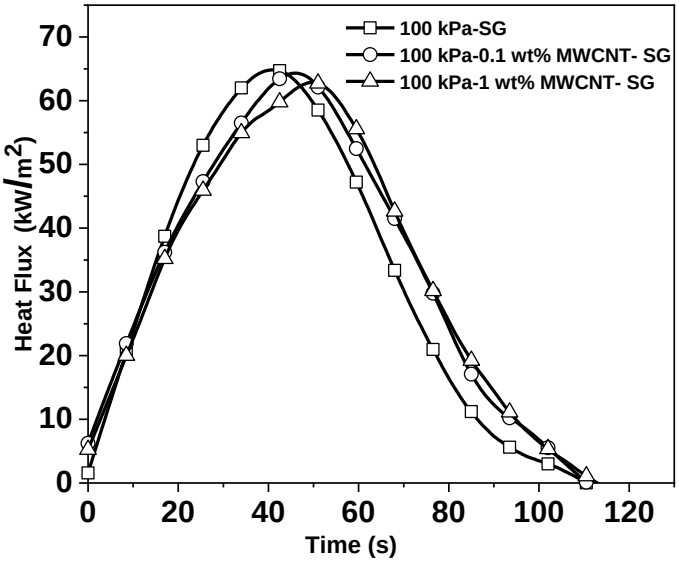

Figure 5.22 Variation of heat flux with time for Cu-Cu interfaces, interfacial conditions: SG, 0.1 wt% MWCNT-SG , 1wt% MWCNT-SG as TIMs and 100kPa

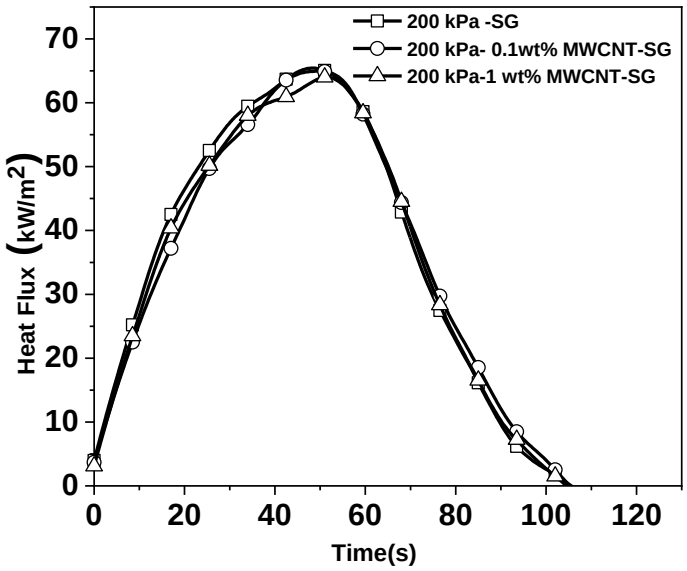

Figure 5.23 Variation of heat flux with time for Cu-Cu interfaces, interfacial conditions: SG, 0.1 wt% MWCNT-SG, 1wt% MWCNT-SG as TIM and 200kPa

The application of 0.1 wt% MWCNTs –SG at no load condition resulted in the peak heat flux to rise to the value of 52.62kW/m^2. Thus, the addition of MWCNTs resulted in a significant rise in peak heat flux as compared to the peak heat flux value of 31.71kW/m^2 when pristine silicone grease was used as TIM. Further, increasing the weight fraction to 1 % resulted in the peak heat flux dipping to a lower value of 43.47kW/m^2. The integral flow values also showed similar trend of an increase when 0.1 wt% MWCNTs were added for no load condition. Further, the integral flow dipped as the weight concentration of MWCNTs was increased to 1wt%. In fact, the integral flow deteriorated for all interfacial pressures when 1 wt% MWCNT – SG was used as TIM as compared to 0.1 wt%-MWCNT-SG. It is clear from the experiments that the addition of silicone based TIMs increases the heat transfer across the interface. The results also indicate that, MWCNT impregnated silicone grease with 0.1 wt% shows superior performance when compared to the silicone grease with 1 wt% MWCNTs. The possible explanation for the deterioration could be based on rheology of the particle laden polymer TIMs. In the present study it is assumed that the MWCNT based silicone greases as being deviating from Newtonian behaviour owing to the addition of MWCNTs in to the matrix. Even though non-Newtonian behaviour holds best for particle laden TIMs with high loading, we assume that the larger aspect ratio of

MWCNTs helps in achieving percolation at lower loading conditions which has been in this case. It has been reported in the literature (Prasher et al. 2003) that higher particle concentration leads to increased viscosity which leads to higher yield stress of TIMs. The increase in viscosity decreases the spreadability of TIMs employed. Thus, increase in MWCNTs from a weight concentration of 0.1 to 1 % results in the enhancement of the resistance to heat transfer. The values of peak het flux and integral flow for Cu-Cu interface with SG, MWCNT-SG TIMs at different interfacial pressure has been tabulated in the Table 7.

Table 7 Peak heat flux and integral heat flow for Cu-Cu interfaces

Sl No	TIM	Interfacial pressure kPa	Peak heat flux (kW/m^2)	Integral heat flow (MJ/m^2)
1	SG	NL	31.71	2.13
2	SG with 0.1 wt % MWCNT	NL	52.62	2.97
3	SG with 1 wt % MWCNT	NL	43.47	2.66
4	SG	40	50.35	2.95
5	SG with 0.1 wt % MWCNT	40	57.94	3.21
6	SG with 1 wt % MWCNT	40	53.50	3.15
7	SG	100	64.86	3.56
8	SG with 0.1 wt % MWCNT	100	64.33	3.78
9	SG with 1 wt % MWCNT	100	62.86	3.76
10	SG	200	65.43	3.94
11	SG with 0.1 wt % MWCNT	200	64.96	3.89
12	SG with 1 wt % MWCNT	200	65.74	3.98

5.3 Assessment of thermal conformance parameters for Cu-Cu metal interfaces.

To assess the thermal conformance of metal–metal interface, a dimensionless source/sink heat transfer parameter, Ƞ was defined. For calculating the parameter Ƞ, the heat required for the source material (Q_1) to reach 70°C and the heat absorbed by the sink (Q_2) during the same time interval were used. Ƞ was calculated as the ratio, Q_2/Q_1. The heat required to reach 70°C for the source (Q_1) was calculated using Newtonian approach and Q_2 was estimated by using inverse method. The heat flux transients were integrated for the time interval during which the source reaches 70°C. The integral value gives the total heat required per unit area for the source to attain 70°C. The values were verified by using the equation $Q= mC_p\Delta T$ where mC_p is the volumetric heat capacity of the source material and ΔT is the temperature difference between 70°C and the initial temperature of the chill/sink. For example, in the case of source/sink combination (Cu/Cu), the total heat estimated was 3708 kJ/m^2 which is in good agreement with the total heat calculated (3684 kJ/m^2) by the mCpΔT equation.

Further, it was found that as the interfacial pressure was increased the Ƞ value also increased for Cu-Cu interfaces. The values of Ƞ for different interfacial pressure have been tabulated in the Table 8. The application of TIMs also resulted in enhanced Ƞ suggesting superior heat transfer. Also, it was observed that with increase in the thermal conformance between the source and the sink, the time (t_g) required for the source to reach the target temperature of 70°C increases. As the overall thermal resistance at the interface decreases, heat from the source is more efficiently transferred to the sink from the beginning of the experiment and as a result the source takes more time to reach the target temperature. Another thermal conformance parameter, dimensionless temperature (Θ) was defined as the ratio of the sink to the source temperatures at the time when the source reaches the target temperature. The ratio increased significantly with the application of interfacial pressure and TIM. The effect of thermal conformance was reflected in the following experimentally measured maximum temperature drop ($\triangle T_{max}$) and estimated heat transfer coefficients corresponding to ($\triangle T_{max}$). The values of $\triangle T_{max}$ and the heat transfer coefficient corresponding to $\triangle T_{max}$ has been tabulated in the Table 9. The heat transfer coefficient

(h) was calculated as the ratio of interfacial heat flux to the temperature drop at the interface.

Table 8 Thermal conformance parameters for Cu-Cu metal interface

Interfacial pressure (kPa)	Heat required for the source to reach 70°C (Q_1) kJ/m^2	Time to reach 70°C(t_g) (s)	Sink temperature T_2 (°C)	$\Theta = T_2/T_1$	Heat absorbed by the sink during t_g (Q_2) kJ/m^2	$\eta = Q_2/Q_1$
Cu-Cu bare interface						
NL	3708	40.2	30.7	0.43	377	0.10
40	3562	44.3	36.98	0.52	753	0.21
100	3780	44.2	40.16	0.57	1127	0.30
200	3855	48.6	44.36	0.63	1611	0.42
Cu-Cu interface with TIM (SG)						
NL	3507	37.6	36.30	0.51	623	0.18
40	3532	47.4	45.36	0.64	1365	0.39
100	3581	52.7	56.35	0.80	2576	0.72
200	3657	59.2	60.94	0.87	2806	0.77

Table 9 HTC and ΔT max parameters for Cu-Cu bare and interfaces with TIMs subjected to various interfacial pressures

Cu-Cu bare interfaces		
Interfacial pressure (kPa)	**ΔT_{max}, (°C)**	**h (W/m^{2}k) at ΔT_{max}**
NL	41.9	423
40	34.07	944
100	30.19	1584
200	25.52	2155
Cu-Cu interfaces with TIM (SG)		
NL	34.72	912
40	24.38	2099
100	14.36	4377
200	9.40	6745

5.4 Assessment of thermal conformance parameters for Al-Al metal interfaces

5.4.1 Results

Thermal conformance of Al-Al interfaces was studied by using inverse heat conduction approach. Figures 5.24 - 5.27 show the thermal history of Al-Al interfaces with different interfacial conditions. Figures 5.28 - 5.29 show the variation of SS_t and SST for Al-Al bare interfaces and for interfaces with SG TIM.

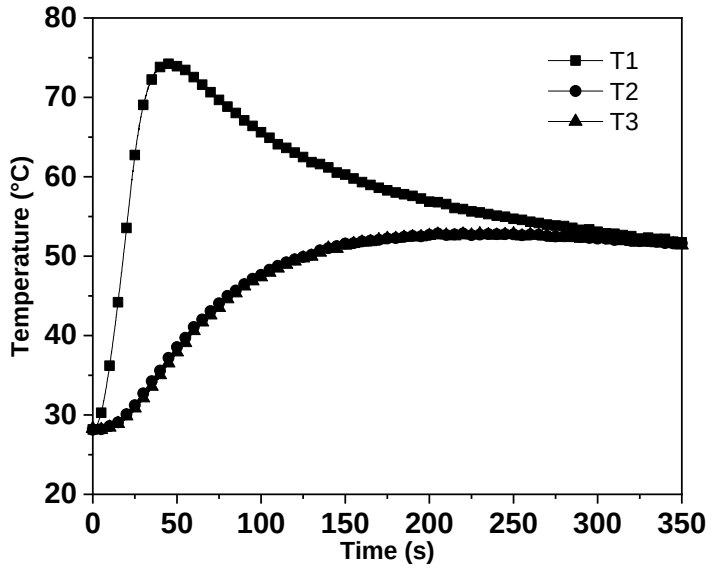

Figure 5.24 Variation of temperature with time for Al-Al bare interfaces under no load

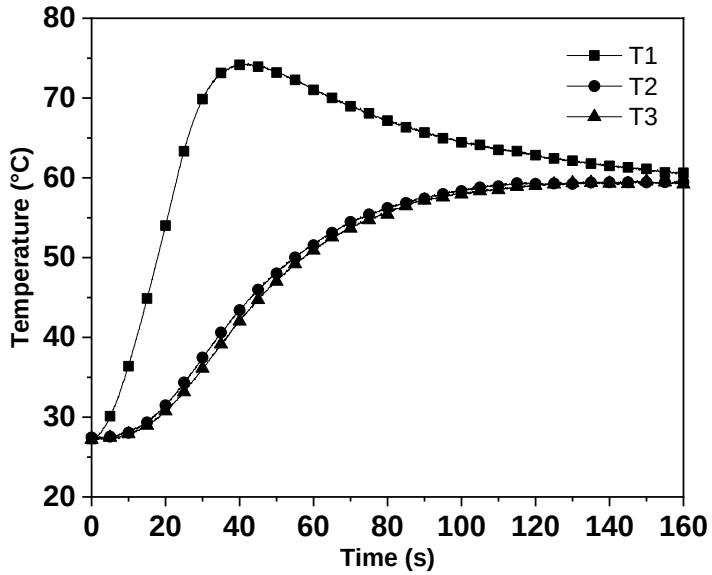

Figure 5.25 Variation of temperature with time for Al-Al interfaces, interfacial conditions: SG TIM, no load

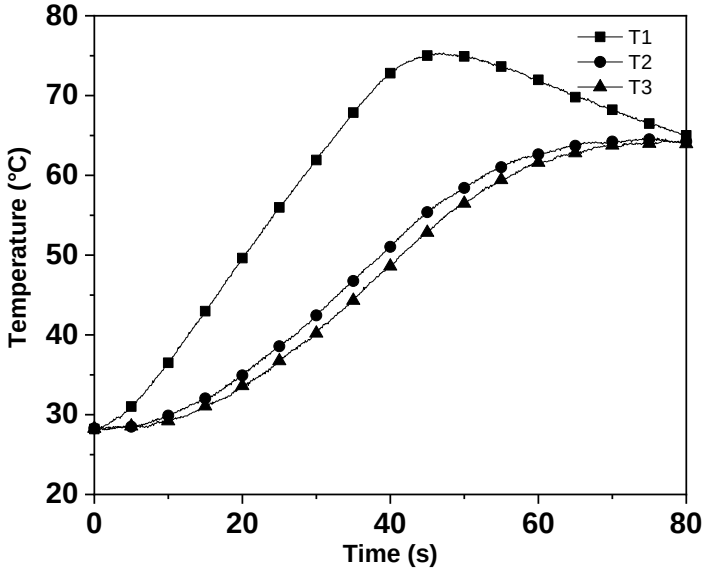

Figure 5.26 Variation of temperature with time for Al-Al bare interfaces under 200kPa

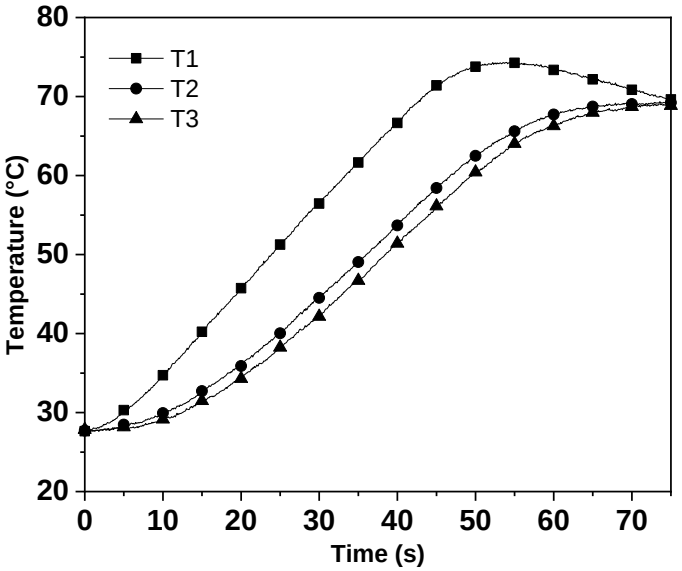

Figure 5.27 Variation of temperature with time for Al-Al interfaces, interfacial condition: SG TIM and 200kPa

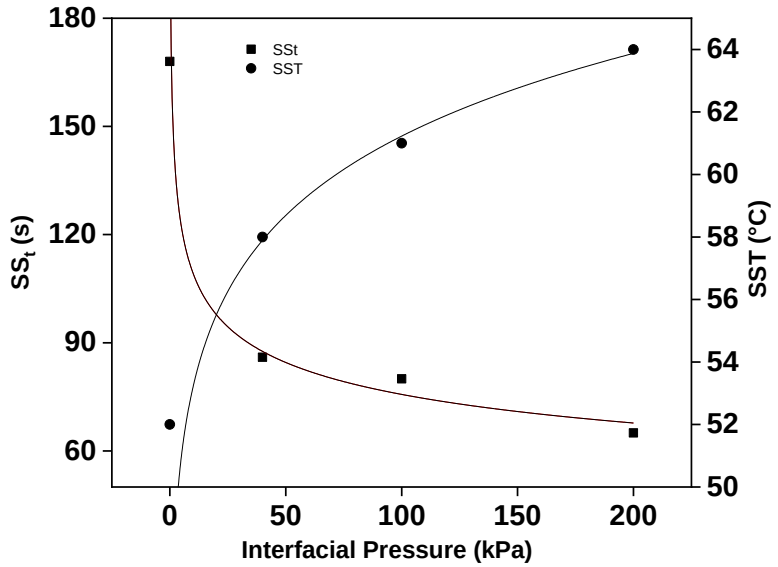

Figure 5.28 Variation of SS_t and SST with interfacial pressure for Al-Al bare interfaces

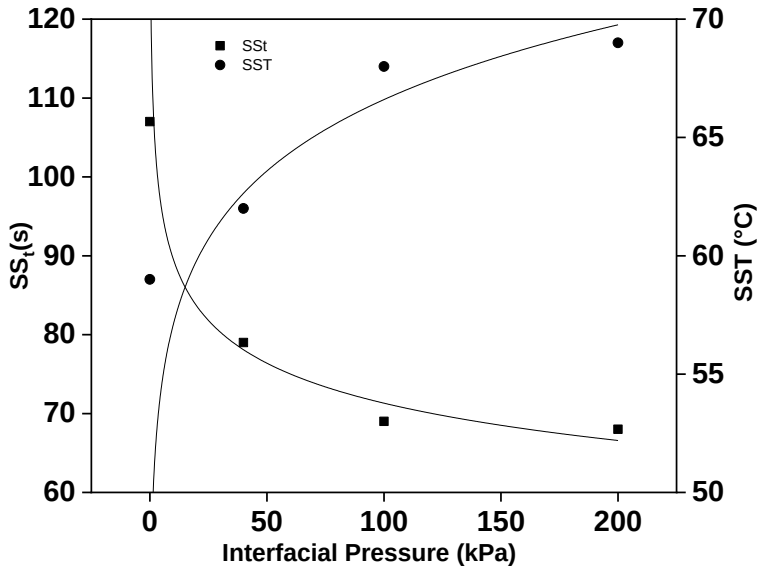

Figure 5.29 Variation of SS_t and SST with interfacial pressure for Al-Al interfaces with SG TIM

5.4.2 Discussion

The thermal conformance was assessed for Al-Al interfaces. Figure 5.30 shows the estimated heat flux transients for a typical Al-Al metal bare contact. The sink heat flux transients were estimated using the inverse heat conduction analysis

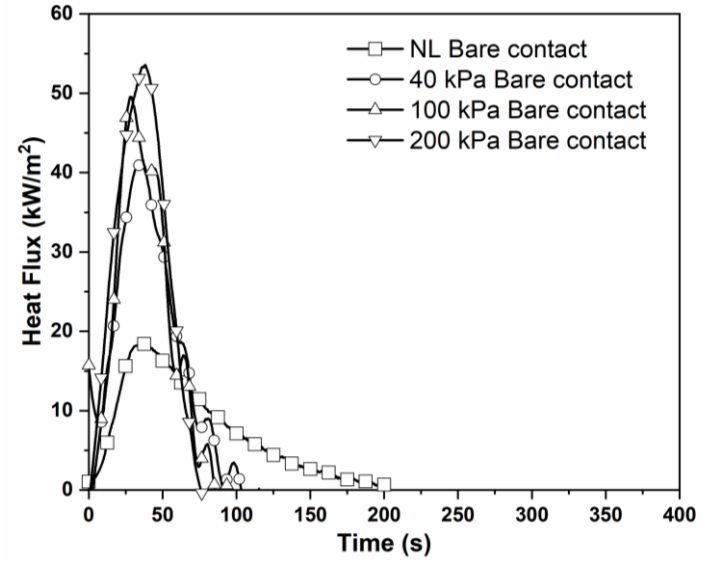

Figure 5.30 Typical plot showing the variation in heat flux with time for Al-Al bare interface for various interfacial loading conditions

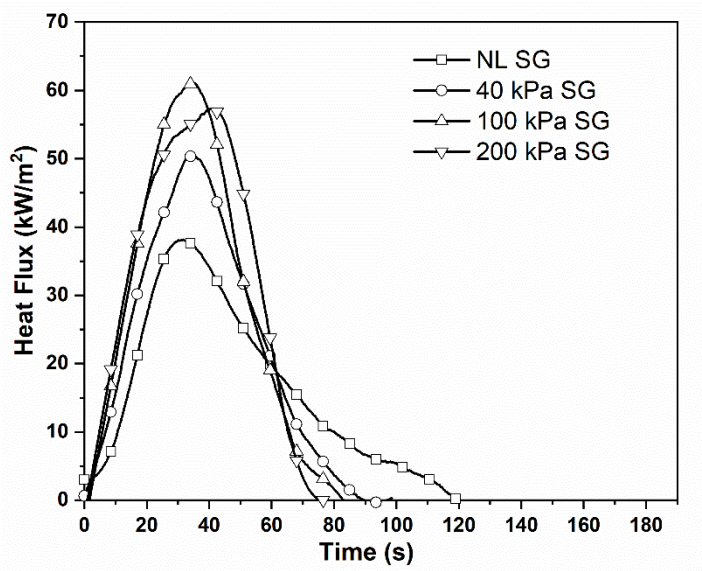

Figure 5.31 Typical plot showing the variation in heat flux with time for Al-Al interface with SG as TIM for various interfacial loading conditions

It is evident that for Al-Al interface the heat flux transients increased with increase in the interfacial pressure. The increase in heat flux was attributed to the increased the contact area at the interface with increase in the interfacial pressure resulting in enhanced heat transfer across the interface. Further, the effect of application of TIMs on heat transfer was studied. Figure 5.31 shows a typical heat flux transient curve for Al-Al interfaces with silicone grease as TIM. The magnitude of the heat flux transients increased with the application of silicone grease TIM. The silicone grease TIM replaces the low thermal conductive air at the interfacial asperities resulting higher degree of thermal conformance. The thermal conformance parameters were estimated and tabulated in the Table 10. The HTC and ΔT_{max} parameters are given in Table 11. The thermal conformance parameters η,Θ, t_g along with HTC were found to increase with the increase in the interfacial pressure and with the application of TIM thus enhancing the thermal conformance of the interfaces. Further, ΔT_{max} reduces with application of TIMs and with enhanced interfacial pressure thus increasing the thermal conformance.

Table 10 Thermal conformance parameters for Al-Al metal interface.

Interfacial Pressure (kPa)	Heat required for the source to reach 70°C (Q_1) kJ/m^2	Time to reach 70°C(t_g) (s)	Sink temperature (°C) T_2	$\Theta = T_2/T_1$	Heat absorbed by the sink during t_g (Q_2) kJ/m^2	$\eta = Q_2/Q_1$
Al-Al Bare Interface						
NL	2606	31.5	33.18	0.47	277	0.10
40	2651	30.8	38.14	0.54	697	0.26
100	2561	33	43.92	0.62	889	0.35
200	2588	37.1	48.60	0.69	1218	0.48
Al-Al Interface with TIM (SG)						
NL	2651.03	30.2	37.52	0.53	572	0.21
40	2654.78	33.2	42.85	0.61	905	0.35
100	2555.64	34.4	50.14	0.71	1315	0.51
200	2621.36	43.4	56.84	0.81	1750	0.67

Table 11 HTC and ΔT_{max} parameters for Al-Al interfaces subjected to various interfacial pressures

Al-Al bare interfaces		
Interfacial pressure (kPa)	**ΔT_{max}, (˚C)**	**h (W/m^{2}k) at ΔT_{max}**
NL	38.27	479
40	33.15	1234
100	26.11	1652
200	21.33	2511
Al-Al interfaces with TIM (SG)		
Interfacial pressure (kPa)	**ΔT_{max}, (˚C)**	**h (W/m^{2}k) at ΔT_{max}**
NL	32.52	1167
40	26.95	1869
100	19.31	3161
200	12.62	4538

5.5 Estimation of thermal conformance parameters (Ƞ,Ɵ,t_g) for dissimilar metal contacts

5.5.1 Results

The thermal conformance was assessed for dissimilar metal-metal interfaces. The experiments were conducted for bare dissimilar interface. Apart from the bare interfaces, interfaces with TIMs were also studied. The TIMs used were SG (Silicone grease) and CTG (commercially available thermal grease). Figures 5.32-5.33 show the variation of temperature with time for Al-Cu bare interfaces under no load and 200kPa interfacial pressure respectively. Figures 5.34-5.35 show the variation in temperature with time for Cu-Al bare interfaces under 40kPa and 100kPa interfacial pressure respectively. Figure 5.36 shows the variation of temperature and time for Al-Cu interfaces with SG TIM under no load. Figure 5.37 shows the variation of temperature and time for Cu-Al interfaces with CTG TIM under no load

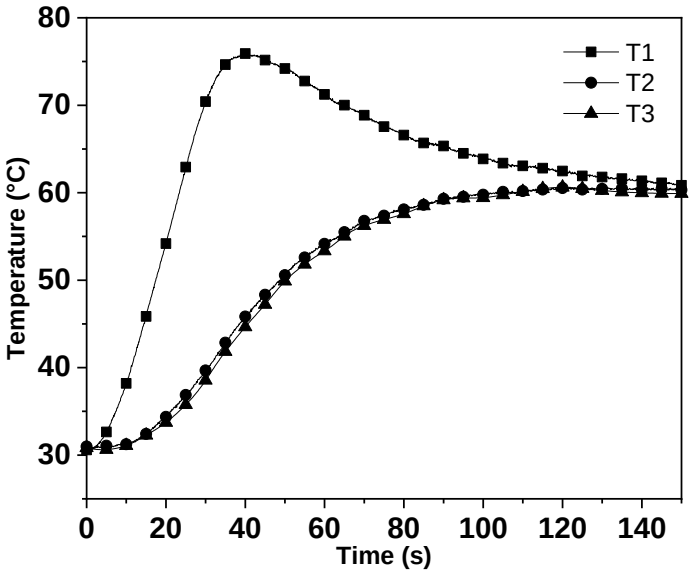

Figure 5.32 Variation of temperature with time for Al-Cu bare interfaces under no load

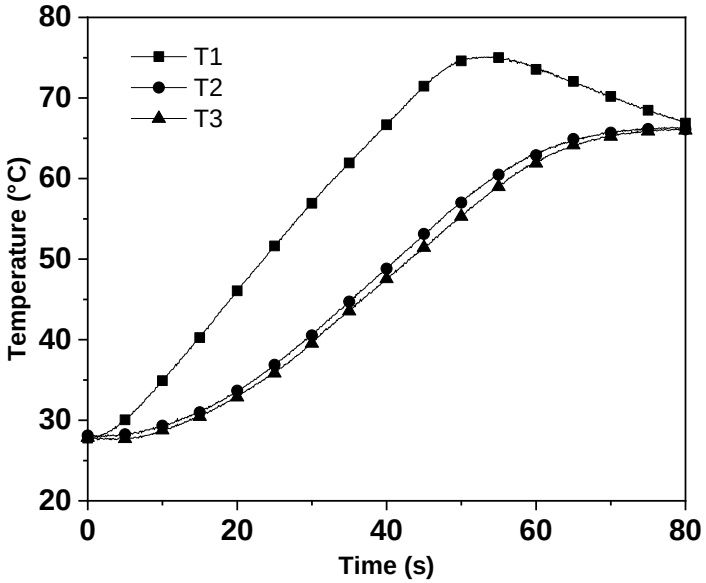

Figure 5.33 Variation of temperature with time for Al-Cu bare interfaces under 200kPa interfacial pressure

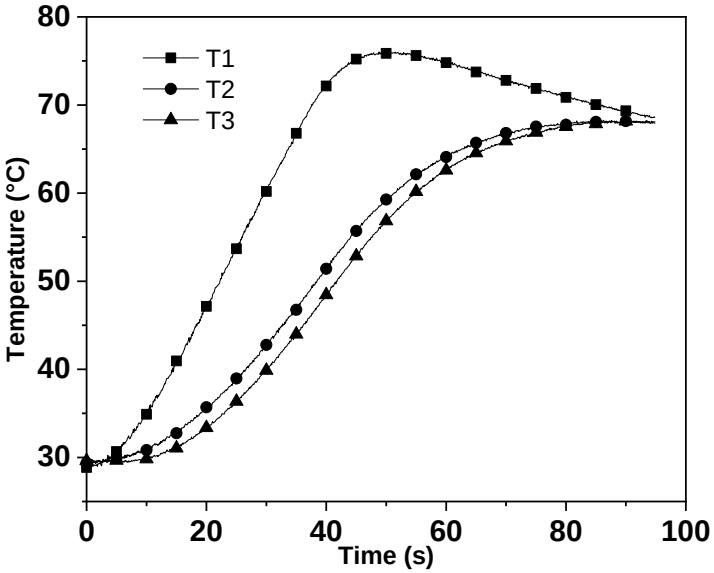

Figure 5.34 Variation of temperature with time for Cu-Al bare interfaces under 40 kPa interfacial pressure

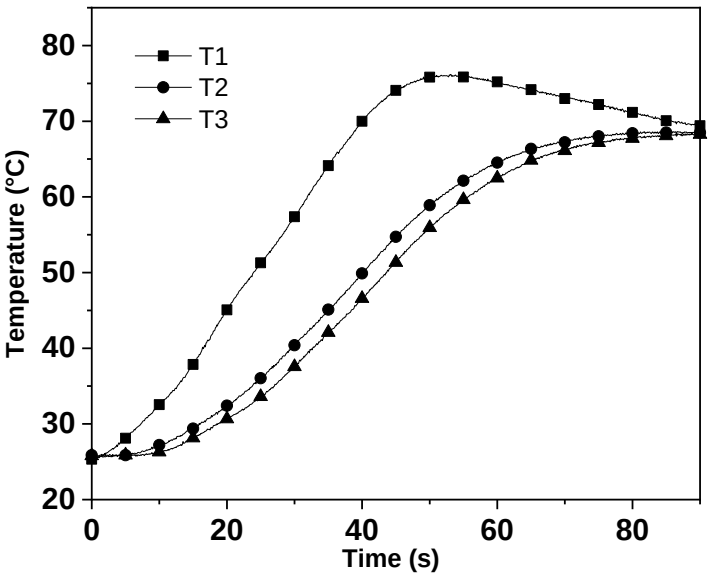

Figure 5.35 Variation of temperature with time for Cu-Al bare interfaces under 100 kPa interfacial pressure

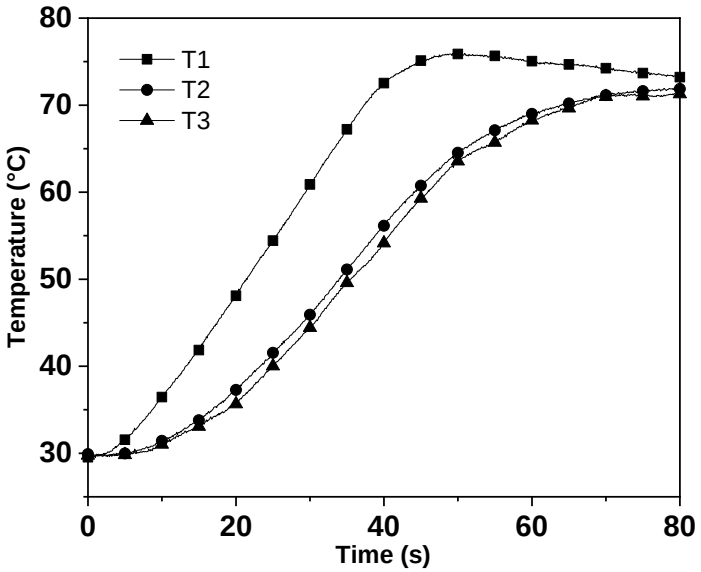

Figure 5.36 Variation of temperature with time for Al-Cu interfaces, interfacial condition: SG TIM and no load

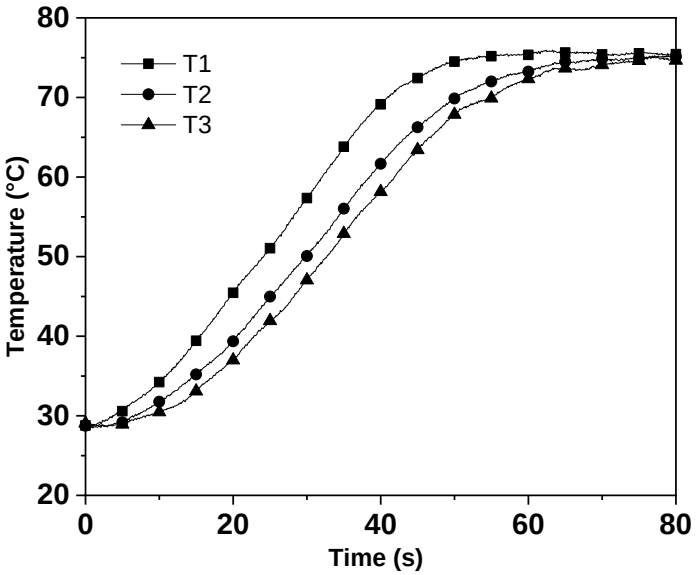

Figure 5.37 Variation of temperature with time for Cu-Al interface, interfacial conditions: CTG TIM and no load

5.5.2 Discussion

Figure 5.38 shows the variation of heat flux with time for Cu-Al bare interfaces. It is clear from the figure that the increase in interfacial pressure leads to enhanced heat transfer across the interface. It is interesting to note that the value of the conformance parameter Ƞ depends not only on the interfacial pressure and the TIM, but is also affected by the source and sink materials. When copper was used as the sink in the presence of interfacial pressure and CTG, the value of the conformance parameter obtained was greater than 1. The interfacial pressure and TIM decrease the thermal contact resistance at the interface by improving the contact condition at the interface. At higher interfacial pressures, the effect of interfacial pressure on the conformance parameter was not significant. Sink materials like copper having high thermal effusivity of 36970 $Jm^{-2}K^{-1}s^{-0.5}$ enhances the ability of the sink to absorb heat. Further, high conductivity copper decreases the thermal resistance offered by the material to the transfer of heat from the source to the sink.

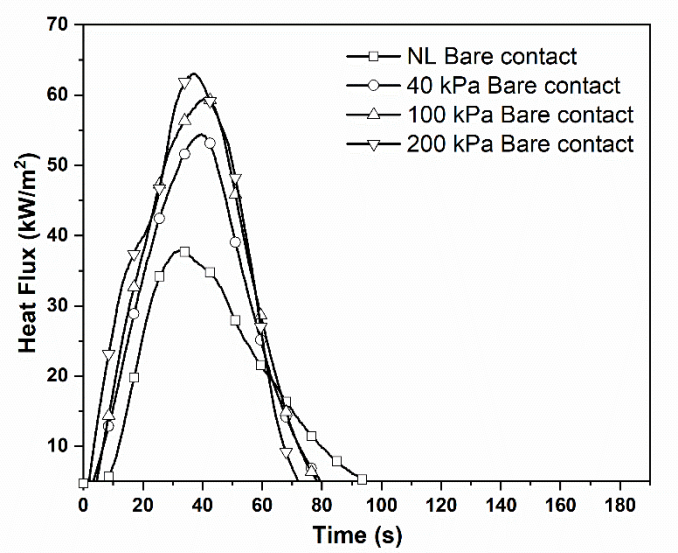

Figure 5.38 Effect of interfacial pressure on heat flux for Cu-Al bare interface

Similarly, high thermal diffusivity source material increases the ability of the source material to dissipate heat to the sink at a faster rate. Also, it was observed that with increase in the thermal conformance between the source and the sink, the time (t_g) required for the source to reach the target temperature of 70°C increases. As the overall thermal resistance at the interface decreases, heat from the source is more efficiently transferred to the sink from the beginning of the experiment and as a result the source

takes more time to reach the target temperature. This is particularly important during heat transfer in microelectronic devices where the device is not expected to reach the upper limit of the specified temperature range generally set for industrial applications. The variations in the thermal conformance parameters of η and t_g for different combinations of dissimilar metal-metal interface has been tabulated in Table 12. From the experiments it has been observed that the heat absorbed at the Cu-Cu bare interface was only 376 kJ/m^2 and the corresponding heat absorbed by the Al-Cu bare interface was 863 kJ/m^2. Further, dimensionless temperature (Θ) increased significantly with the application of interfacial pressure and TIM. The ratio was minimum (~0.43) for the Cu/Cu bare interface and maximum (~0.92) for Cu-Al and Al-Cu dissimilar metals under interfacial pressure of 200kPa and with CTG as the TIM. Experiments revealed that even in case of dissimilar metal-metal interfaces, the interfacial pressure and TIMs has an effect on the thermal conformance. As the interfacial pressure increases the ΔT_{max} decreases and the HTC increases indicating superior heat transfer. The values of ΔT_{max} and the HTC for various combinations of dissimilar metal-metal contacts with TIMs of varying thermal conductivity has been tabulated in the Table 13.

Table 12 Thermal conformance parameter of Ƞ,Ɵ,tg for dissimilar metal contacts

Interfacial Pressure (kPa)	Heat required for the source to reach 70°C (Q_1) kJ/m^2	Time to reach 70°C(t_g) (s)	Source temperature (°C) T_1	Sink temperature (°C) T_2	Ɵ= T_2/T_1	Heat absorbed by the sink during t_g (Q_2) kJ/m^2	Ƞ = Q_2/Q_1
Al-Cu bare Interface							
NL	2438	29.7	70	39.48	0.56	863	0.36
40	2515	32.3	70	44.81	0.64	1220	0.49
100	2580	36.9	70	47.66	0.68	1705	0.67
200	2635	43.5	70	51.79	0.73	1920	0.73
Al-Cu Interface with TIM(SG)							
NL	2509	37.4	70	53.57	0.76	2076	0.83
40	2573	42.8	70	59.90	0.85	2630	1.03
100	2598	45.6	70	62.68	0.89	2976	1.15
200	2581	48.7	70	64.40	0.92	3079	1.2
Al-Cu Interface with TIM (CTG)							
NL	2487	39.1	70	58.59	0.83	2475	0.99
40	2504	42.4	70	62.24	0.88	2805	1.12
100	2473	44	70	62.60	0.89	2828	1.14
200	2596	47.8	70	64.10	0.91	3068	1.19
Cu-Al bare Interface							
NL	3544	32.4	70	41.01	0.58	619	0.18
40	3551	37.6	70	49.47	0.70	1129	0.32
100	3850	40.2	70	50.07	0.71	1542	0.40
200	3709	42	70	55.53	0.79	1716	0.47
Cu-Al Interface with TIM (SG)							
NL	3445	38.6	70	56.52	0.80	1586	0.47
40	3531	39.9	70	58.08	0.82	1799	0.50
100	3526	41.7	70	63.17	0.90	1934	0.55
200	3649	45.1	70	64.01	0.91	2093	0.58
Cu-Al Interface with TIM (CTG)							
NL	3548	40.9	70	62.59	0.89	2058	0.59
40	3918	44.7	70	65.23	0.93	2174	0.56
100	3629	44.5	70	65.08	0.92	2125	0.59
200	3694	46.5	70	65.14	0.93	2249	0.60

Table 13 HTC and △T max parameters for dissimilar contacts

Al-Cu Bare interfaces		
Interfacial pressure (kPa)	**ΔT_{max}, (°C)**	**h (W/m^2K) at ΔT_{max}**
NL	31.59	1695
40	25.26	2870
100	21.89	3547
200	18.58	3827
Al-Cu TIM (SG)		
NL	16.11	5429
40	9.92	8407
100	6.99	12406
200	5.41	15096
Al-Cu TIM (CTG)		
NL	10.92	8554
40	7.37	12495
100	6.96	12483
200	5.36	15213
Cu-Al Bare interfaces		
NL	29.18	1297
40	20.33	2672
100	19.59	3035
200	13.66	4227
Cu-Al TIM (SG)		
NL	13.31	4872
40	11.40	5627
100	6.74	9444
200	5.62	10793
Cu-Al TIM (CTG)		
NL	7.02	10171
40	5.73	13137
100	4.38	14886
200	4.40	14041

5.6 Estimation of thermal conformance assessment parameter (TCAP) for various metal-metal contacts

To assess the thermal conformance between the source and the sink materials, a thermal conformance assessment parameter (TCAP) was proposed and is given by

$$TCAP = (A*B) + C^{0.25} \quad (5.3)$$

Where A is the thermal diffusivity of the source material, $k/(\rho C_p)$, B is the thermal effusivity of the sink material, $\sqrt{k\rho C_p}$, C is the interfacial pressure.

The variations of the η, ΔT_{max}, Θ and HTC at ΔT_{max} were modelled as function of TCAP and load for the various combinations and are shown in figures 5.39-5.42. TCAP was normalized with respect to its maximum value so that the maximum and minimum values lie between zero and one. It was observed that all combinations excluding Cu-Cu interfaces showed a linear trend with the TCAP. The discrepancy was attributed to the high thermal conductivity of Cu-Cu interfaces with the interface becoming the overriding factor affecting the heat transfer across the source/sink interface. Hence, for Cu-Cu interfaces, only load was considered to quantify the heat flux parameters. Cu-Cu interfacial heat transfer depended only on the interfacial pressure and the thermophysical properties of the copper had no significant effect. Figure 5.43 shows the variation of estimated time vs TCAP for bare and interfaces with TIM (SG). It is evident from the graph that for a given TCAP the estimated time to reach tg increases with the application of TIMs. Thus, the application of TIMs enhances heat transfer across the interface.

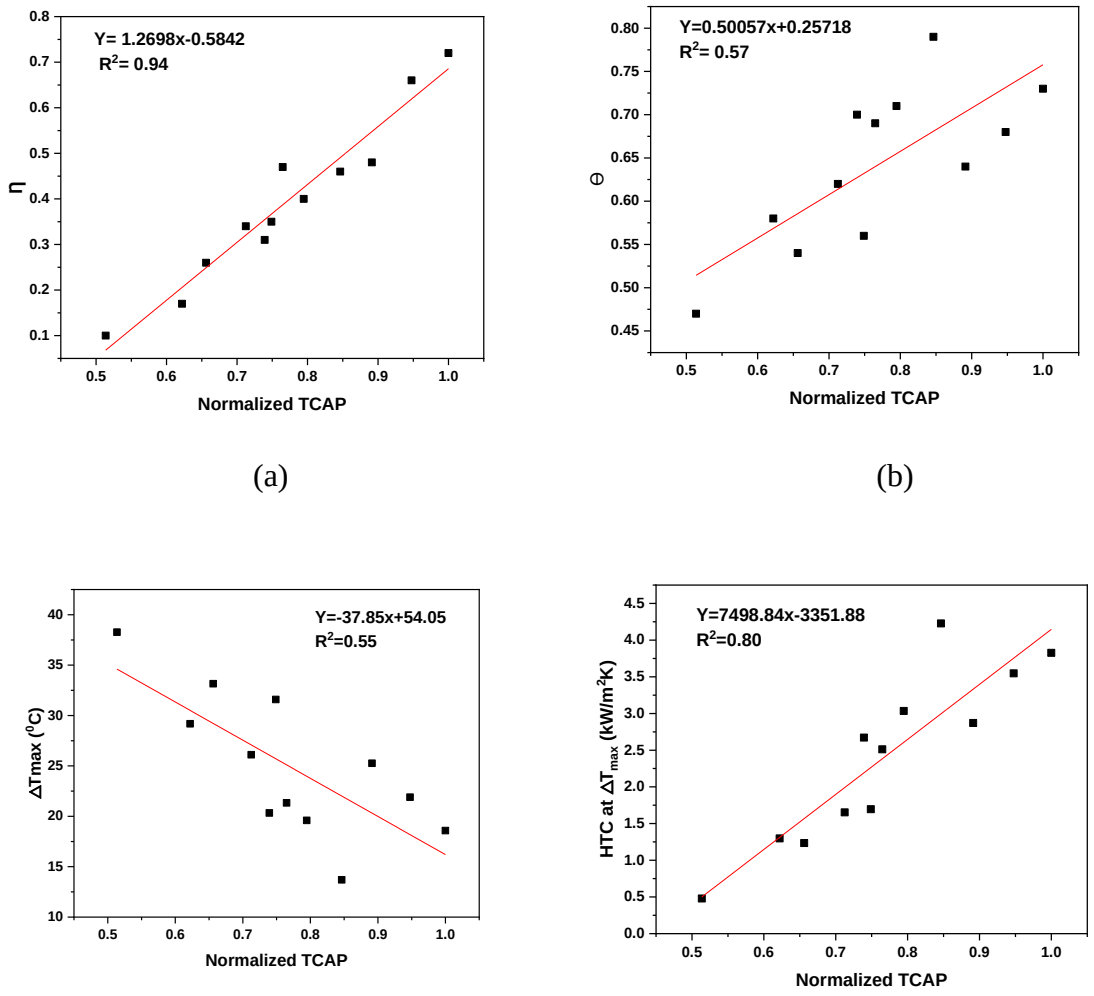

Figure 5.39 Variation of a) η b) Θ, c) ΔT_{max} and d) HTC at ΔT_{max} with Normalized TCAP for Al-Al, Al-Cu, Cu-Al Bare interfaces

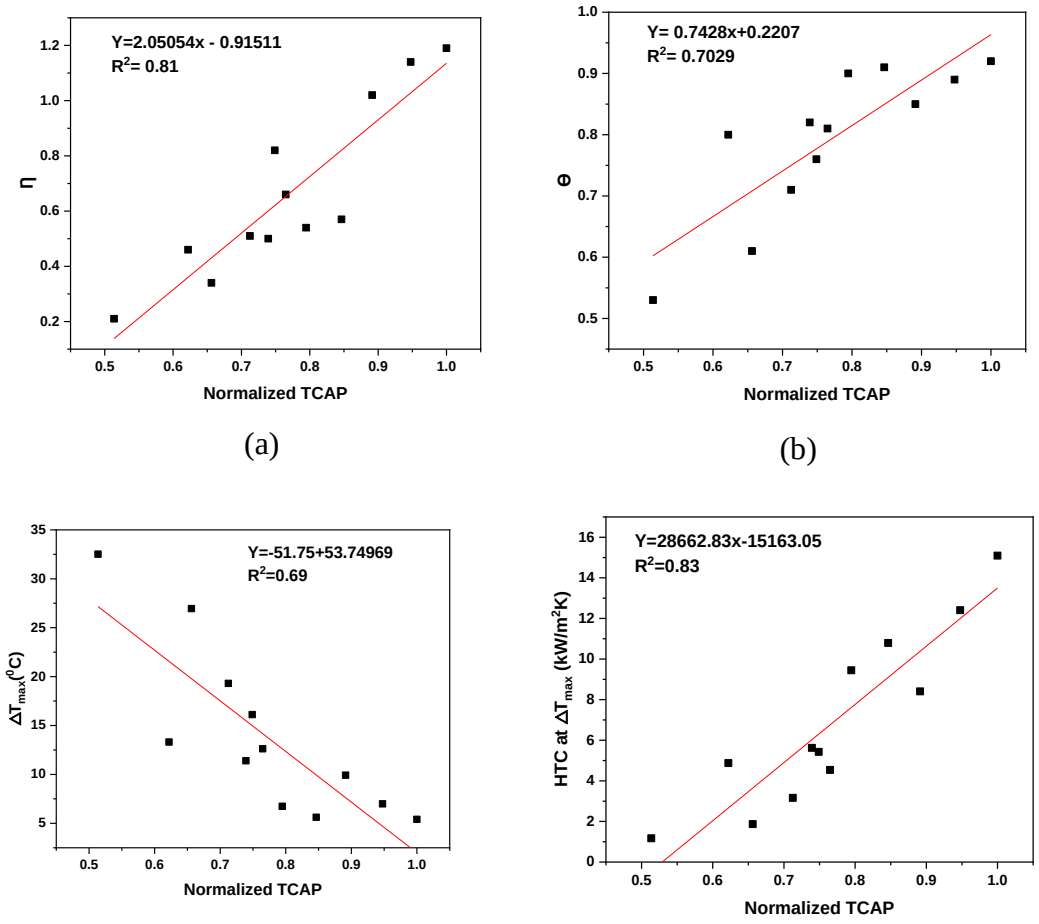

Figure 5.40 Variation of a) η b) Θ, c) ΔTmax and d) HTC at ΔTmax with Normalized TCAP for Al-Al, Al-Cu, Cu-Al interfaces with TIM (SG)

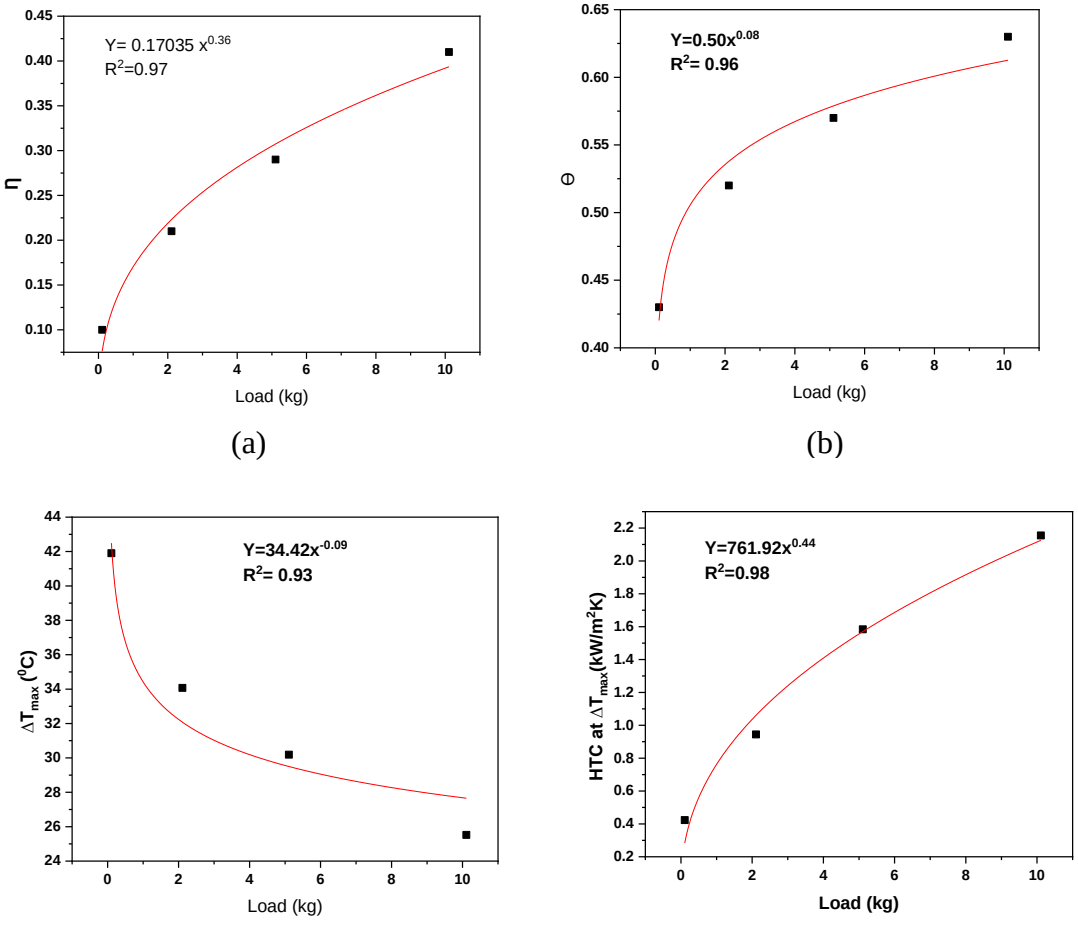

Figure 5.41 Variation of a) η b) Θ, c) ΔT_{max} and d) HTC at ΔT_{max} with interfacial pressure for Cu-Cu bare interfaces

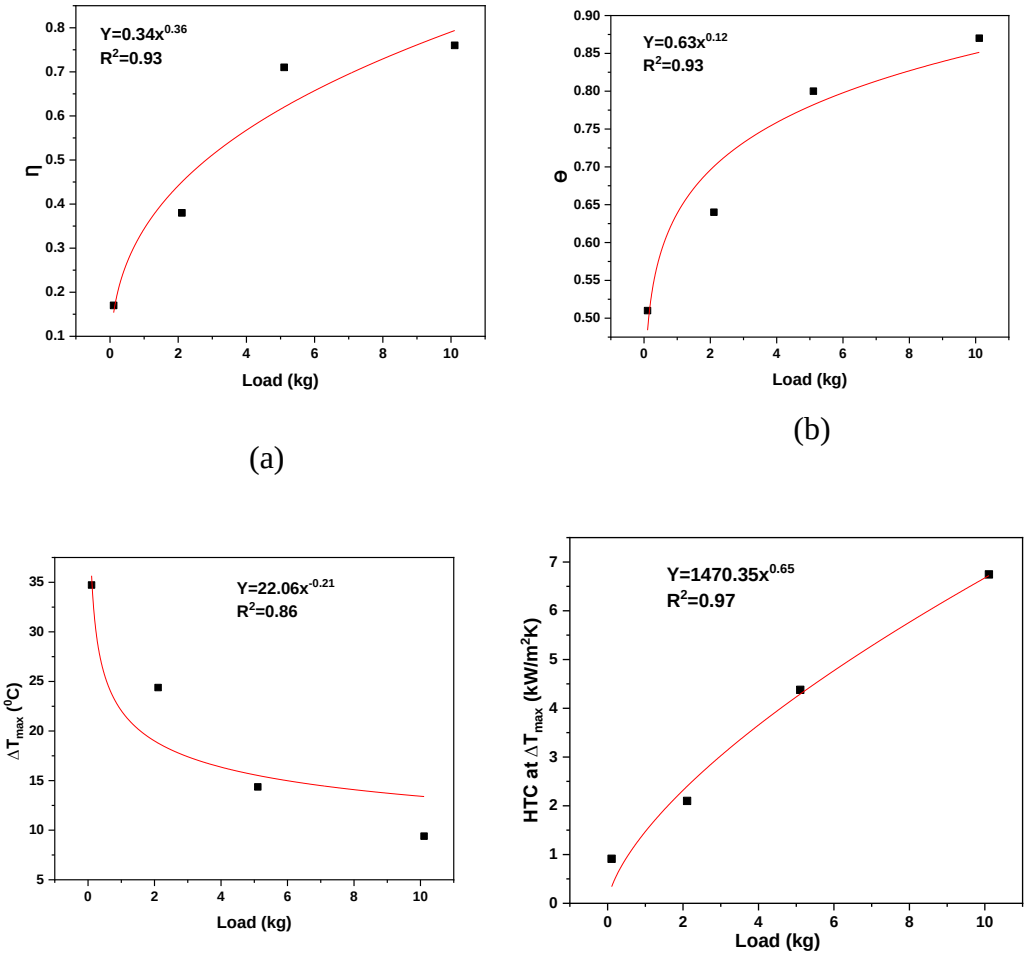

Figure 5.42 Variation of a) η b) Θ, c) ΔT_{max} and d) HTC at ΔT_{max} with interfacial pressure for Cu-Cu interfaces with TIM (SG)

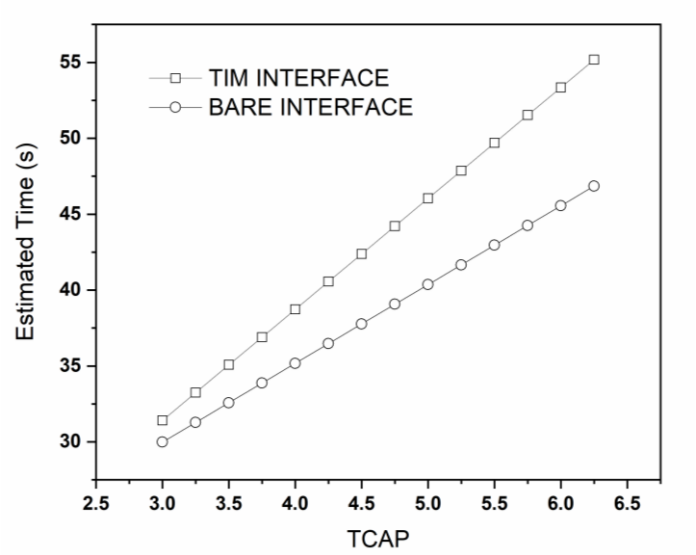

Figure 5.43 Variation of estimated time vs TCAP for bare and interfaces with TIM (SG)

5.7 Effect of Surface roughness and high thermal conductive TIMs on thermal conformance of Cu- Cu interface.

5.7.1 Results

Thermal conformance analysis was conducted for Cu-Cu interfaces with smooth surface finish. The thermal history of the specimens was measured. Figure 5.44 and 5.45 show the variation in temperature with time for Cu-Cu bare interfaces and Cu-Cu interfaces with SG TIM under no load respectively. Figure 5.46 and 5.47 show the thermal history for Cu-Cu interfaces with CTG TIM and STP TIM respectively.

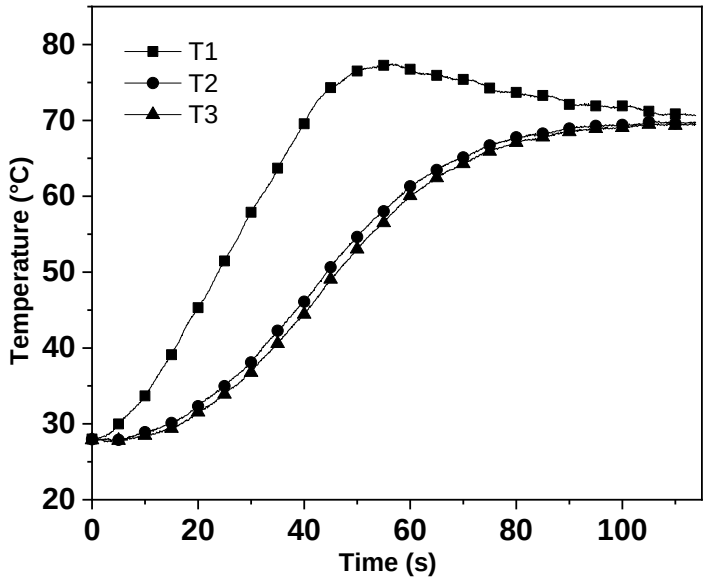

Figure 5.44 Variation of temperature with time for Cu-Cu bare interfaces, interfacial conditions: no load, smooth surface finish

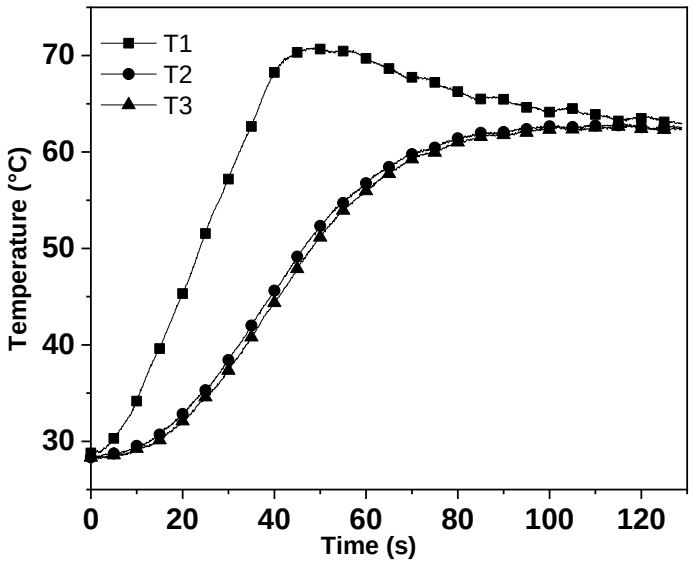

Figure 5.45 Variation of temperature with time for Cu-Cu interfaces, interfacial conditions: SG TIM, no load, smooth surface finish

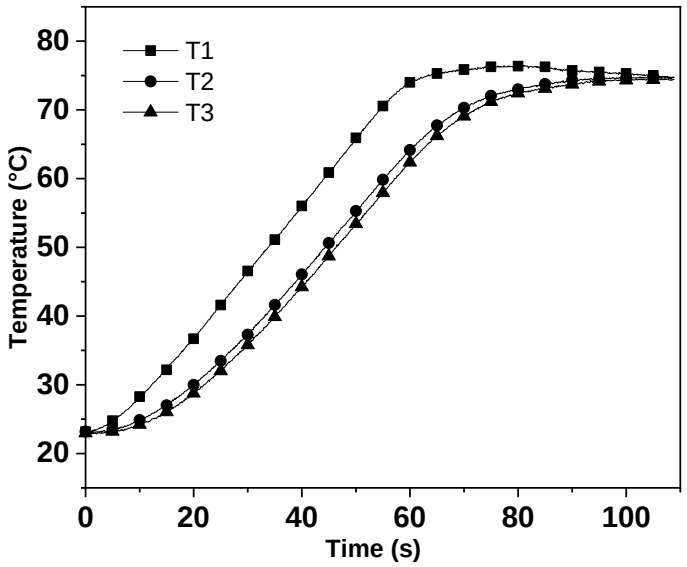

Figure 5.46 Variation of temperature with time for Cu-Cu interfaces, interfacial conditions: CTG TIM, no load, smooth surface finish

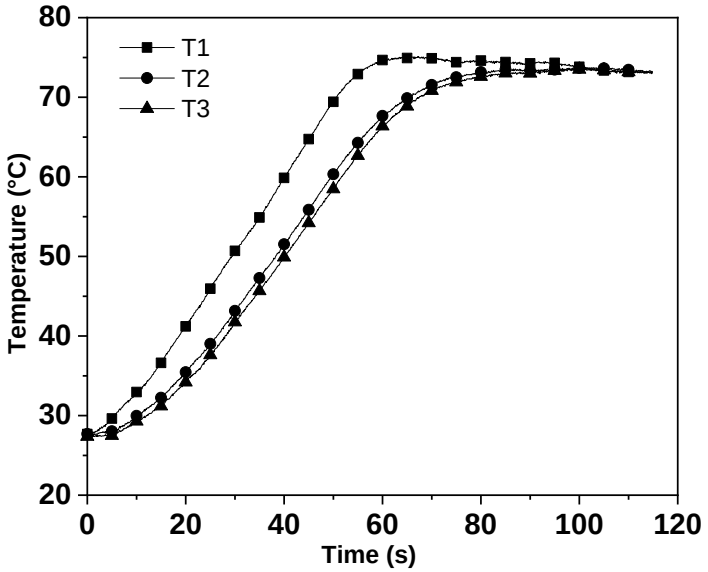

Figure 5.47 Variation of temperature with time for Cu-Cu interfaces, interfacial conditions: STP TIM, no load, smooth surface finish

5.7.2 Discussion

The thermal conformance of Cu-Cu interfaces with smooth surface finish was ascertained. The average surface roughness values (Ra) of the interfaces were 21.5 nm± 4.94nm. The conformance was studied by subjecting the interfaces to interfacial pressure from no load up to the range of 200kPa. The experiments were initially conducted for bare interfaces. Subsequently the interfaces were laced with TIMs with thermal conductivity ranging from 0.025W/m K to 7W/m K. The results of the experiments were tabulated in the Tables 14-17. It is evident from the experiments that for bare interfaces, increasing the interfacial pressure resulted in enhanced heat transfer. Similar trend was also observed for Cu-Cu interfaces with relatively rough surface finish. The experiments indicate that smooth surface finish results in enhanced thermal conformance. Among the TIMs employed, the application of STP resulted in superior heat transfer owing to the higher thermal conductivity. Further, beyond 40kPa, the application of interfacial pressure resulted in insignificant changes in the heat transfer across the interface.

Table 14 Effect of interfacial pressure on thermal conformance of bare Cu-Cu interface of smooth surface finish

Interfacial pressure (kPa)	η	Θ	t_g (s)
NL	0.44±0.04	0.65±0.03	42.53±2.95
40	0.62±0.01	0.78±0.005	47.23±1.22
100	0.61±0.01	0.77±0.005	47.8±2.56
200	0.68±0.04	0.82±0.02	53.16±2.73

Table 15 Effect of interfacial pressure on thermal conformance of smooth surface finish Cu-Cu interface with SG TIM

Interfacial pressure (kPa)	η	Θ	t_g (s)
NL	0.53±0.09	0.73±0.05	43.73±1.41
10	0.7±0.02	0.82±0.01	52.16±0.70
20	0.71±0.01	0.83±0.01	51.13±0.87
40	0.77±0.05	0.88±0.02	48.9±3.12
100	0.82±0.01	0.90±0.01	50.66±1.80
200	0.8±0.01	0.89+0.005	51.56±1.80

Table 16 Effect of interfacial pressure on thermal conformance of smooth surface finish Cu-Cu interface with CTG TIM

Interfacial pressure (kPa)	η	Θ	t_g(s)
NL	0.74	0.85	52.7±2.68
10	0.77±0.01	0.865±0.007	51.15±1.20
20	0.80±0.007	0.895±0.007	50.7±0.98
40	0.82±0.02	0.91±0.01	52.93±1.89
100	0.82±0.02	0.90±0.01	53.33±0.28
200	0.84±0.01	0.91±0.005	56.73±1.55

Table 17 Effect of interfacial pressure on thermal conformance of smooth surface finish Cu-Cu interface with STP TIM

Interfacial pressure (kPa)	η	Θ	t_g (s)
NL	0.75±0.005	0.87	49.7±0.95
10	0.80±0.01	0.89	53.5±1.37
20	0.84±0.01	0.91±0.005	55.16±1.20
40	0.87±0.01	0.93	55.5±2.06
100	0.86±0.005	0.93	53.8
200	0.90	0.95±0.005	61.13±2.02

5.8 The effect of interfacial pressure on heat transfer between Brass-Brass metallic contacts with interfacial media of varying thermal conductivity

5.8.1 Results

Figures 5.48 - 5.53 show the thermal history of Brass-Brass interfaces for various interfacial conditions.

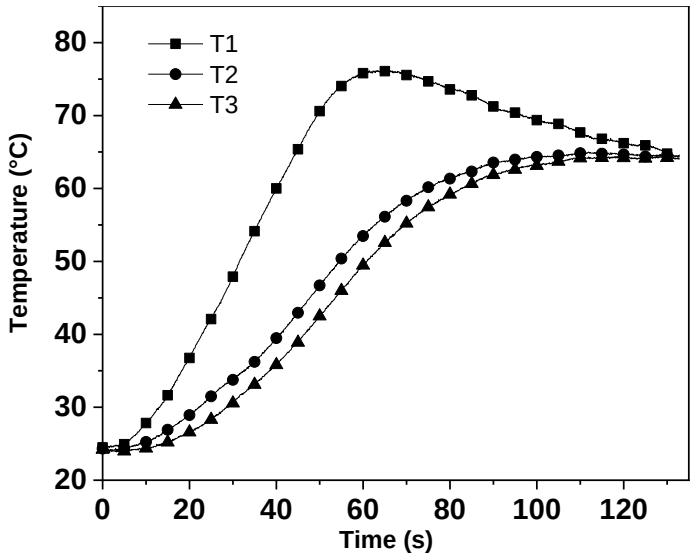

Figure 5.48 Variation of temperature with time for Brass-Brass bare interfaces under 10kPa interfacial pressure

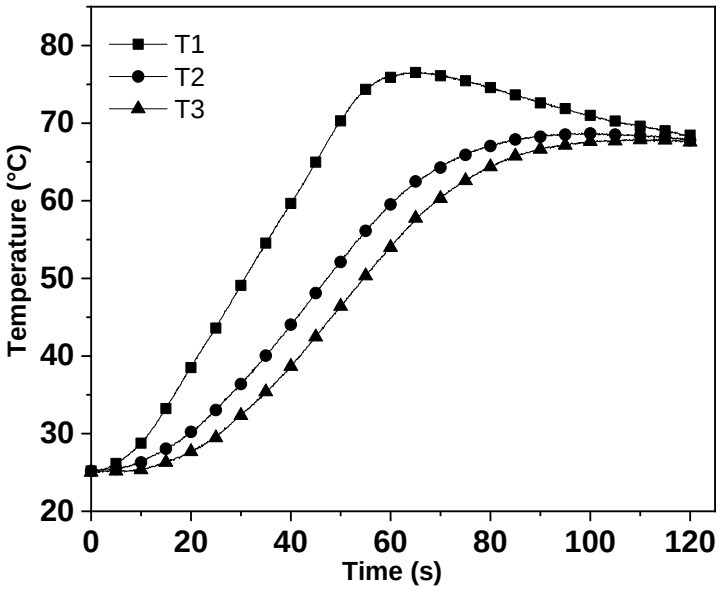

Figure 5.49 Variation of temperature with time for Brass-Brass bare interfaces under 20kPa interfacial pressure

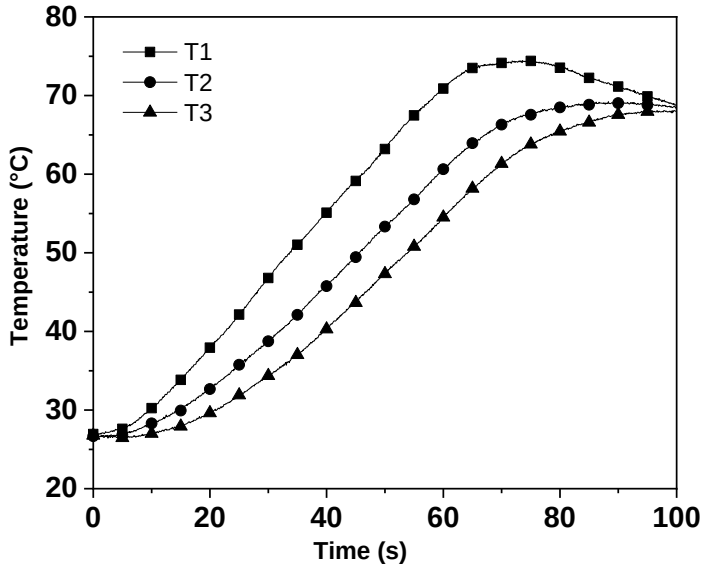

Figure 5.50 Variation of temperature with time for Brass-Brass bare interfaces under 200kPa interfacial pressure

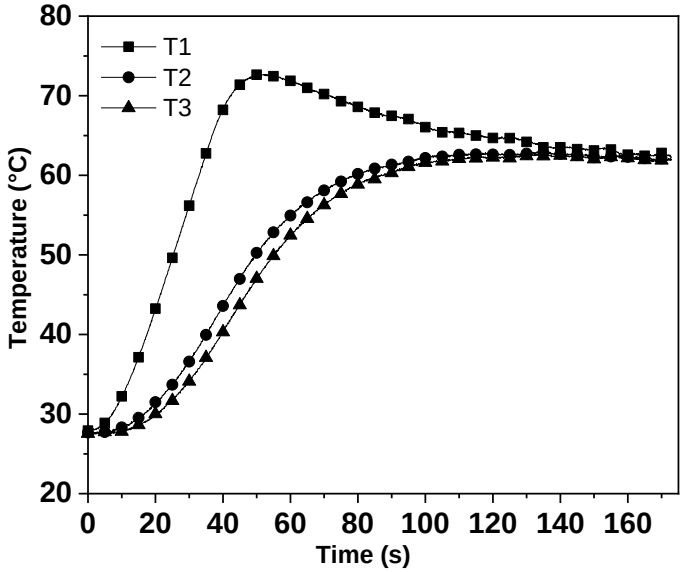

Figure 5.51 Variation of temperature with time for Brass-Brass interfaces, interfacial conditions: SG TIM and no load

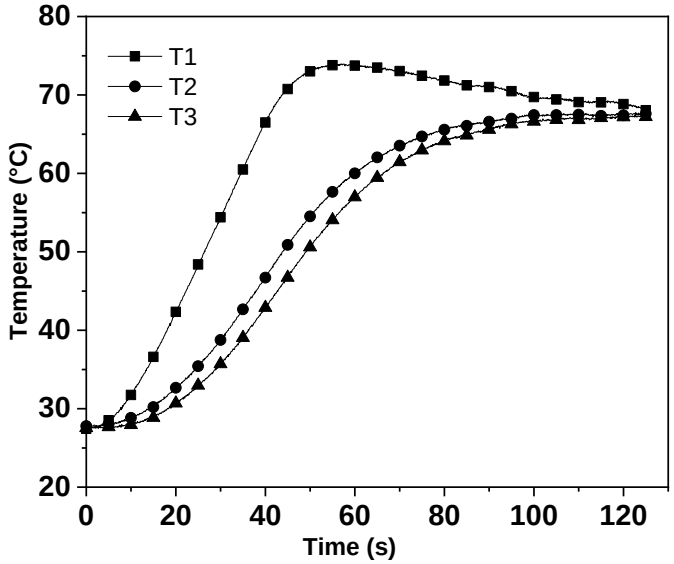

Figure 5.52 Variation of temperature with time for Brass-Brass interfaces, interfacial conditions: CTG TIM and no load

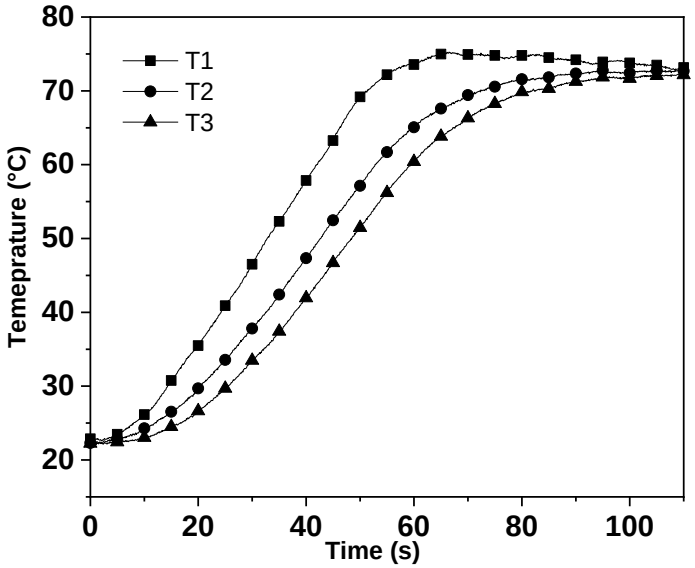

Figure 5.53 Variation of temperature with time for Brass-Brass interfaces, interfacial conditions: STP TIM and no load

5.8.2 Discussion

The thermal conformance of brass-brass interface was studied by subjecting the interfaces for interfacial pressure conditions ranging from no load to 200kPa with TIMs having varied thermal conductivity. The results of the experiments were tabulated in the Tables 18-21. It is evident from the experiments that for bare interfaces, increasing the interfacial pressure resulted in enhanced heat transfer. Similar trend was also found for Cu-Cu interfaces. The experiments indicate that superior surface finish results in enhanced thermal conformance. Among the TIMs employed, the application of STP resulted in superior heat transfer owing to the higher thermal conductivity.

Table 18 Effect of interfacial pressure on thermal conformance of bare brass-brass interface

Interfacial pressure (kPa)	**η**	**Θ**	**t_g (s)**
NL	0.20	0.52±0.015	40.03±2.62
40	0.48±0.01	0.72	44.76±1.44
100	0.50±0.03	0.73±0.02	45.56±0.30
200	0.59±0.015	0.78±0.005	54.3±1.81

Table 19 Effect of interfacial pressure on thermal conformance of brass-brass interface with SG TIM

Interfacial pressure (kPa)	η	Θ	t_g (s)
NL	0.37±0.02	0.65	42.05±0.21
10	0.48±0.02	0.71±0.02	48.55±1.34
20	0.56±0.03	0.76±0.02	49.03±1.19
40	0.71±0.01	0.86±0.01	49.4±0.26
100	0.72	0.88	49.16±0.73
200	0.77	0.91	55.83±0.75

Table 20 Effect of interfacial pressure on thermal conformance of brass-brass interface with CTG TIM

Interfacial pressure (kPa)	η	Θ	t_g (s)
NL	0.45	0.7±0.01	44.8±1.41
10	0.71±0.01	0.86	55.76±2.04
20	0.73±0.02	0.88	55.2±3.67
40	0.76±0.01	0.89	54.96±2.65
100	0.76±0.01	0.89	54.06±2.13
200	0.79	0.92	58.03±0.35

Table 21 Effect of interfacial pressure on thermal conformance of brass-brass interface with STP TIM

Interfacial pressure (kPa)	η	Θ	t_g (s)
NL	0.69	0.83	51.4
10	0.74	0.88	54.3±0.8
20	0.73	0.88	53.2±0.36
40	0.73	0.88	47.16±1.32
100	0.73	0.89	45.56±0.63
200	0.76	0.9	50.8±0.4

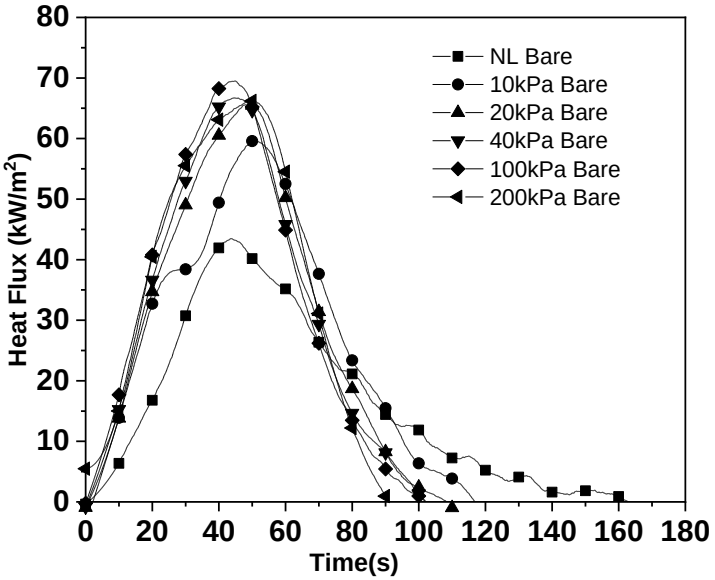

Figure 5.54 Effect of interfacial pressure on heat flux for the Brass-Brass bare interface

Figure 5.54 shows the variation of heat flux transients with time for Brass-Brass bare interfaces subjected to various interfacial pressures in the range of no load to 200kPa. It was found that increasing the interfacial pressure results in enhanced heat flux

transients across the interface. Figure 5.55 shows the effect of interfacial conditions on the heat transfer for Brass-Brass interfaces. Experiments reveal that the thermal conductivity of the TIMs play a role in determine the magnitude of heat transfer. Increasing the thermal conductivity of TIMs results in enhancement of heat transfer. Among the TIMs, application of STP TIM results in superior heat transfer when compared to SG TIM and CTG TIM owing to greater thermal conductivity of STP TIM. At higher loads, there was no significant difference in heat flux transient values of interfaces with SG TIM when compared to interfaces with CTG TIM. This could be attributed to the fact that the difference in thermal conductivity of SG TIM and CTG TIM is very minimal.

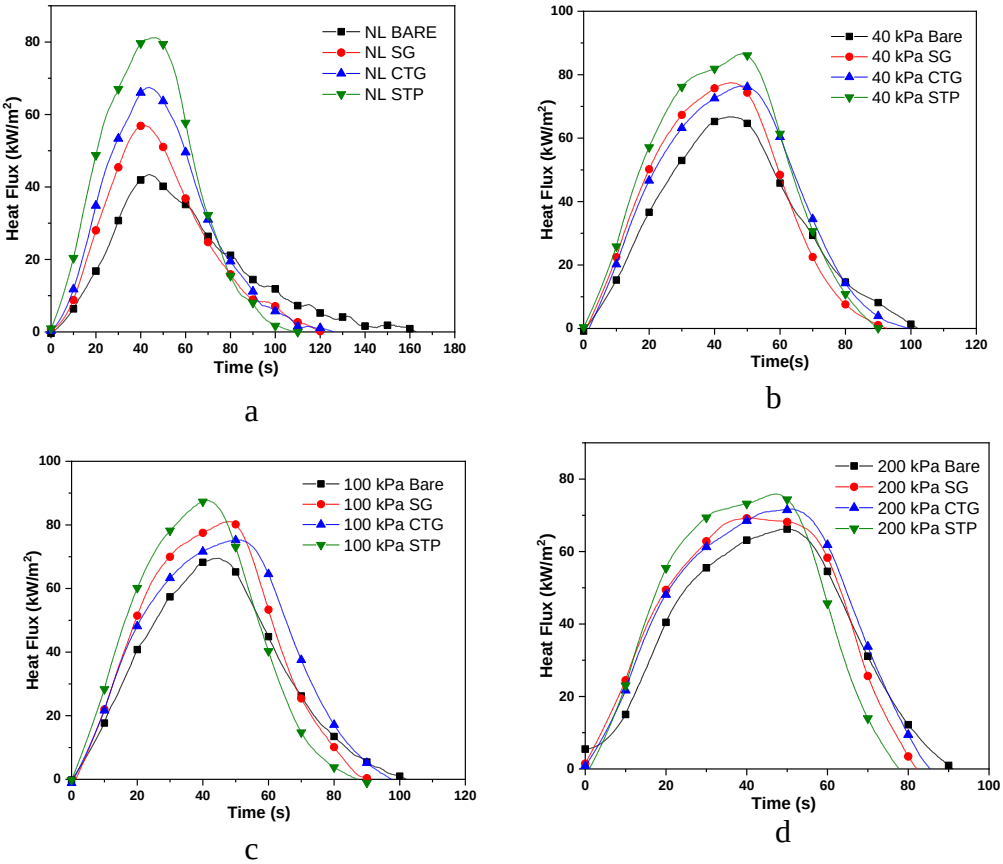

Figure 5.55 Effect of the interfacial condition on heat flux transients for Brass-Brass interface: (a) 2kPa (b) 40kPa (c) 100 kPa and (d) 200 kPa

Figures 5.56 - 5.59 show the effect of interfacial pressure on heat transferred (Q_2) to the sink in the case of bare, SG TIM, CTG TIM and STP TIM respectively. Experiments reveal that as the thermal conductivity increases the limiting value of the interfacial

pressure reduces. In case of STP TIM which has the highest thermal conductivity among the TIMs studied in the present study, the effect of interfacial pressure was insignificant suggesting that the role of interfacial pressure diminishes as the TIM with higher thermal conductivity is applied.

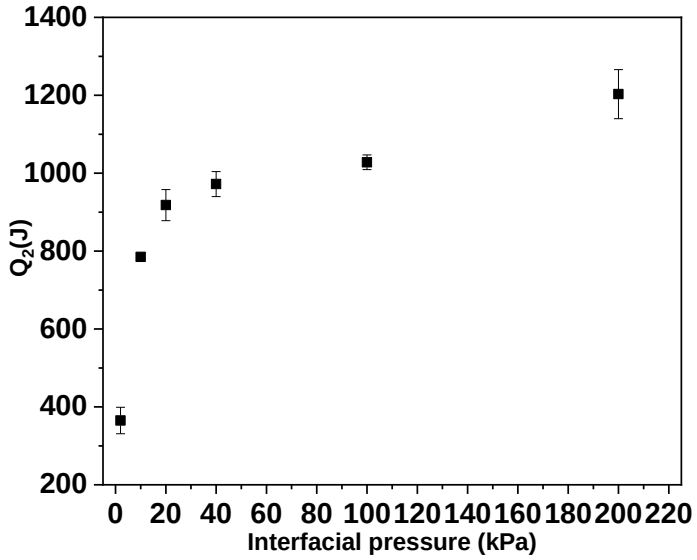

Figure 5.56 The effect of interfacial pressure on heat transferred (Q_2) to the sink for Brass-Brass bare interface (interfacial medium is air)

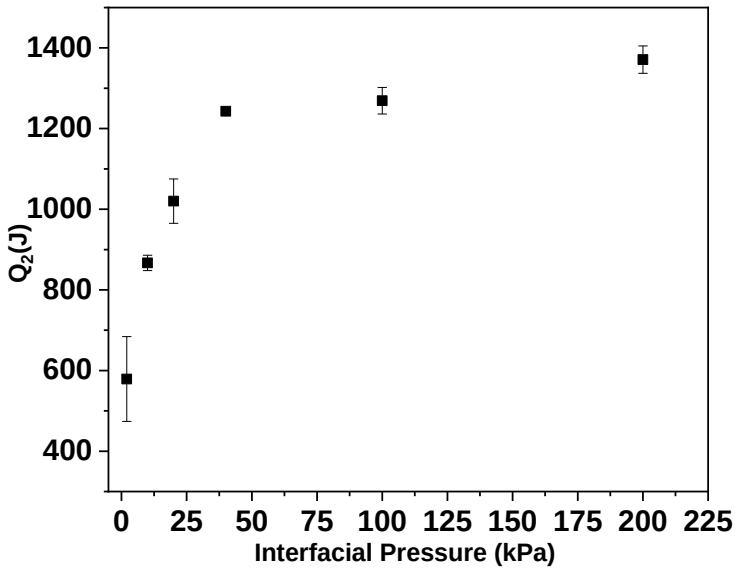

Figure 5.57 The effect of interfacial pressure on heat transferred (Q_2) to the sink for Brass-Brass interface with TIM (SG)

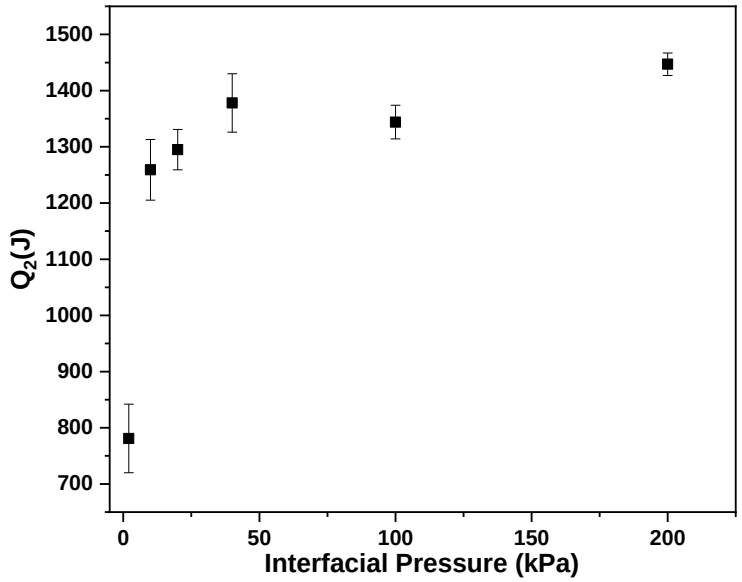

Figure 5.58 The effect of interfacial pressure on heat transferred (Q_2) to the sink for Brass-Brass interface with TIM (CTG)

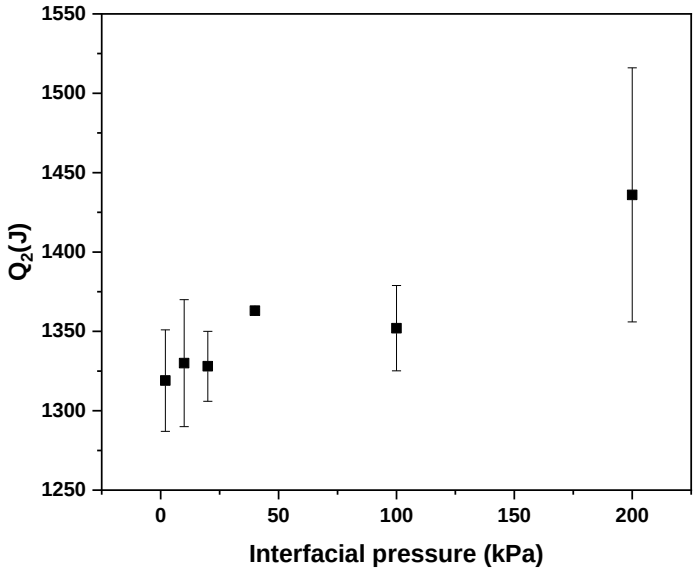

Figure 5.59 The effect of interfacial pressure on heat transferred (Q_2) to the sink for Brass-Brass interface with TIM (STP)

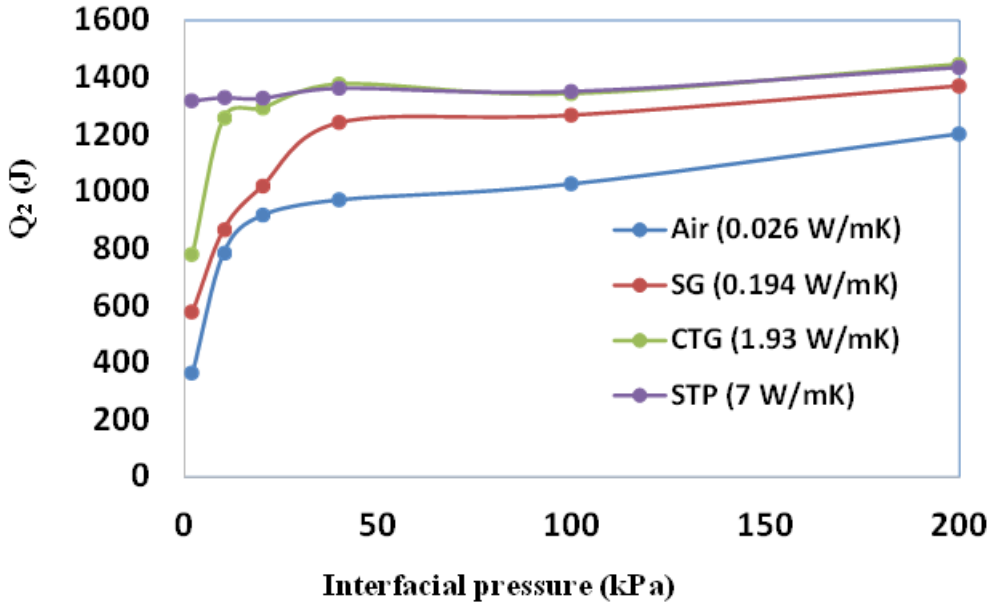

Figure 5.60 The effect of thermal conductivity of TIMs on heat transferred to the sink

The effect of interfacial pressure and thermal conductivity of the interfacial medium on heat transfer was determined by estimating the magnitude of heat absorbed by the sink material. The average surface roughness (R_a) of the brass source and sink were 23.32 ± 7.67 nm and 19.08 ± 9.70nm respectively. The heat flux transients were integrated till the source material reached a target temperature of 70°C. The integrated values were multiplied by the contact area to obtain the total heat flow (Q_2) to the sink material. Q_1 is the heat required to raise the temperature of the source to the target temperature of 70°C. Figure 5.56 shows the variation of Q_2 with the interfacial pressure for Brass-Brass bare interfaces. As the interfacial pressure was increased from no pressure condition to higher interfacial pressure conditions, the heat flux also increases. This is attributed to the increase in contact area at the interface as the interfacial pressure is increased. Apart from the heat flux the, average value heat transferred to the sink (Q_2) in case of bare interfaces for NL, 10kPa, 20kPa, 40kPa, 100kPa and 200kPa is 365,785,918,972,1028,1203 J respectively. Thus, the effect of interfacial pressure on heat transfer in the case of Brass-Brass bare interfaces was significant. It can be concluded that as the interfacial pressure increases the Q_2 also increases. However, the rate at which the Q_2 increases decrease with the increase in interfacial pressure. The experiments were conducted for interfaces with SG as TIM. Under no load conditions, as SG was applied, the average heat transferred was recorded to be 579 J. Thus, there was a 59 pct increase in the heat transferred across the interface upon application of SG TIM when compared to bare interfaces under no load conditions. Figure 5.57 shows the effect of interfacial pressure on heat transferred (Q_2) to the sink with TIM (SG) at the interface. The heat transfer values were 867J and 1020J when the pressure was increased to 10kPa and 20kPa respectively. The experiments revealed that the application of TIM resulted in enhancement in heat transferred across the interface. Further, as the interfacial pressure was increased to 40kPa, there was a 114 pct increase in heat transfer for interfaces with SG as TIM when compared to interfaces with SG as TIM under no load conditions. However, beyond 40kPa the enhancement in heat transfer is insignificant as there was only about 10 pct increase in the heat transferred across the interface with the increase in load from 40kPa to 200kPa. The amount of heat transferred across the interface for interfaces with SG as TIM for 10kPa, 20kPa, 40kPa, 100kPa and 200kPa was 867, 1020, 1243,1269,1371J respectively. Further, when

compared to the bare interfaces, interfaces with SG as TIM showed superior heat transfer for all the loading condition owing to the replacement of poor conductive air by SG TIM. In case of interfaces with SG as TIM 40kPa is the limiting value of pressure beyond which the increase in heat flux is insignificant. Experiments were conducted for interfaces with commercially available thermal grease (CTG) as TIM. Figure 5.58 shows the effect of interfacial pressure on heat transferred (Q_2) to the sink with TIM (CTG) at the interface. The application of CTG further increase the heat transfer across the interface. The application of CTG as TIM resulted in average heat transfer value of 781J. Thus, application of CTG as TIM resulted in higher magnitudes of heat transfer across the interface when compared to SG as TIM owing to higher thermal conductivity of CTG. Increase in the interfacial pressure resulted in even higher magnitudes of heat transfer values. The magnitude of heat transfer across interface with CTG as TIM for 10 kPa was estimated to be 1259 J. Raising the interfacial pressure to 20 kPa led to a slight increase in heat transfer, bringing the value to 1295 J. There was no significant increase in the heat transfer beyond 10 kPa. Thus, 10 kPa is the limiting value of pressure beyond which the increase in heat transfer value is insignificant. However, for all the interfacial pressure conditions the magnitude of heat transfer was higher in case of interfaces with CTG as TIM when compared to SG TIM. The effect of interfacial pressure on heat transferred (Q_2) to the sink with TIM (STP) was studied. The variation of Q_2 with the interface pressure is shown in the figure 5.59. The application of STP as TIM resulted in heat transfer value of 1319 J under no load condition, which about 69 pct higher when compared to interfaces CTG as TIM. When compared to bare interfaces and interfaces with SG as TIM the increase was 261% and 129% respectively for interfaces with STP as TIM. However, increase in the interfacial pressure did not affect the heat transfer values indicating that, upon application of high thermal conductive TIMs the interfacial pressure has no effect on the heat transfer.

Figure 5.60 shows the effect of thermal conductivity of TIMs on the heat transfer across the Brass-Brass interface. Experiments revealed that as the thermal conductivity of the TIM increased the heat transferred to the sink (Q_2) also increases especially at lower interfacial pressures. The effect of interfacial pressure on heat transfer was found to be minimal when a TIM of high thermal conductivity is used. The increase in interfacial

pressure and the application of TIMs both increase the heat transfer across the interface. However, in microelectronic applications, the application of high conductivity TIMs is a better option for obtaining superior performance. The application of higher interfacial pressures when TIMs are being used may also result in flow out of TIMs leading to a possible reduction in heat transfer across the interface. The use of high performance TIMs therefore reduces the need for the use of high interfacial pressures in applications where such high pressures are not feasible.

5.9 Effect of interfacial pressure and TIM on heat transfer on metal-metal contacts with L/D ratio of 5.

5.9.1 Results

The experiments were conducted for interfaces with L/D=5. Figure 5.61 shows the variations in Temperature vs Time for Cu-Cu bare interfaces under no load. Figure 5.62 shows the variations in Temperature vs Time for Cu-Cu bare interfaces under 200 kPa interfacial pressure. Figure 5.63 and 5.64 show the variations in temperature vs time for Cu-Cu interfaces with SG TIM under no load and 200kPa interfacial pressure respectively.

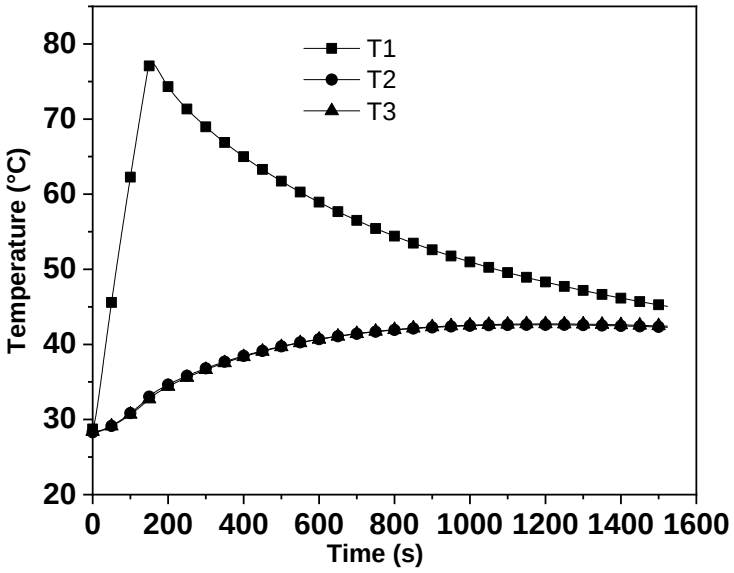

Figure 5.61 Variations in temperature with time for Cu-Cu bare interfaces under no load

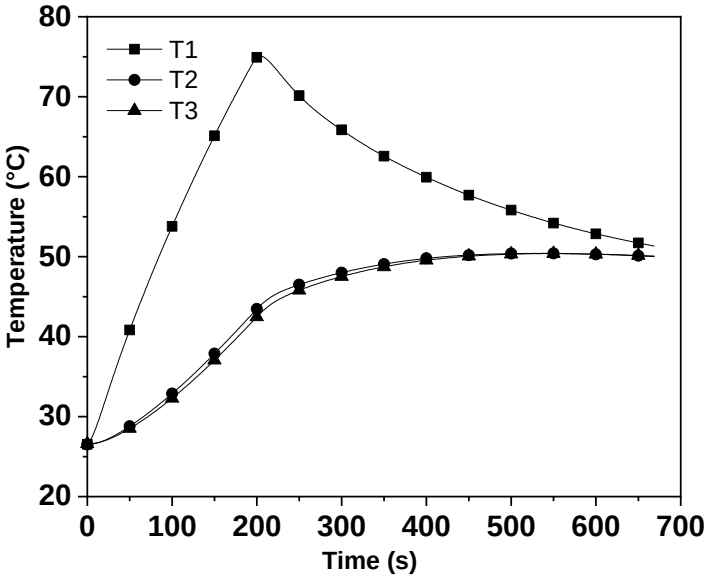

Figure 5.62 Variations in temperature with time for Cu-Cu bare interfaces under 200 kPa interfacial pressure

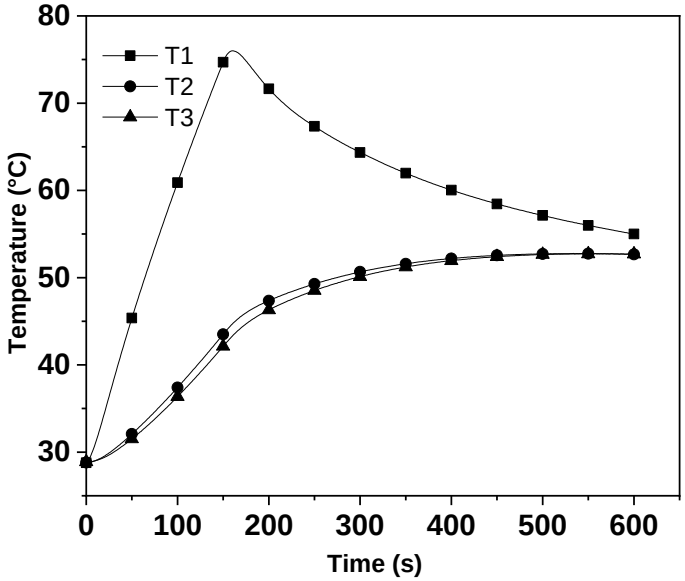

Figure 5.63 Variations in temperature with time for Cu-Cu interfaces with SG TIM under no load

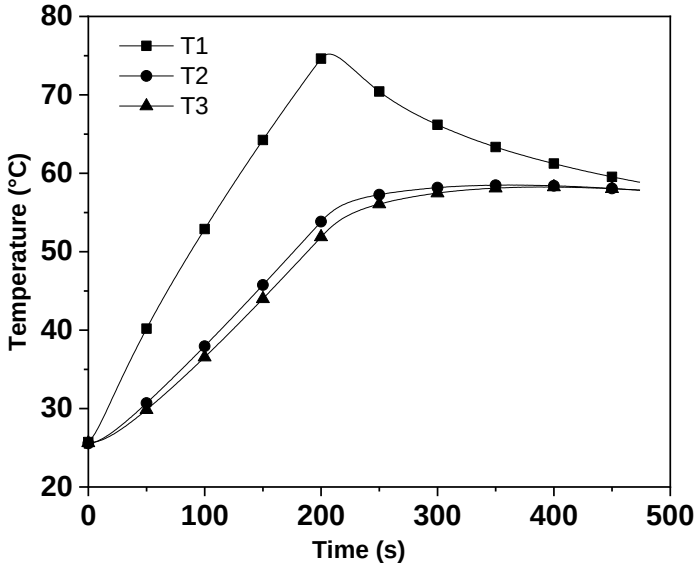

Figure 5.64 Variations in temperature with time for Cu-Cu interfaces with SG TIM under 200 kPa interfacial pressure

5.9.2 Discussion

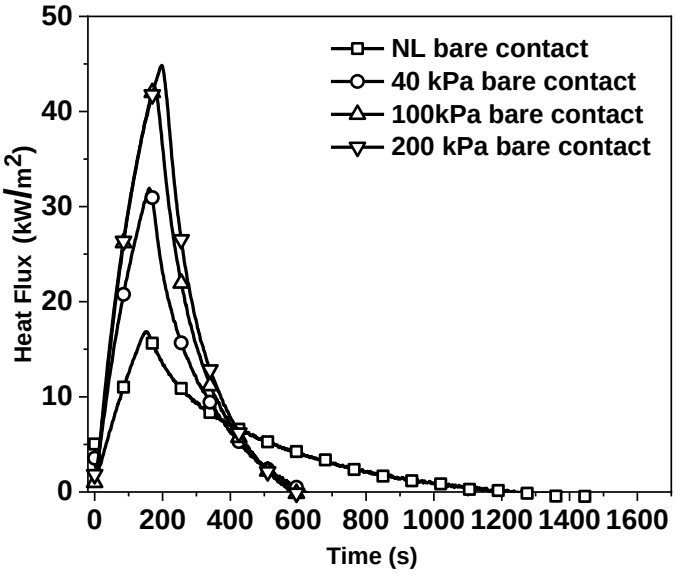

Figure 5.65 Variation of heat flux with time for Cu-Cu bare interfaces subjected to varying interfacial pressures.

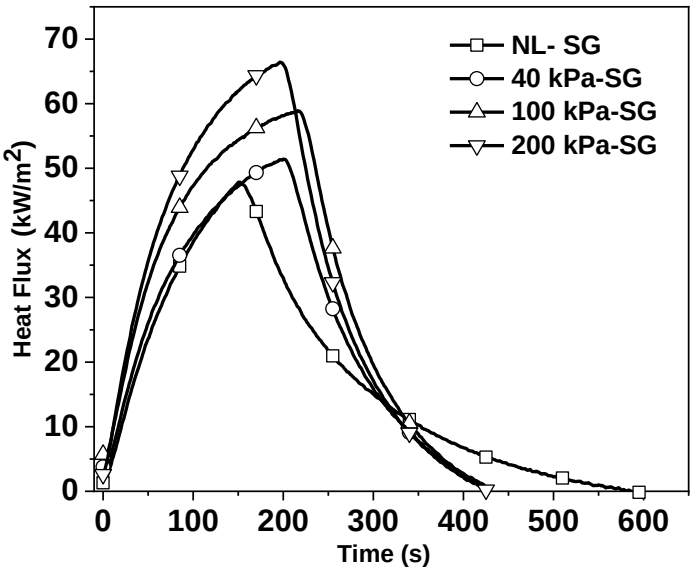

Figure 5.66 Variation of heat flux with time for Cu-Cu interfaces with SG TIM subjected to varying interfacial pressures.

Experiments were conducted for Cu-Cu interfaces with L/D ratio of 5. The variation in the heat flux values for bare interface and for interface with silicone grease is plotted in figures 5.65 and 5.66 respectively. With the increase in the interfacial pressure, the peak heat flux also increased. Similar trends were observed for specimens with L/D ratio of 1. The application of silicone grease as TIM resulted in enhancement of peak heat flux values. The peak heat flux values for no load, 40kPa, 100kPa and 200kPa for the interfaces with SG as TIM were 47.85kW/m^2, 51.42kW/m^2, 58.91kW/m^2 and 66.42kW/m^2 respectively. Similarly, the corresponding peak heat flux for bare interfaces were 16.83kW/m^2, 31.94kW/m^2, 42.60kW/m^2 and 44.84kW/m^2 respectively.

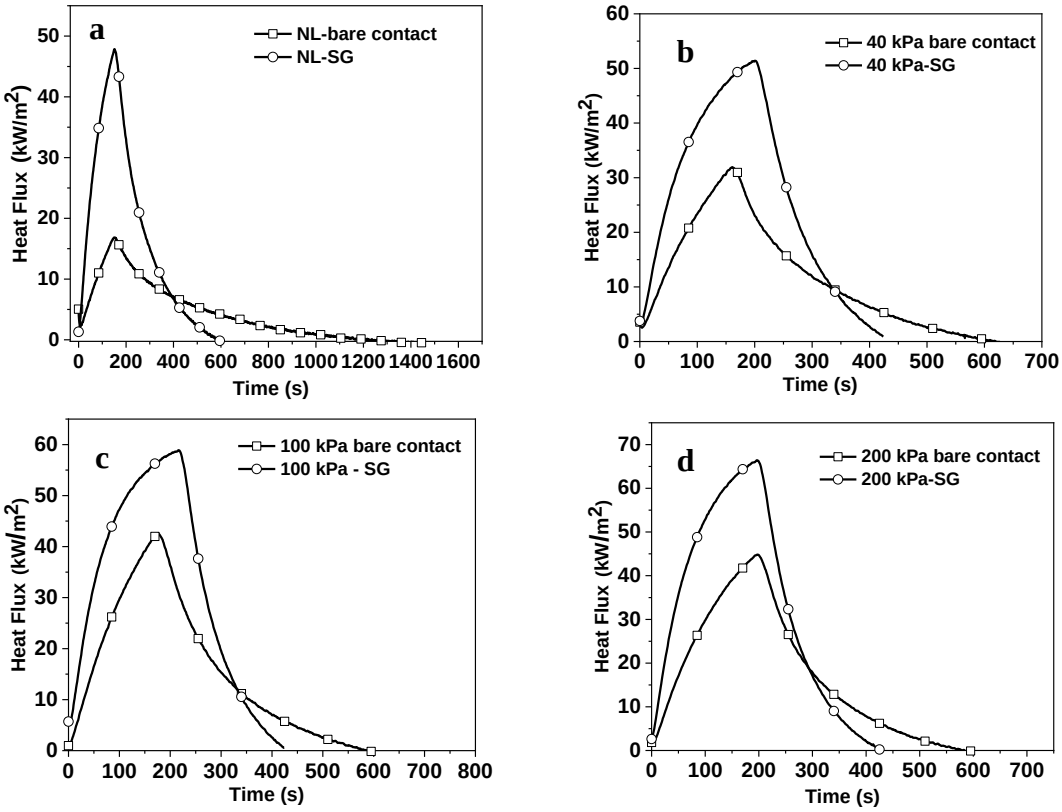

Figure 5.67 Variation of heat flux with time for bare and for interfaces with TIM for Cu-Cu interfaces a) No load b) 40kPa c) 100kPa d) 200kPa interfacial pressure

Figure 5.67 shows the comparison of heat flux with time for bare and for interfaces with silicone grease as TIM for specimens with L/D ratio of 5. The application of silicone grease as TIM resulted in the rise in peak heat flux for each of the loading conditions. Thus, it can be concluded that the addition of silicone grease as TIM results in increase in peak heat flux values irrespective of L/D ratio employed. The introduction of silicone grease replaces poor conductive air at the interface resulting in enhanced heat transfer.

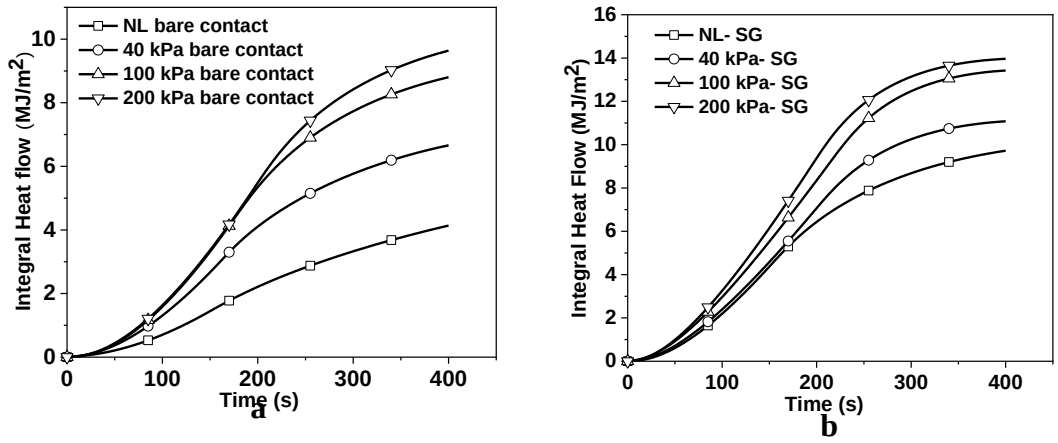

Figure 5.68 Variation of Integral heat flow with time for specimens a) bare interface b) interface with TIM.

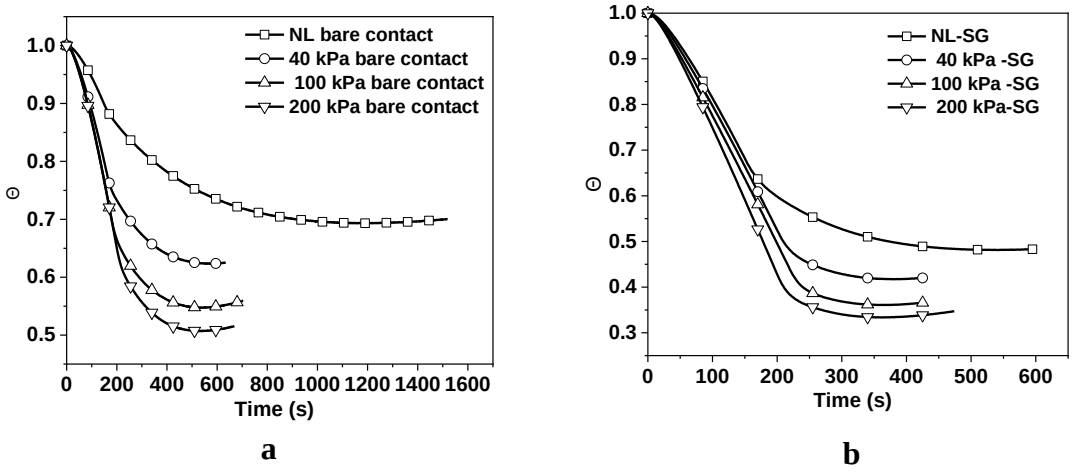

Figure 5.69 Variation in dimensionless transient temperature with time for specimens a) bare contacts b) interfaces with TIM

The determination of integral heat flow showed that with the application of silicone grease, there is a significant improvement in heat transfer across the interface. Also, the integral heat flow was found to increase with the increase in interfacial pressure even for specimens with L/D ratio of 5. Figure 5.68 show the variation in the integral heat flow with time for interfaces with and without TIM.

The integral curve for 400 seconds was plotted. The integral values are shown in Table 22 and were calculated. For, bare interfaces, the increase in integral heat flow as the interfacial pressure was applied from no load condition to 40kPa and further from

40kPa to 100kPa resulted in an increase of 61% and 32% respectively. Furthermore, increasing the interfacial pressure to 200kPa from 100kPa resulted in just over 9% in the values of integral heat flow. Similar trends were noticed in the case of L/D ratio of 1. The analysis of integral curve and peak heat flux reveals that addition of silicone grease as TIM results in efficient heat transfer across interfaces owing to the replacement of air with comparatively higher thermal conductive silicone grease TIM. The increase in integral heat flow was observed for all the loading conditions, with an increase as high as 135% for no load condition and an increase of 44% in case of interfacial pressure of 200kPa. For interfaces with silicone grease as TIM, increasing the interfacial pressure beyond 100kPa to 200kPa did not result in significant changes in heat flow value. The possible reason has already been discussed for the case of specimens with L/D ratio of 1. The explanation also holds good for specimens with L/D ratio of 5.

The experiments also showed that in the case of specimens with L/D ratio of 5, for bare contacts, increasing the interfacial pressure from no load condition to 200kPa resulted in a rise of 133% in the integral heat flow value, whereas in the case of interfaces with silicone grease, an increase in the interfacial pressure from no load condition to 200kPa resulted in 43.62% rise in the value. This indicates that the effect of interfacial pressure on thermal contact resistance is significant when TIM was not used, even under the case of transient conditions.

Table 22 Values of peak heat flux and integral heat flow for Cu-Cu interfaces with L/D =5

Sl No	TIM/interface condition	Interfacial pressure (kPa)	Peak heat flux (kW/m^2)	Integral heat flow (MJ/m^2)
1	bare contact	NL	16.83	4.13
2	bare contact	40	31.94	6.66
3	bare contact	100	42.60	8.80
4	bare contact	200	44.84	9.63
5	silicone grease	NL	47.85	9.72
6	silicone grease	40	51.42	11.07
7	silicone grease	100	58.91	13.42
8	silicone grease	200	66.42	13.96

The analysis of dimensionless transient temperature for specimens with L/D of 5 showed that, increasing the load and the application of TIM at the interfaces results in higher heat absorption by heat sinks (figure 5.69). For bare contacts, the time taken by the heat sink to reach 70% of the maximum temperature is about 700s. However, with the application of silicone grease TIM, the heat sink took just around 180s. As the interfacial pressure was increased to 200kPa for bare interfaces, the time taken by the heat sink to reach about 70% of the maximum temperature was about 200s. However, as the interfacial pressure gets increased to 200kPa for interfaces with silicone grease, about 70% of maximum temperature attained by the heat sink by around 120s. Hence, it was concluded that the interfacial pressure and the TIM have an effect on the conformance of the contacting surfaces even in the case of L/D ratio of 5. Similar effect was found in case of specimens with L/D ratio of 1.

5.10 Effect addition of MWCNT in heat transfer across the metal-metal interface with L/D=5

5.10.1 Results

Experiments were carried out to study the effect of the addition of MWCNT to the interface material on contact heat transfer for Cu-Cu interfaces with L/D ratio of 5. Figure 5.70 -5.71 shows the variation of temperature with time for Cu-Cu interfaces with 0.1wt% MWCNT-SG TIM and 1 wt % MWCNT- SG TIM under no load conditions.

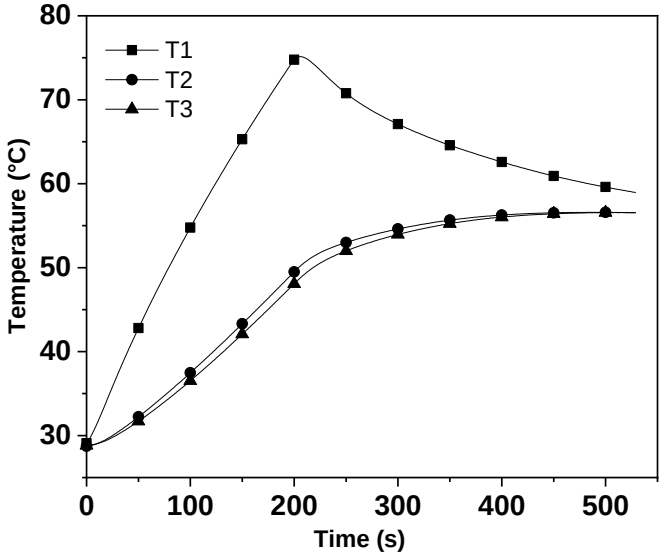

Figure 5.70 Variation of temperature with time for Cu-Cu interfaces, interfacial conditions: 0.1 wt % MWCNT- SG TIM under no load

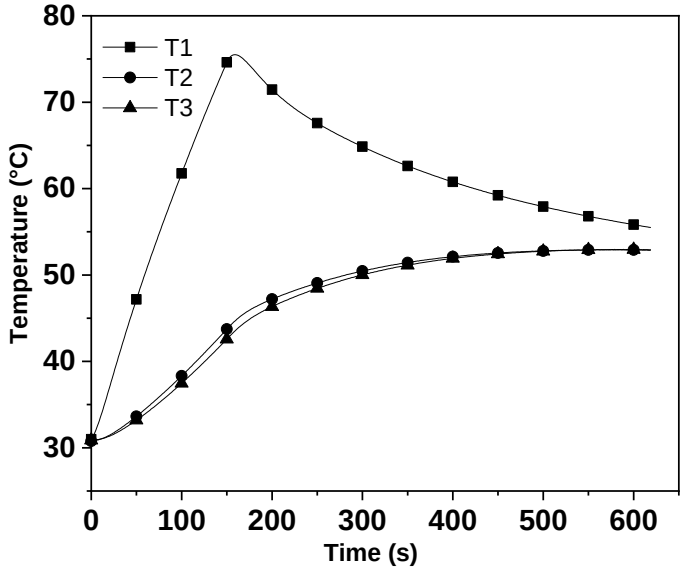

Figure 5.71 Variation of temperature with time for Cu-Cu interfaces, interfacial conditions: 1 wt % MWCNT- SG TIM under no load

5.10.2 Discussion

Experiments were carried out to study the effect of the addition of MWCNTs to the interface material on contact heat transfer for Cu-Cu interfaces with L/D of 5. Figure 5.72 - 5.75 show the interfacial heat flux transients when silicone grease and MWCNT-SG were used as TIM for NL, 40kPa, 100kPa and 200kPa interfacial pressure respectively.

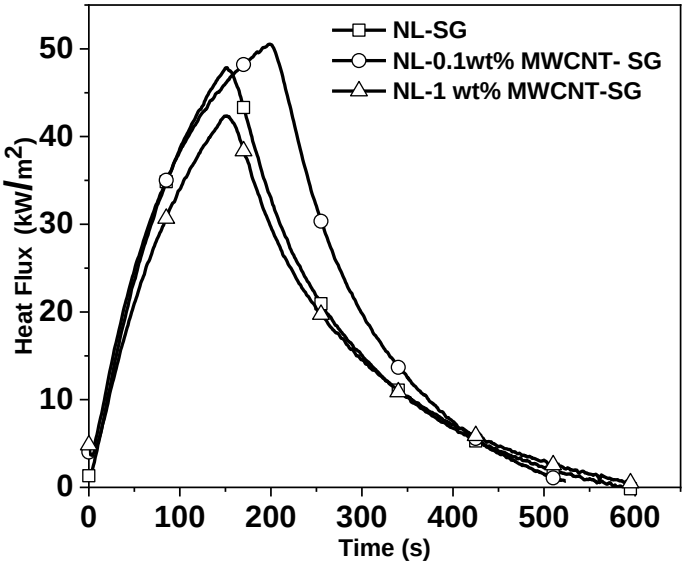

Figure 5.72 Variation of heat flux with time for Cu-Cu interfaces, interfacial conditions: SG TIM, MWCNT-SG TIM, no load condition

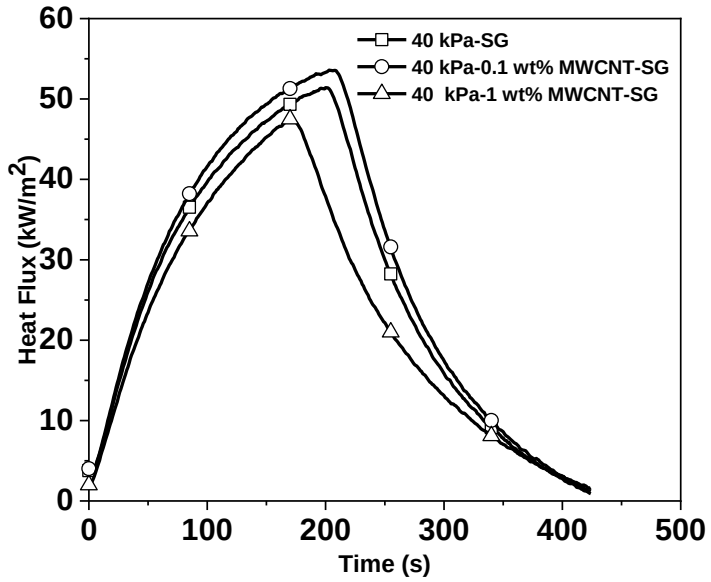

Figure 5.73 Variation of heat flux with time for Cu-Cu interfaces, interfacial conditions: SG TIM, MWCNT-SGTIM, 40kPa

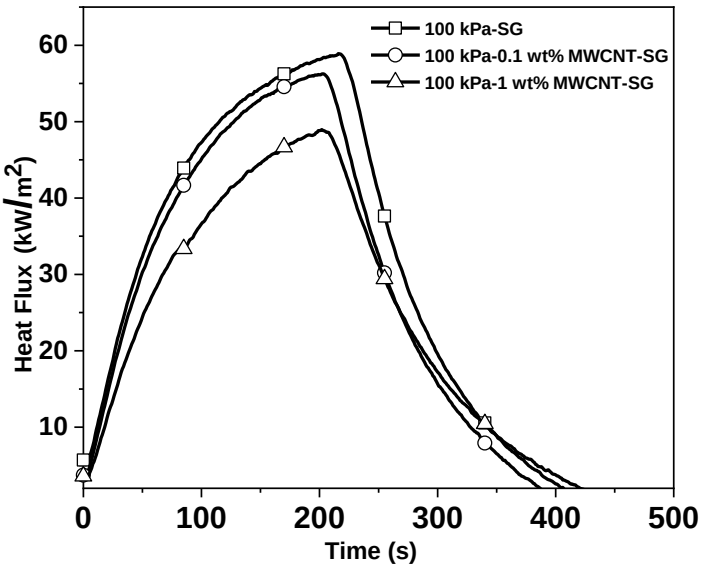

Figure 5.74 Variation of heat flux with time for Cu-Cu interfaces interfacial conditions: SGTIM, MWCNT-SGTIM,100kPa

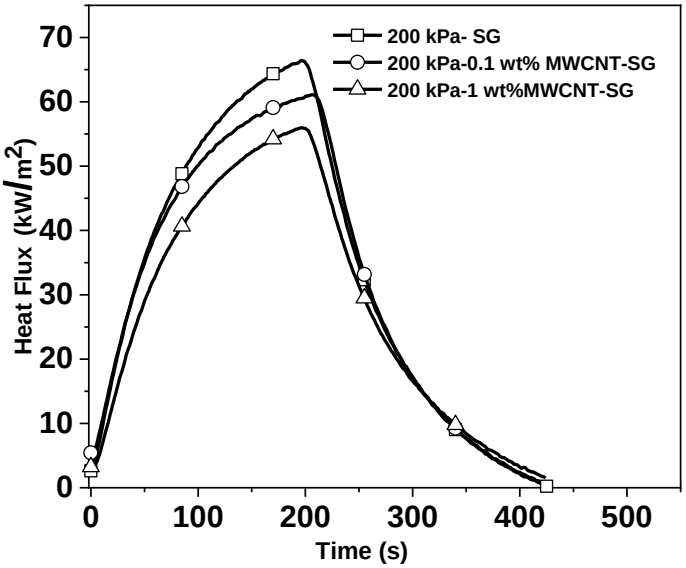

Figure 5.75 Variation of heat flux with time for Cu-Cu interfaces, interfacial conditions: SG TIM, MWCNT-SGTIM, 200kPa

Experiments were carried out to study the effect of the addition of MWCNTs to the interface material on contact heat transfer. For no load condition, the addition 0.1 MWCNTs to silicone grease resulted in increase in peak heat flux and the integral heat flow. Table 23 shows the values of peak heat flux and integral heat flow values across interface for specimens with L/D ratio of 5. The study found that the addition of MWCNT to silicone grease at 0.1 wt% resulted in enhancement of heat flow. This could be attributed to the ability of MWCNTs to attain percolation at lower fractions (Hansson et al. 2018). However, the heat flow deteriorated at higher interfacial pressures. Further, increase in the MWCNT fraction to 1 wt% resulted in deterioration in heat flow values under all interfacial loading conditions. It is clear from the experiments that the addition of silicone based TIMs increases the heat transfer across the interface irrespective of the L/D ratio of the metal-metal contacts employed. The results also indicate that, MWCNT impregnated silicone grease with 0.1 wt% shows superior performance when compared to the silicone grease with 1 wt% MWCNTs. The possible explanation for the deterioration could be based on rheology of the particle laden polymer TIMs (Prasher et al. 2003) as discussed in the earlier case where the metal-metal contacts with

L/D ratio of 1 was used. (Fabris et al. 2011) in their study also noted that increasing the CNT results in formation of paste that is thick and difficult to spread resulting in higher viscosity of TIMs causing enhanced thermal contact resistance. Table 24 shows the contact resistance values for specimens with L/D ratio of 1 and 5 for various interfacial conditions and for interfaces with and without TIMs. The experiments reveal that the contact resistance decreases with the increase in the interfacial pressure and the application of TIMs.

Table 23 Peak heat flux and integral heat flow under curve for specimens with L/D of 5

Sl No	TIM	Interfacial pressure (kPa)	Peak heat flux (kW/m^2)	Integral heat flow (MJ/m^2)
1	SG	NL	47.85	9.72
2	SG with 0.1 wt % MWCNT	NL	50.53	11.49
3	SG with 1 wt % MWCNT	NL	42.34	8.88
4	SG	40	51.42	11.07
5	SG with 0.1 wt % MWCNT	40	53.59	11.80
6	SG with 1 wt % MWCNT	40	47.49	9.54
7	SG	100	58.91	13.42
8	SG with 0.1 wt % MWCNT	100	56.26	12.13
9	SG with 1 wt % MWCNT	100	48.96	10.82
10	SG	200	66.42	13.96
11	SG with 0.1 wt % MWCNT	200	61.11	13.54
12	SG with 1 wt % MWCNT	200	55.97	12.05

Table 24 Contact resistance values for specimens with L/D ratio of 1 and 5 for various interfacial conditions

Contact resistance → / Interfacial condition ↓	Peak thermal contact resistance (cm^2 °C/W) for specimens with L/D=1	Mean thermal Contact resistance (cm^2 °C/W) for specimens with L/D=1	Peak thermal contact resistance (cm^2 °C/W) for specimens with L/D=5	Mean thermal Contact resistance (cm^2 °C/W) for specimens with L/D=5
NL	24.52	24.33	29.12	24.85
40kPa	11.60	10.76	12.34	10.81
100kPa	7.07	6.4	9.30	7.93
200kPa	5.87	4.63	7.88	7.01
NL SG	11.71	11.1	7.14	6.45
40kPa SG	5.90	4.99	4.52	4.50
100kPa SG	4.14	2.26	3.70	3.71
200kPa SG	3.06	1.47	3.28	3.21
NL 0.1wt% MWCNT	5.84	4.86	5.13	4.99
40kPa 0.1wt% MWCNT	4.78	3.33	4.29	4.28
100kPa 0.1wt% MWCNT	3.72	2.42	3.91	3.79
200kPa 0.1wt% MWCNT	3.17	1.95	3.14	3.10
NL 1wt% MW CNT	7.74	7.18	7.95	7.28
40kPa 1wt% MWCNT	5.62	4.81	6.14	5.74
100kPa 1 wt% MWCNT	3.78	2.69	5.32	5.16
200kPa 1wt% MWCNT	2.88	1.65	3.93	3.86

To compare the effect of L/D ratio on heat flow, R_T (thermal contact resistance) vs $\triangle T_{max}$ was plotted. Figure 5.76a shows the variation of R_T with maximum temperature difference ($\triangle T_{max}$) for both specimens of L/D ratio of 1 and 5. The analysis shows that, as the maximum temperature difference between the upper specimen and lower specimen increases, the thermal contact resistance also increases exponentially. From the figure 5.76b it is evident that with the increase in the maximum temperature

difference, the heat extracted by the lower specimen also decreases. The study reveals that thermal contact resistance depends on $\triangle T_{max}$ for all interfacial conditions irrespective of L/D ratio used.

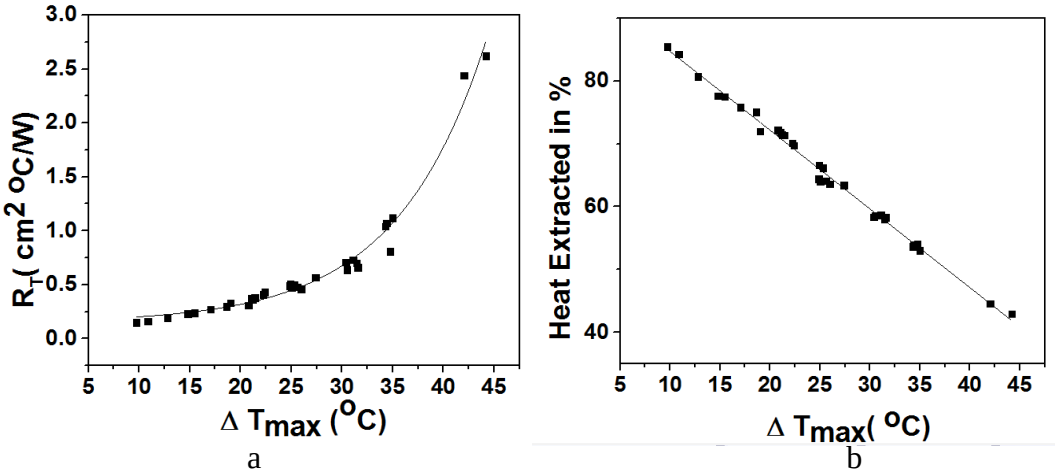

Figure 5.76 Variation of a) Thermal contact resistance (R_T) vs $\triangle T_{max}$ b) Heat extracted vs $\triangle T_{max}$

5.11 Effect of 1-Methyl-2 pyrrolidone (NMP) on the enhancement of heat transfer across the metal- metal interface.

5.11.1 Results

Experiments were conducted to study the effect of 1-Methyl-2 pyrrolidone (NMP) on the heat transfer enhancement across the metal- metal interface. Figure 5.77 and 5.78 show the variation of temperature with time for NMP treated Cu-Cu and Brass-Brass interfaces with L/D ratio of 1 under no load conditions respectively.

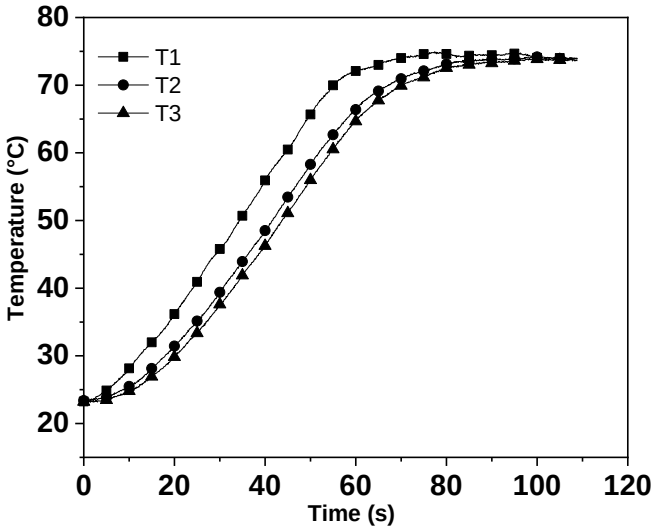

Figure 5.77 Variation of temperature with time for Cu-Cu interfaces, interfacial conditions: NMP treated, no load

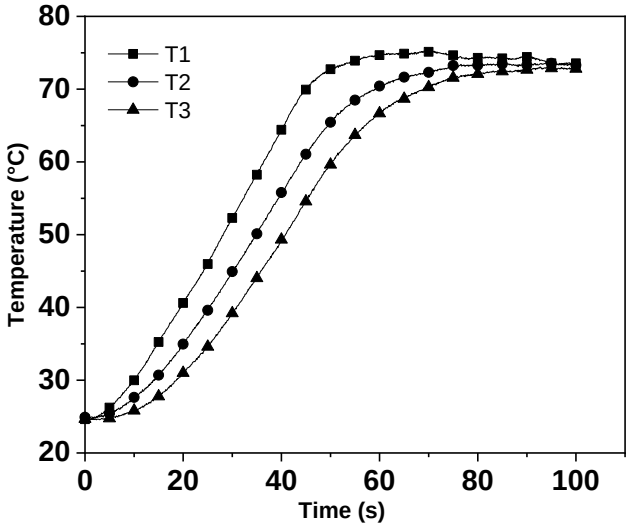

Figure 5.78 Variation of temperature with time for Brass-Brass interface, interfacial conditions: NMP treated, no load

The surface roughness parameters measured for the Cu-Cu and Brass-Brass interfaces are given in Table 25.

Table 25 Surface roughness values of Cu and Brass specimens with and without NMP treatment

Material	Without NMP		NMP treated	
	R_a (nm)	R_z (nm)	R_a (nm)	R_z (nm)
Cu	21.25	189.6	11.07	110
Brass	26.25	480.5	24.5	387.5

5.11.2 Discussion

Table 26 gives the thermal conformance of Cu-Cu, Brass-Brass NMP treated surfaces under no load and 200kPa interfacial pressure.

Table 26 Thermal conformance parameters for NMP treated metal-metal interface

Material	Interfacial pressure (kPa)	Q_1 (kJ/m^2)	Q_2 (kJ/m^2)	η	Θ	t_g (s)
Cu-Cu	NL	3791±280	3074±277	0.82±0.007	0.89	53.5±2.12
Cu-Cu	200	3848±7.07	3416±3.53	0.88	0.93	59
Brass-Brass	NL	3622±176	2557±160	0.7±0.014	0.865±0.007	43.5±2.12
Brass-Brass	200	3522±16.97	2563±18.38	0.72±0.007	0.88	50±1.414

When NMP was used, the thermal conformance of interfaces was better compared to bare interfaces and interfaces with polymer based TIMs. The enhancement in conformance is probably due to the removal of oxide layer adhering to metallic surfaces of the source and sink resulting in enhanced heat transfer. The presence of the oxide film offers resistance to the transfer of heat. The degree of conformance under no load conditions was higher than that obtained with contacting surfaces not subjected to NMP

treatment. The change in thermal conformance was negligible when interfacial pressure was increased.

A schematic sketch representing mechanism of heat transfer between interfaces is shown in Figure 5.79. Figure 5.79a represents bare metal interface. The metal interfaces consisting of source and sink when exposed to the ambient undergo oxidation. The oxide layers formed at both the source and sink surface provide resistance to the heat flow in addition to the voids present. Thus, the total resistance is the sum of (i) resistance offered by the oxide film at the source surface (R_1), (ii) resistance offered by the air present in the voids formed due to the irregular contacting surfaces of the source and sink (R_{air}), and (iii) resistance offered by the oxide film on the sink surface (R_3). The total resistance is given by,

$$R_{bare\ interface} = R_1 + R_{air} + R_3 \qquad (5.4)$$

The heat transfer takes place via the contacting points though conduction which is a small fraction of the entire contacting surface. In the case of figure 5.79b, the voids are filled with TIMs whose thermal conductivity is greater than air. However, the presence of oxide film contributes to the thermal resistance. Thus,

$$R_{TIM\ \ interface} = R_1 + R_{TIM} + R_3 \qquad (5.5)$$

The interfacial resistance in cases with interfaces with TIMs is the summation of R_1, R_{TIM} and R_3. The total thermal resistance offered by the interfaces with TIM is lower compared to bare interface without NMP treatment as air with lower thermal conductivity in voids was replaced by TIM. Figure 5.79c shows the thermal contact of the interfaces cleaned with the NMP solvent. The application of the solvent results in the removal of the oxide film thus eliminating R_1 and R_3 in equation 5.4

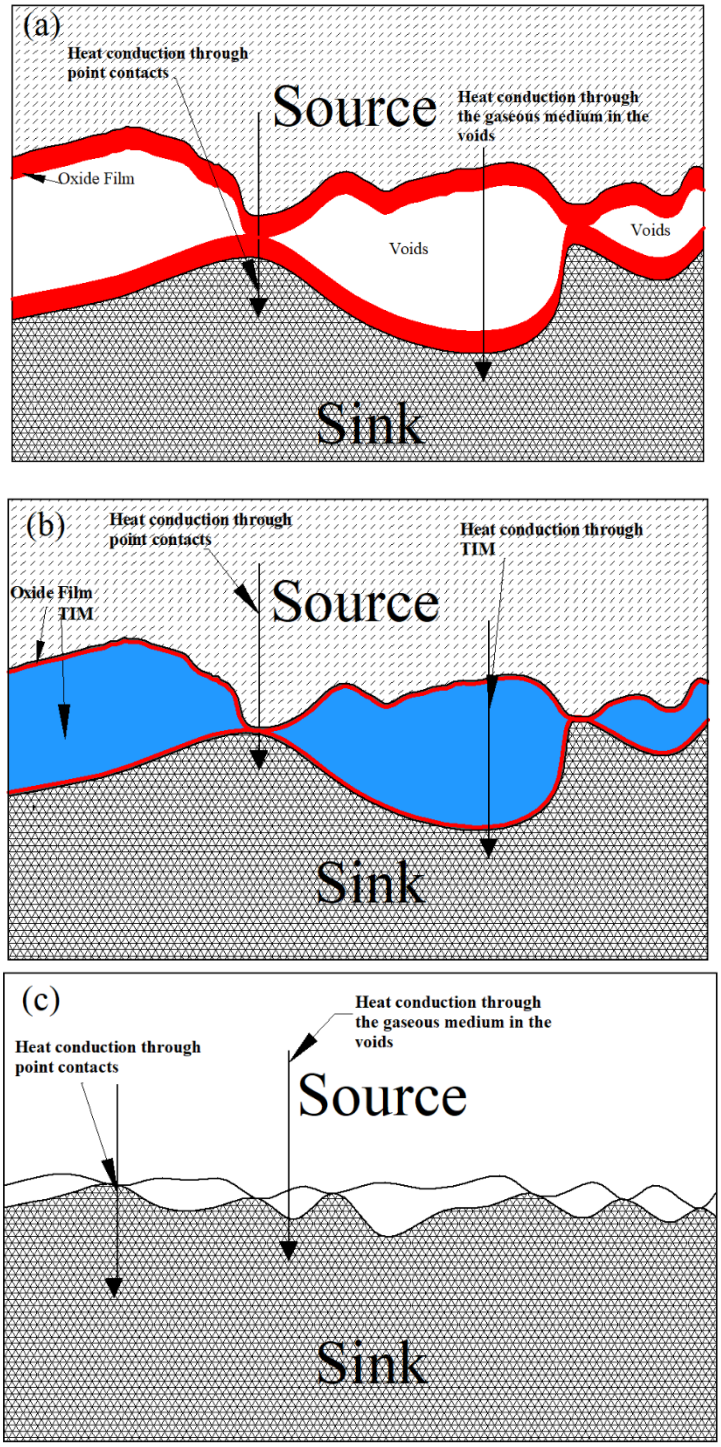

Figure 5.79 Schematic representation of the mechanism of heat transfer at source-sink interface for a) bare interfaces b) interfaces with TIM c) surfaces treated with 1-Methyl-2-pyrrolidone/NMP

The removal of oxide films by the application of NMP results in larger degree of enhancement in the interfacial heat transfer primarily due to the elimination of R_1 and R_3 components and owing to the direct metal-metal conformance at the contacting points. The conforming point contacts offer no resistance to the transfer of heat. The thermal conductivity of the contacting metals is high resulting in enhanced conductive transfer. Thus, the interfaces with the NMP solvent results in enhanced heat transfer when compared to the bare interfaces and interfaces with TIMs. Thus, the NMP treated surfaces offer the lowest thermal contact resistance compared to the bare interface and the interface filled with TIM.

Surface roughness measurements were carried out to assess the effect of NMP on the surface texture. Experimental results revealed that the application of NMP results in smoother surface finish of the surfaces. In the case of copper surfaces, R_a and R_z values before NMP treatment was 21.25 nm and 189.6 nm respectively. The application of NMP resulted in improvement of the surface finish. The R_a and R_z was 11nm and 110 nm respectively after the application of NMP. Similar results were obtained with brass surfaces as shown in Table 25. The application of NMP smoothens the surface increasing the microscopic contacts and reducing the voids. The surface smoothening result obtained when NMP was applied on the source and sink metallic surfaces effectively reduces the mean gap width enhancing the thermal conformance at the interface. In the absence of direct experimental evidence of the removal of oxide films, it is possible that the surface smoothening mechanism is mainly responsible for the enhancement of thermal conformance parameters in the case of NMP treated surfaces.

Chapter 6 Conclusions

An experimental set-up was designed and fabricated to assess the transient heat transfer and thermal conformance between metallic contacts. Based on the results and discussion of the present investigation, the following conclusions were drawn.

- For all materials in contact, heat flux transients increased with the increase in interfacial pressure and application of TIMs.
- The effect of interfacial pressure on heat transfer across the interface is significant for bare contacts. For interfaces with TIMs, the effect of interfacial pressure was not significant compared to that for bare contacts.
- For high thermal conductive interfaces of Cu-Cu, the thermal conformance and the magnitude of heat flux transients increased on the application of interfacial pressure and TIMs. Increasing the surface finish of the contacting metals further enhanced the thermal conformance. For bare interfaces under no load conditions improving the surface finish from a R_a value of 165nm to 21.5nm, resulted in an enhancement of thermal conformance by 340%. The corresponding increase was only 60% when the interfaces were subjected to 200kPa.
- For interfaces with smooth surface finish, there exists a limiting value of interfacial pressure (~40kPa) beyond which the increase in thermal conformance was found to be negligible. The limiting interfacial pressure reduces to 10 kPa when TIMs are applied at the interface. The limiting value increased to 100 kPa for rough surface finish.
- The increase in thermal conductivity of the TIM enhanced the thermal conformance of the interfaces under no load conditions. For Cu-Cu interfaces with smooth surface finish, the thermal conformance values increased by 20%, 68%, and 70% respectively, when SG, CTG and STP were to be applied as TIMs, compared to that for bare Cu-Cu interfaces.
- Increasing the L/D ratio of the source and sink materials from 1 to 5 increased the thermal resistance at the interface for Cu-Cu interfaces. In both cases, the contact resistances decreased with increase in the interfacial pressure and the use of TIMs.

- The application of MWCNT at a low concentration of 0.1 wt% in SG for specimens with L/D of 1 and 5 increased the heat flux transients. However, increasing the CNT content beyond 0.1 wt% resulted in decreased heat transfer, possibly due to the agglomeration of MWCNTs. Further, at interfacial pressures beyond 100 kPa, the peak heat flux and the integral heat flow show negligible effects of the adding of MWCNTs to the TIM.
- Higher heat flux transients were obtained for dissimilar materials consisting of Al-Cu interfaces with Cu as the sink material.
- Thermal conformance parameters (η, Θ, t_g) were proposed to quantify the metal-metal interfacial heat transfer under transient conditions. A Thermal Conformance Assessment Parameter (TCAP) was proposed to assess the effect of process variables on the contact condition between a metallic heat source and a heat sink. TCAP was defined as, TCAP =(A*B) + $C^{0.25}$. where, A, B, and C are the thermal diffusivity [$k/(\rho C_p)$], of the source material, thermal effusivity [$(\sqrt{k\rho C_p})$] of the sink material, and the interfacial pressure respectively.
- For Al-Al, Al-Cu, and Cu-Al, combinations, η and Θ parameters were increased linearly with the Thermal Conformance Assessment Parameter (TCAP).
- The peak temperature difference between the source and the sink materials dropped significantly with an increase in the TCAP for Al-Al, Al-Cu, Cu-Al combinations. For Cu-Cu interfaces, a similar trend was observed with increase in the interfacial pressure indicating enhanced heat transfer. The application of TIMs also resulted in a reduction of $\triangle T_{max}$ indicating superior heat transfer for both similar and dissimilar combinations.
- The magnitude of heat transferred across the interface for brass-brass metallic contacts increased significantly on the application of the pressure for the bare interface when air is the interfacial medium. The increase in interfacial pressure from no load interfacial conditions to 200 kPa resulted in a 230 pct in the heat flow to the sink material.
- The application of SG as TIM resulted in 59 pct enhancement in the heat transfer across the interface compared to bare interfaces for no load conditions in the case of brass-brass metallic interface. The corresponding increases in the case of CTG and STP was 114 pct and 261 pct, respectively.

- For the brass- brass interfaces with SG as TIM, 40kPa was the limiting interfacial pressure beyond which the interfacial pressure did not have any significant effect on the heat transfer across the thermal interface. The limiting interfacial pressure for interfaces with CTG was 10kPa. However, the role of interfacial pressure was insignificant on the application of STP. The increase in thermal conductivity of the interfacial medium enhances the thermal conformance of the interfaces. Further, application of high thermal conductive TIMs resulted in the reduction of limiting interfacial pressure beyond which there was minimal effect on heat transfer enhancement.
- The effect of the thermal conductivity of TIM is not a significant factor at higher interfacial pressures for all combinations.
- A cleaning solvent 1-Methyl-2-pyrrolidone (NMP), generally used in the semiconductor industry, was used to clean the source and sink surfaces before its use in the heat transfer experiments to assess its effect on the contact heat transfer. When NMP was applied, all thermal conformance parameters and heat flux transients increased significantly without TIM and no load conditions. The degree of increase was comparable to that when 200 kPa interfacial pressure was applied in the presence of TIMs.
- The increase in the heat transfer on application of NMP was due to two reasons: (i) the application of NMP possibly removes the source and sink surface oxide films that offer more resistance to the interfacial heat transfer, and (ii) when NMP was used on the surface, it smoothens the surface increasing the microscopic contacts and reducing the voids which were confirmed by the surface roughness measurements carried out on the source and sink metallic surfaces before and after the application of NMP.

References

Abdullah, M. Z., Yau, Y. C., Alauddin, and, Z. A. Z., and Seetharamu, K. N. (2017). "Effects of pressure on thermal contact resistance for rough mating surfaces." *ASEAN J. Sci. Technol. Dev.*

Bahrami, M., Yovanovich, M. M., and Culham, J. R. (2005). "Thermal contact resistance at low contact pressure: Effect of elastic deformation." *Int. J. Heat Mass Transf.*, 48(16), 3284–3293.

Bai, J. G., Zhang, Z. Z., Lu, G., and Hasselman, D. P. H. (2005). "Measurement of Solder / Copper Interfacial Thermal Resistance by the Flash Technique." *Int. J. Thermophys.*, 26(5), 1607–1615.

Beck, J. V. (1970). "Nonlinear estimation applied to the nonlinear inverse heat conduction problem." *Int. J. Heat Mass Transf.*, 13(4), 703–716.

Becker, G., Lee, C., and Lin, Z. (2005). "Thermal in advanced chips conductivity." *Adv. Packag.*, 14(7), 14–16.

Bhanushali, S., Ghosh, P. C., Simon, G. P., and Cheng, W. (2017). "Copper Nanowire-Filled Soft Elastomer Composites for Applications as Thermal Interface Materials." *Adv. Mater. Interfaces*, 4(17), 1–12.

Burggraf, O. R. (1964). "An exact solution of the inverse problem in heat conduction theory and applications." *J. Heat Transfer*, 86(3), 373–380.

Carlberg, B., Wang, T., Liu, J., and Shangguan, D. (2009). "Polymer-metal nano-composite films for thermal management." *Microelectron. Int.*, 26(2), 28–36.

Chano, K., Poliskie, G. M., and Fregoso, J. (2017). "Rheology of Thermal Interface Materials Composed of Silicone Gels." *IEEE Trans. Components, Packag. Manuf. Technol.*, 7(2), 217–220.

Chen, H., Wei, H., Chen, M., Meng, F., Li, H., and Li, Q. (2013). "Enhancing the effectiveness of silicone thermal grease by the addition of functionalized carbon

nanotubes.” *Appl. Surf. Sci.*, 283, 525–531.

Chiu, C. P., Solbrekken, G. L., and Chung, Y. D. (1997). “Thermal modeling of grease-type interface material in PPGA application.” *Annu. IEEE Semicond. Therm. Meas. Manag. Symp.*, 57–63.

Choi, Y. S., and Kim, M. S. (2014). “Experiments on thermal contact conductance between metals below 100 K.” *AIP Conf. Proc.*, 1573(February), 1070–1077.

Chu, W. X., Tseng, P. H., and Wang, C. C. (2019). “Utilization of low-melting temperature alloy with confined seal for reducing thermal contact resistance.” *Appl. Therm. Eng.*, 163(August), 114438.

Chung, D. D. L. (2001). “Thermal Interface Materials.” *J. Mater. Eng. Perform.*, 10(1), 56–59.

Cola, B. A., Xu, J., and Fisher, T. S. (2009). “Contact mechanics and thermal conductance of carbon nanotube array interfaces.” *Int. J. Heat Mass Transf.*, 52(15–16), 3490–3503.

Cola, B. A., Xu, X., and Fisher, T. S. (2007). “Increased real contact in thermal interfaces: A carbon nanotube/foil material.” *Appl. Phys. Lett.*, 90(9), 88–91.

Cook, R. S., Token, K. H., and Calkins, R. L. (1984). “A novel concept for reducing thermal contact resistance.” *J. Spacecr. Rockets*, 21(1), 122–124.

Cui, T., Li, Q., Xuan, Y., and Zhang, P. (2015). “Preparation and thermal properties of the graphene-polyolefin adhesive composites: Application in thermal interface materials.” *Microelectron. Reliab.*, 55(12), 2569–2574.

Dai, Y. J., Gou, J. J., Ren, X. J., Bai, F., Fang, W. Z., and Tao, W. Q. (2018). “A test-validated prediction model of thermal contact resistance for Ti-6Al-4V alloy.” *Appl. Energy*, 228(November 2017), 1601–1617.

DeSorgo, M. (1996). “Thermal Interface Materials | Electronics Cooling.” *https://www.electronics-cooling.com/1996/09/thermal-interface-materials-2/*.

Dmitriev, A. S., and Valeev, A. R. (2017). “Graphene nanocomposites as thermal interface materials for cooling energy devices.” *J. Phys. Conf. Ser.*, 891(1).

Due, J., and Robinson, A. J. (2013). “Reliability of thermal interface materials: A review.” *Appl. Therm. Eng.*, 50(1), 455–463.

Fabris, D., Rosshirt, M., Cardenas, C., Wilhite, P., Yamada, T., and Yang, C. Y. (2011). “Application of carbon nanotubes to thermal interface materials.” *J. Electron. Packag. Trans. ASME*, 133(2).

Fletcher, L. S. (1990). “A review of thermal enhancement techniques for electronic systems.” 136–148.

Gao, Y., and Liu, J. (2012). “Gallium-based thermal interface material with high compliance and wettability.” *Appl. Phys. A Mater. Sci. Process.*, 107(3), 701–708.

Gao, Y., Wang, X., Liu, J., and Fang, Q. (2017). “Investigation on the Optimized Binary and Ternary Gallium Alloy as Thermal Interface Materials.” *J. Electron. Packag. Trans. ASME*, 139(1), 1–8.

Goel, N., Anoop, T. K., Bhattacharya, A., Cervantes, J. A., Mongia, R. K., Machiroutu, S. V., Lin, H. L., Huang, Y. C., Fan, K. C., Denq, B. L., Liu, C. H., Lin, C. H., Tien, C. W., and Pan, J. H. (2008). “Technical review of characterization methods for Thermal Interface Materials (TIM).” *2008 11th IEEE Intersoc. Conf. Therm. Thermomechanical Phenom. Electron. Syst. I-THERM*, 248–258.

Goli, P., Legedza, S., Dhar, A., Salgado, R., Renteria, J., and Balandin, A. A. (2014). “Graphene-enhanced hybrid phase change materials for thermal management of Li-ion batteries.” *J. Power Sources*, 248(September), 37–43.

Gowda, A., Esler, D., Paisner, S. N., Tonapi, S., Nagarkar, K., and Srihari, K. (2005). “Reliability Testing of Silicone-based Thermal Greases Department of Systems Science and Industrial Engineering.” *Semi-Therm*.

Gowda, A., Esler, D., Tonapi, S., Nagarkar, K., and Srihari, K. (2004). “Voids in thermal interface material layers and their effect on thermal performance.” *Proc. 6th*

Electron. Packag. Technol. Conf. EPTC 2004, 41–46.

Grujicic, M., Zhao, C. L., and Dusel, E. C. (2005). "The effect of thermal contact resistance on heat management in the electronic packaging." *Appl. Surf. Sci.*, 246(1–3), 290–302.

Gwinn, J. P., Saini, M., and Webb, R. L. (2002). "Apparatus for accurate measurement of interface resistance of high performance thermal interface materials." *Intersoc. Conf. Therm. Thermomechanical Phenom. Electron. Syst. ITHERM*, 2002-Janua, 644–650.

Gwinn, J. P., and Webb, R. L. (2002). "Performance and testing of thermal interface materials." 201–210.

Gwinn, J. P., and Webb, R. L. (2003). "Performance and testing of thermal interface materials." *Microelectronics J.*, 34(3), 215–222.

Haight, A. E., Green, C. E., and Cola, B. A. (2016). "Vertically aligned carbon nanotube based thermal interface materials for low contact pressure and low ambient pressure applications." *Proc. 15th Intersoc. Conf. Therm. Thermomechanical Phenom. Electron. Syst. ITherm 2016*, 1261–1266.

Hamdan, A., Mclanahan, A., Richards, R., and Richards, C. (2011). "Characterization of a liquid – metal microdroplet thermal interface material." *Exp. Therm. Fluid Sci.*, 35(7), 1250–1254.

Hansson, J., Nilsson, T. M. J., Ye, L., and Liu, J. (2018). "Novel nanostructured thermal interface materials: A review." *Int. Mater. Rev.*, 63(1), 22–45.

Hansson, J., Ye, L., and Liu, J. (2017). "Fabrication and characterization of a carbon fiber solder composite thermal interface material." *2017 IMAPS Nord. Conf. Microelectron. Packag. Nord. 2017*, 97–100.

Hansson, J., Zandén, C., Ye, L., and Liu, J. (2016). "Review of current progress of thermal interface materials for electronics thermal management applications." *16th Int. Conf. Nanotechnol. - IEEE NANO 2016*, 371–374.

Hao, M., Huang, Z., Saviers, K. R., Xiong, G., Hodson, S. L., and Fisher, T. S. (2017). "Characterization of vertically oriented carbon nanotube arrays as high-temperature thermal interface materials." *Int. J. Heat Mass Transf.*, 106, 1287–1293.

Heerden, D. Van, Rude, T., Newson, J., Knio, O., Weihs, T. P., and Gailus, D. W. (2004). "Thermal behavior of a soldered Cu-Si interface." *Annu. IEEE Semicond. Therm. Meas. Manag. Symp.*, 20, 46–49.

Hill, R. F., and Strader, J. L. (2006). "Practical Utilization of Low Melting Alloy Thermal Interface Materials." *22nd IEEE SEMI-THERM Symp.*

Hu, K., and Chung, D. D. L. (2011). "Flexible graphite modified by carbon black paste for use as a thermal interface material." *Carbon N. Y.*, 49(4), 1075–1086.

Hu, X., Jiang, L., and Goodson, K. E. (2004). "Thermal characterization of eutectic alloy thermal interface materials with void-like inclusions." *Annu. IEEE Semicond. Therm. Meas. Manag. Symp.*, 20(650), 98–103.

Huilong Yan, J. Y. and G. Z. (2019). "Heat transfer of liquid metal alloy on copper plate deposited with film of different surface free energy." *Chinese Phys. B*.

Ji, Y., Li, G., Chang, C., Sun, Y., and Ma, H. (2015). "Investigation on carbon nanotubes as thermal interface material bonded with liquid metal alloy." *J. Heat Transfer*, 137(9), 1–9.

Ji, Y., Yan, H., Xiao, X., Xu, J., Li, Y., and Chang, C. (2020). "Excellent thermal performance of gallium-based liquid metal alloy as thermal interface material between aluminum substrates." *Appl. Therm. Eng.*, 166, 114649.

Kargar, F., Barani, Z., Salgado, R., Debnath, B., Lewis, J. S., Aytan, E., Lake, R. K., and Balandin, A. A. (2018). "Thermal Percolation Threshold and Thermal Properties of Composites with High Loading of Graphene and Boron Nitride Fillers." *ACS Appl. Mater. Interfaces*, 10(43), 37555–37565.

Kumar, S., and Tariq, A. (2017). "Determination of thermal contact conductance of flat and curvilinear contacts by transient approach." *Exp. Therm. Fluid Sci.*, 88, 261–276.

Kusuma, W. J., Fadarina, and Hasan, A. (2019). “Sodium Silicate Composite Filled by Zinc Oxide as Low Resistance Thermal Grease.” *J. Phys. Conf. Ser.*, 1167(1).

Leong, C. K., and Chung, D. D. L. (2003). “Carbon black dispersions as thermal pastes that surpass solder in providing high thermal contact conductance.” *Carbon N. Y.*, 41(13), 2459–2469.

Leong, C. K., and Chung, D. D. L. (2004). “Carbon black dispersions and carbon-silver combinations as thermal pastes that surpass commercial silver and ceramic pastes in providing high thermal contact conductance.” *Carbon N. Y.*, 42(11), 2323–2327.

Lewis, J. S., Perrier, T., Mohammadzadeh, A., Kargar, F., and Balandin, A. A. (2020). “Power Cycling and Reliability Testing of Epoxy-Based Graphene Thermal Interface Materials.” *C — J. Carbon Res.*, 6(2), 26.

Li, A., Zhang, C., and Zhang, Y. (2017a). “Composites : Part A RGO / TPU composite with a segregated structure as thermal interface material.” 101, 108–114.

Li, G., Ji, Y., Wu, M., and Ma, H. (2017b). “Ht2016-7374.” *Proc. ASME 2016 Heat Transf. Summer Conf. HT2016*, 1–6.

Lin, W., Zhang, R., Moon, K. S., and Wong, C. P. (2010). “Synthesis of high-quality vertically aligned carbon nanotubes on bulk copper substrate for thermal management.” *IEEE Trans. Adv. Packag.*, 33(2), 370–376.

Liu, C., and Hu, G. (2015). “Highly efficient reduction of graphene oxide by sub/supercritical water and their application for thermal interface materials.” *Appl. Therm. Eng.*, 90, 193–198.

Liu, H., Liu, H., Lin, Z., and Chu, S. (2018). “AlN/Ga-based Liquid Metal/PDMS Ternary Thermal Grease for Heat Dissipation in Electronic Devices.” *Xiyou Jinshu Cailiao Yu Gongcheng/Rare Met. Mater. Eng.*, 47(9), 2668–2674.

Liu, J., Feng, H., Luo, X., Hu, R., and Liu, S. (2010). “A simple setup to test thermal contact resistance between interfaces of two contacted solid materials.” *Proc. - 2010 11th Int. Conf. Electron. Packag. Technol. High Density Packag. ICEPT-HDP 2010,*

116–120.

Liu, Z., and Chung, D. D. L. (2006a). “Boron nitride particle filled paraffin wax as a phase-change thermal interface material.” *J. Electron. Packag. Trans. ASME*, 128(4), 319–323.

Liu, Z., and Chung, D. D. L. (2006b). “Boron Nitride Particle Filled Paraffin Wax as a Phase-Change.” *J. Electron. Packag.*, 128(December), 319–323.

Loeblein, M., Tsang, S. H., Pawlik, M., Phua, E. J. R., Yong, H., Zhang, X. W., Gan, C. L., and Teo, E. H. T. (2017). “High-Density 3D-Boron Nitride and 3D-Graphene for High-Performance Nano-Thermal Interface Material.” *ACS Nano*, 11(2), 2033–2044.

Luo, X., Xu, Y., and Chung, D. D. L. (2001). “Thermal Stability of Thermal Interface Pastes, Evaluated by Thermal Contact Conductance Measurement.” *J. Electron. Packag.*, 123(3), 309.

Luo, X., Zhang, Y., Zandén, C., Murugesan, M., Cao, Y., Ye, L., and Liu, J. (2014). “Novel thermal interface materials: Boron nitride nanofiber and indium composites for electronics heat dissipation applications.” *J. Mater. Sci. Mater. Electron.*, 25(5), 2333–2338.

Ma, K., and Liu, J. (2007). “Liquid metal cooling in thermal management of computer chips.” *Front. Energy Power Eng. China*, 1(4), 384–402.

Macris, C. G., Sanderson, T. R., Ebel, R. G., and Leyerle, C. B. (2004). “Performance, reliability, and approaches using a low melt alloy as a thermal interface material.” *Int. Microelectron. Packag. Soc.*, 1–6.

Mahadevan, B. K., Naghibi, S., Kargar, F., and Balandin, A. A. (2019). “Non-Curing Thermal Interface Materials with Graphene Fillers for Thermal Management of Concentrated Photovoltaic Solar Cells.” *C — J. Carbon Res.*, 6(1), 2.

Mallik, S., Ekere, N., Best, C., and Bhatti, R. (2011). “Investigation of thermal management materials for automotive electronic control units.” *Appl. Therm. Eng.*, 31(2–3), 355–362.

Martin, Y., Kessel, T. Van, Heights, Y., Martin, Y., and Kessel, T. Van. (2007). “IBM Research Report High Performance Liquid Metal Thermal Interface for Large Volume Production for Large Volume Production.” 24372.

Matayabas Jr, J. C. et al. (2005). “Gel thermal interface materials comprising fillers having low melting point and electronic packages comprising these gel thermal interface materials.” *US Pat. 6841867-B2*, 2(12).

McNamara, A. J., Joshi, Y., and Zhang, Z. M. (2015). “Thermal resistance of thermal conductive adhesive anchored carbon nanotubes interface material.” *Int. J. Therm. Sci.*, 96, 221–226.

Nagabandi, N., Yegin, C., Feng, X., King, C., Oh, J. K., Narumanchi, S., and Akbulut, M. (2017). “Metallic nanocomposites as next-generation thermal interface materials.” *Proc. 16th Intersoc. Conf. Therm. Thermomechanical Phenom. Electron. Syst. ITherm 2017*, (September), 400–406.

Naghibi, S., Kargar, F., Wright, D., Huang, C. Y. T., Mohammadzadeh, A., Barani, Z., Salgado, R., and Balandin, A. A. (2020). “Noncuring Graphene Thermal Interface Materials for Advanced Electronics.” *Adv. Electron. Mater.*, 6(4), 1–9.

Narayana, S. R., and Narayan, P. K. (2014). “Effect of load and interface materials on thermal contact resistance between similar and dissimilar materials.” *Appl. Mech. Mater.*, 592–594, 1493–1497.

Otiaba, K. C., Ekere, N. N., Bhatti, R. S., Mallik, S., Alam, M. O., and Amalu, E. H. (2011). “Thermal interface materials for automotive electronic control unit: Trends, technology and R&D challenges.” *Microelectron. Reliab.*, 51(12), 2031–2043.

Park, W., Guo, Y., Li, X., Hu, J., Liu, L., Ruan, X., and Chen, Y. P. (2015). “High-Performance Thermal Interface Material Based on Few-Layer Graphene Composite.” *J. Phys. Chem. C*, 119(47), 26753–26759.

Peacock, M. A., Roy, C. K., Hamilton, M. C., Wayne Johnson, R., Knight, R. W., and Harris, D. K. (2016). “Characterization of transferred vertically aligned carbon

nanotubes arrays as thermal interface materials." *Int. J. Heat Mass Transf.*, 97, 94–100.

Pei, Y., Zhong, H., Wang, M., Zhang, P., and Zhao, Y. (2018). "Effect of contact pressure on the performance of carbon nanotube arrays thermal interface material." *Nanomaterials*, 8(9), 1–10.

Peterson, A. L. (1990). .. "I." *40th Conf. Proc. Electron. Components Technol. (pp. 613-619). IEEE.*, 613–619.

Poirier, D. R., and Geiger, G. H. (2016). *Transport Phenomena in Materials Processing*. The Minerals, Metals \& Materials Series, Springer Cham.

Prabhu, K. N., and Ashish, A. A. (2002). "Inverse modeling of heat transfer with application to solidification and quenching." *Mater. Manuf. Process.*, 17(4), 469–481.

Prasher, R. (2006). "Thermal interface materials: Historical perspective, status, and future directions." *Proc. IEEE*, 94(8), 1571–1586.

Prasher, R. S., and Matayabas, J. C. (2004). "Thermal contact resistance of cured gel polymeric thermal interface material." *Thermomechanical Phenom. Electron. Syst. - Proceedings Intersoc. Conf.*, 1(4), 28–35.

Prasher, R. S., Shipley, J., Prstic, S., Koning, P., and Wang, J. (2003). "Thermal Resistance of Particle Laden Polymeric Thermal Interface Materials." *J. Heat Transfer*, 125(6), 1170.

Qingyun, T., and Weifang, Z. (2016). "International Journal of Heat and Mass Transfer The effect of pressure on thermal contact conductance of superalloys under high temperature." *Int. J. Heat Mass Transf.*, 103, 1208–1213.

R.S Cook, K. H. T. and R. L. C. (1983). "A Novel Concept for Reducing Thermal Contact Resistance." *3rd Jt. Thermophys. Fluids, Plasma Heat Transf. Conf.*, 21(1), 122–124.

Ramakrishna Devananda P and K NarayanPrabhu. (2019). "The effect of load and addition of MWCNTs on silicone based TIMs on thermal contact heat transfer across

Cu/Cu interface." *Mater. Res. Express*, 6(11).

Rauch, B. (2000). "Understanding the performance characteristics of phase-change thermal interface materials." *2000 Inter Soc. Conf. Therm. Phenomen*, 42–47.

Raza, M. A., and Westwood, A. (2019). "Thermal contact resistance of various carbon nanomaterial-based epoxy composites developed for thermal interface applications." *J. Mater. Sci. Mater. Electron.*, 30(11), 10630–10638.

Raza, M. A., Westwood, A., and Stirling, C. (2015). "Comparison of carbon nanofiller-based polymer composite adhesives and pastes for thermal interface applications." *Mater. Des.*, 85, 67–75.

Raza, M. A., Westwood, A., and Stirling, C. (2018). "Graphite nanoplatelet/rubbery epoxy composites as adhesives and pads for thermal interface applications." *J. Mater. Sci. Mater. Electron.*, 29(10), 8822–8837.

Renteria, J., Legedza, S., Salgado, R., Balandin, M. P., Ramirez, S., Saadah, M., Kargar, F., and Balandin, A. A. (2015). "Magnetically-functionalized self-aligning graphene fillers for high-efficiency thermal management applications." *Mater. Des.*, 88, 214–221.

Roy, C. K. (2016). "Application of Low Melt Alloys as Compliant Thermal Interface Materials: A Study of Performance and Degradation under Thermal Duress ;Dissertation submitted to Auburn university."

Roy, C. K., Bhavnani, S., Hamilton, M. C., Johnson, R. W., Knight, R. W., and Harris, D. K. (2016). "Thermal performance of low melting temperature alloys at the interface between dissimilar materials." *Appl. Therm. Eng.*, 99, 72–79.

Roy, C. K., Bhavnani, S., Hamilton, M. C., Johnson, R. W., Nguyen, J. L., Knight, R. W., and Harris, D. K. (2015). "Investigation into the application of low melting temperature alloys as wet thermal interface materials." *Int. J. Heat Mass Transf.*, 85, 996–1002.

Saadah, M., Hernandez, E., and Balandin, A. A. (2017). "Thermal management of

concentrated multi-junction solar cells with graphene-enhanced thermal interface materials." *Appl. Sci.*, 7(6).

Sartre, V., and Lallemand, M. (2001). "Enhancement of thermal contact conductance for electronic systems." *Appl. Therm. Eng.*, 21(2), 221–235.

Sarvar, F., Whalley, D. C., and Conway, P. P. (2006). "Thermal Interface Materials - A Review of the State of the Art." *Electron. Syst. Technol. Conf. Dresden, Ger.*, 1292–1302.

Shahil, K. M. F., and Balandin, A. A. (2012). "Graphene-multilayer graphene nanocomposites as highly efficient thermal interface materials." *Nano Lett.*, 12(2), 861–867.

Skuriat, R., Li, J. F., Agyakwa, P. A., Mattey, N., Evans, P., and Johnson, C. M. (2013). "Microelectronics Reliability Degradation of thermal interface materials for high-temperature power electronics applications." *Microelectron. Reliab.*, 53, 1933–1942.

Snaith, B., O'Callaghan, P. W., and Probert, S. D. (1984). "Use of Interstitial Materials for Thermal Contact Conductance Control." *AIAA Pap.*

Stewart, W. E. (1972). "Scholars' Mine Determination of thermal contact resistance between metals using a pulse technique." *Determ. Therm. contact Resist. between Met. using a pulse Tech.*

Stolz, G. (1960). "Numerical solutions to an inverse problem of heat conduction for simple shapes." *J. Heat Transfer*, 82(1), 20–25.

Swamy, K., and Satyanarayan. (2019a). "Study on thermal resistance of brass with and without coating of metallic surface." *Mater. Today Proc.*, 35(xxxx), 335–339.

Swamy, M. C. K., and Satyanarayan. (2019b). "A Review of the Performance and Characterization of Conventional and Promising Thermal Interface Materials for Electronic Package Applications." *J. Electron. Mater.*, 48(12), 7623–7634.

Tang, B., Hu, G., Gao, H., and Hai, L. (2015). "Application of graphene as filler to

improve thermal transport property of epoxy resin for thermal interface materials." *Int. J. Heat Mass Transf.*, 85, 420–429.

Taphouse, J. H., Smith, O. L., Marder, S. R., and Cola, B. A. (2014). "A pyrenylpropyl phosphonic acid surface modifier for mitigating the thermal resistance of carbon nanotube contacts." *Adv. Funct. Mater.*, 24(4), 465–471.

Tariq, A., and Asif, M. (2016). "Experimental investigation of thermal contact conductance for nominally flat metallic contact." *Heat Mass Transf. und Stoffuebertragung*, 52(2), 291–307.

Tong, T., Zhao, Y., Delzeit, L., Kashani, A., Meyyappan, M., and Majumdar, A. (2007). "Dense vertically aligned multiwalled carbon nanotube arrays as thermal interface materials." *IEEE Trans. Components Packag. Technol.*, 30(1), 92–100.

Uetani, K., Ata, S., Tomonoh, S., Yamada, T., Yumura, M., and Hata, K. (2014). "Elastomeric thermal interface materials with high through-plane thermal conductivity from carbon fiber fillers vertically aligned by electrostatic flocking." *Adv. Mater.*, 26(33), 5857–5862.

Veilleux, E. D. (1968). "Use of thermal greases to conduct heat across sheet-metal interfaces." *J. Spacecr. Rockets*, 5(10), 1238–1240.

Viswanath, R., Wakharkar, V., Watwe, A., and Lebonheur, V. (2000). "Thermal Performance Challenges from Silicon to Systems." *Intel Techology J.*, (Q3), 1–16.

Wang, S., Cheng, Y., Wang, R., Sun, J., and Gao, L. (2014). "Highly Thermal Conductive Copper Nanowire Composites with Ultralow Loading : Toward Applications as Thermal Interface Materials."

Xu, J., and Fisher, T. S. (2006). "Enhancement of thermal interface materials with carbon nanotube arrays." *Int. J. Heat Mass Transf.*, 49(9–10), 1658–1666.

Xu, Y., and Chung, X. L. D. D. L. (2000). "Interface Material for High." *Trans. ASME*, 122(June), 128–131.

Xu, Y., Leong, C. K., and Chung, D. D. L. (2007). “Carbon nanotube thermal pastes for improving thermal contacts.” *J. Electron. Mater.*, 36(9), 1181–1187.

Xu, Y., Zhang, Y., Suhir, E., and Wang, X. (2006). “Thermal properties of carbon nanotube array used for integrated circuit cooling.” *J. Appl. Phys.*, 100(7).

Yang, E., Guo, H., Guo, J., Shang, J., and Wang, M. (2014). “Thermal performance of low-melting-temperature alloy thermal interface materials.” *Acta Metall. Sin. (English Lett.*, 27(2), 290–294.

Yovanovich, M. M., Culham, J. R., and Teertstra, P. (1997). “Calculating interface resistance.” *Electron. Cool.*, 1–9.

Yu, A., Ramesh, P., Itkis, M. E., Bekyarova, E., and Haddon, R. C. (2007). “Graphite nanoplatelet-epoxy composite thermal interface materials.” *J. Phys. Chem. C*, 111(21), 7565–7569.

Yu, H. (2012). “Thermal and insulating properties of epoxy/aluminum nitride composites used for thermal interface material.” *J. Appl. Polym. Sci.*, 124(1), 669–677.

Yu, H., Li, L., and Zhang, Y. (2012). “Silver nanoparticle-based thermal interface materials with ultra-low thermal resistance for power electronics applications.” *Scr. Mater.*, 66(11), 931–934.

Yu, W., Xie, H., Chen, L., Zhu, Z., Zhao, J., and Zhang, Z. (2014). “Graphene based silicone thermal greases.” *Phys. Lett. Sect. A Gen. At. Solid State Phys.*, 378(3), 207–211.

Yu, W., Xie, H., Yin, L., Zhao, J., Xia, L., and Chen, L. (2015). “Exceptionally high thermal conductivity of thermal grease: Synergistic effects of graphene and alumina.” *Int. J. Therm. Sci.*, 91, 76–82.

Yujun, G., Zhongliang, L., Guangmeng, Z., and Yanxia, L. (2014). “Effects of multi-walled carbon nanotubes addition on thermal properties of thermal grease.” *Int. J. Heat Mass Transf.*, 74, 358–367.

Yunsheng Xu, Xiangcheng Luo, D. D. L. C. (2000). “Sodium Silicate Based Thermal Interface Material for High Thermal Contact Conductance.” *Trans. ASME*, 122(June), 128–131.

Zahid, M., Masood, M. T., Athanassiou, A., and Bayer, I. S. (2018). “Sustainable thermal interface materials from recycled cotton textiles and graphene nanoplatelets.” *Appl. Phys. Lett.*, 113(4).

Zandén, C., Luo, X., Ye, L., and Liu, J. (2014). “A new solder matrix nano polymer composite for thermal management applications.” *Compos. Sci. Technol.*, 94, 54–61.

Zhang, P., Li, Q., and Xuan, Y. (2014a). “Thermal contact resistance of epoxy composites incorporated with nano-copper particles and the multi-walled carbon nanotubes.” *Compos. Part A Appl. Sci. Manuf.*, 57, 1–7.

Zhang, P., Xuan, Y., and Li, Q. (2014b). “A high-precision instrumentation of measuring thermal contact resistance using reversible heat flux.” *Exp. Therm. Fluid Sci.*, 54, 204–211.

Zhang, P., Zeng, J., Zhai, S., Xian, Y., Yang, D., and Li, Q. (2017). “Thermal Properties of Graphene Filled Polymer Composite Thermal Interface Materials.” *Macromol. Mater. Eng.*, 302(9), 1–18.

Zhang, R., Cai, J., Wang, Q., Li, J., Hu, Y., Du, H., and Li, L. (2014c). “Thermal Resistance Analysis of Sn-Bi Solder Paste Used as Thermal Interface Material for Power Electronics Applications.” *J. Electron. Packag.*, 136(1), 011012.

Zhang, W., Kong, Q. Q., Tao, Z., Wei, J., Xie, L., Cui, X., and Chen, C. M. (2019). “3D Thermally Cross-Linked Graphene Aerogel–Enhanced Silicone Rubber Elastomer as Thermal Interface Material.” *Adv. Mater. Interfaces*, 6(12), 1–8.

Zhang, Y. F., Ren, Y. J., and Bai, S. L. (2018). “Vertically aligned graphene film/epoxy composites as heat dissipating materials.” *Int. J. Heat Mass Transf.*, 118, 510–517.

Zhao, J. W., Zhao, R., Huo, Y. K., and Cheng, W. L. (2019a). “Effects of surface roughness, temperature and pressure on interface thermal resistance of thermal

interface materials.” *Int. J. Heat Mass Transf.*, 140, 705–716.

Zhao, L., Chu, S., Chen, X., and Chu, G. (2019b). “Efficient heat conducting liquid metal/CNT pads with thermal interface materials.” *Bull. Mater. Sci.*, 42(4), 1–5.

Zhong, Y., Zhou, M., Huang, F., Lin, T., and Wan, D. (2013). “Effect of graphene aerogel on thermal behavior of phase change materials for thermal management.” *Sol. Energy Mater. Sol. Cells*, 113, 195–200.

APPENDIX A

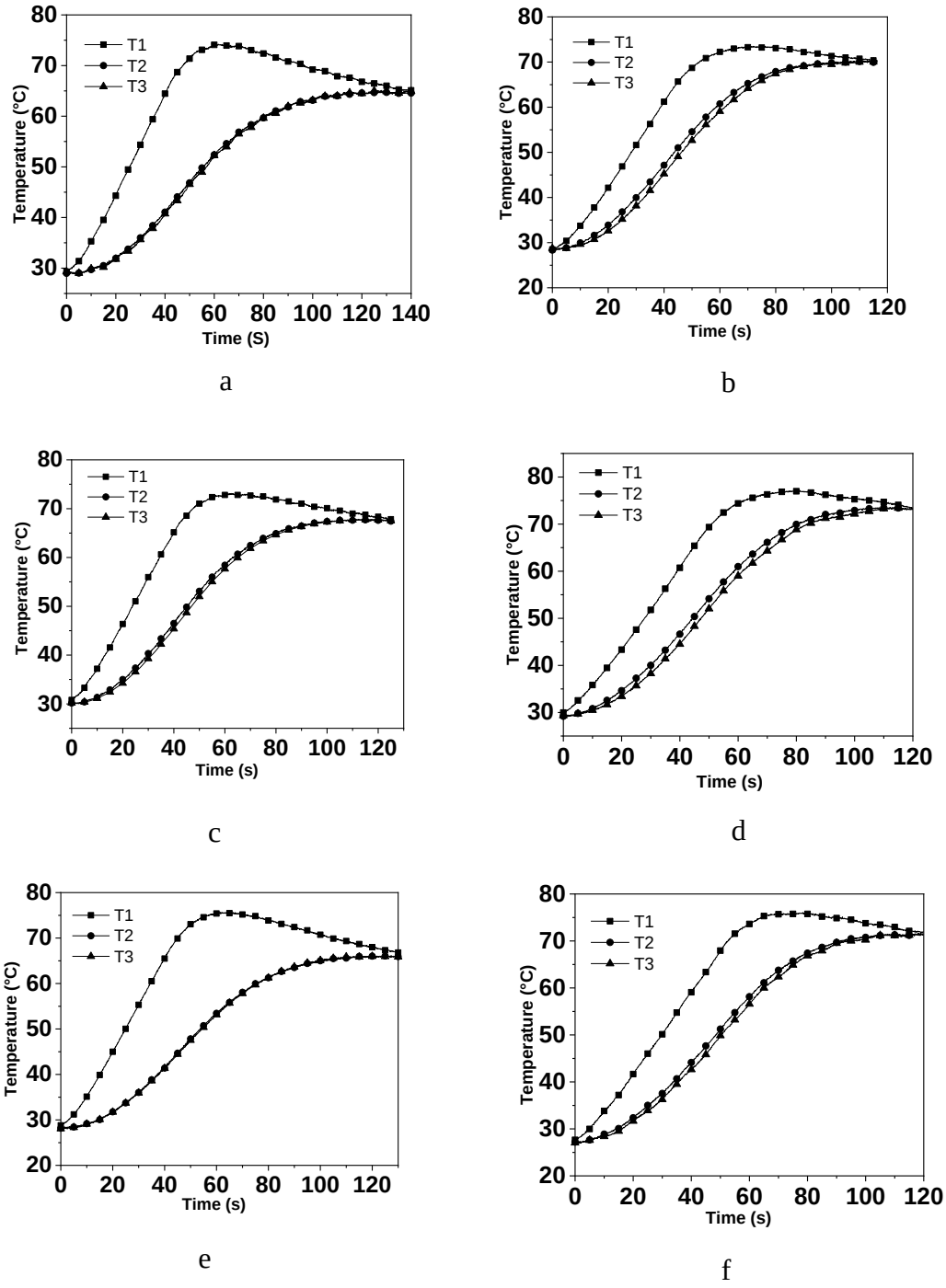

Fig A 1 Variation of temperature with time for Cu-Cu interfaces with a) SG TIM-40kPa b) SG TIM- 100kPa c) SG MWCNT 0.1 WT%- 40kPa d) SG MWCNT 0.1 WT %-100kPa e) SG MWCNT 1 WT% 40 kPa f) SG MWCNT 1 WT% 100kPa

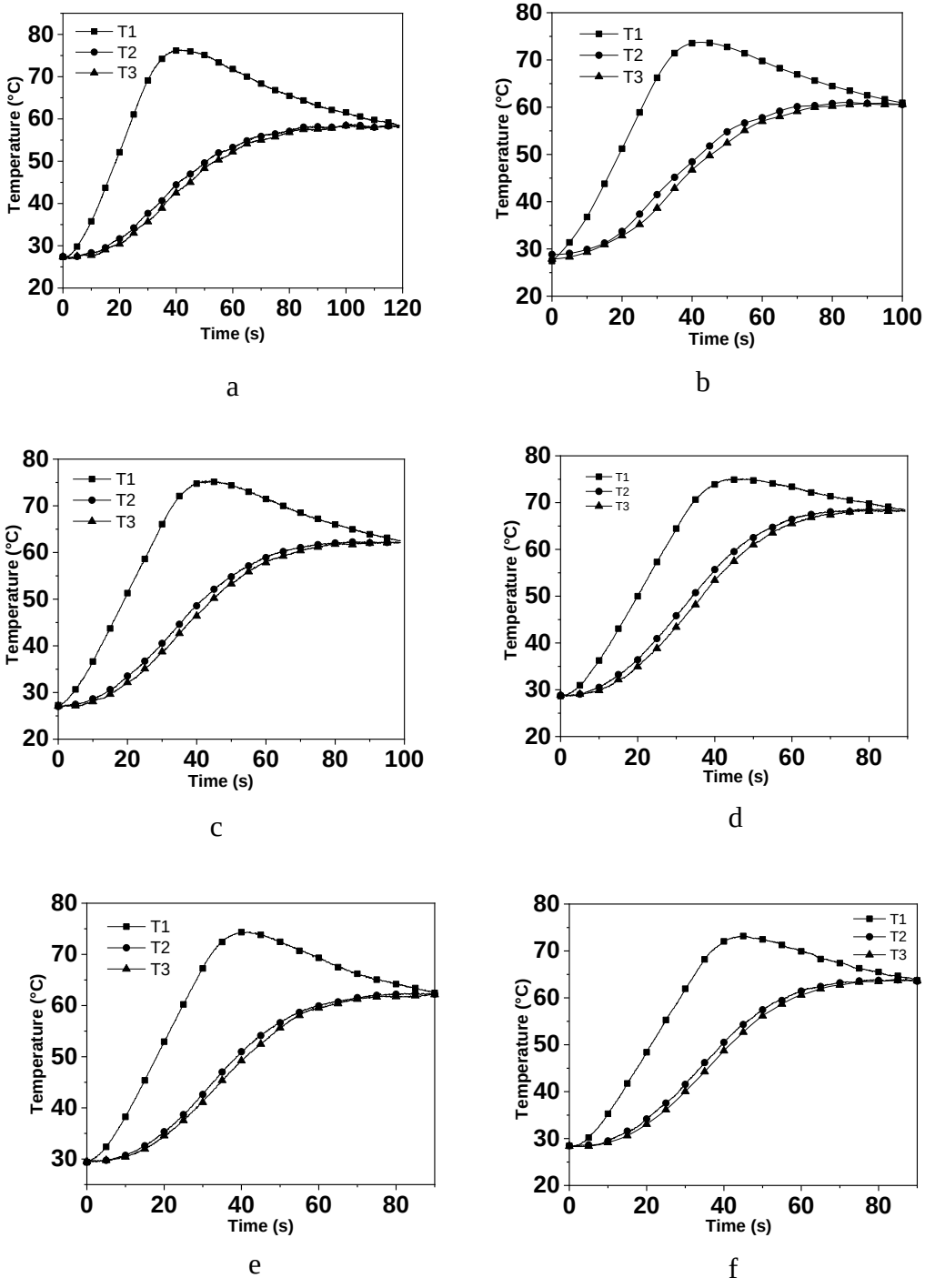

Fig A 2 Variation of temperature with time for a) Al-Al bare interface -40kPa b) Al-Al bare interface -100kPa c) Al-Al SG TIM -40kPa d) Al-Al SG TIM -100kPa e) Al-Cu bare -40kPa f) Al-Cu bare-100kPa

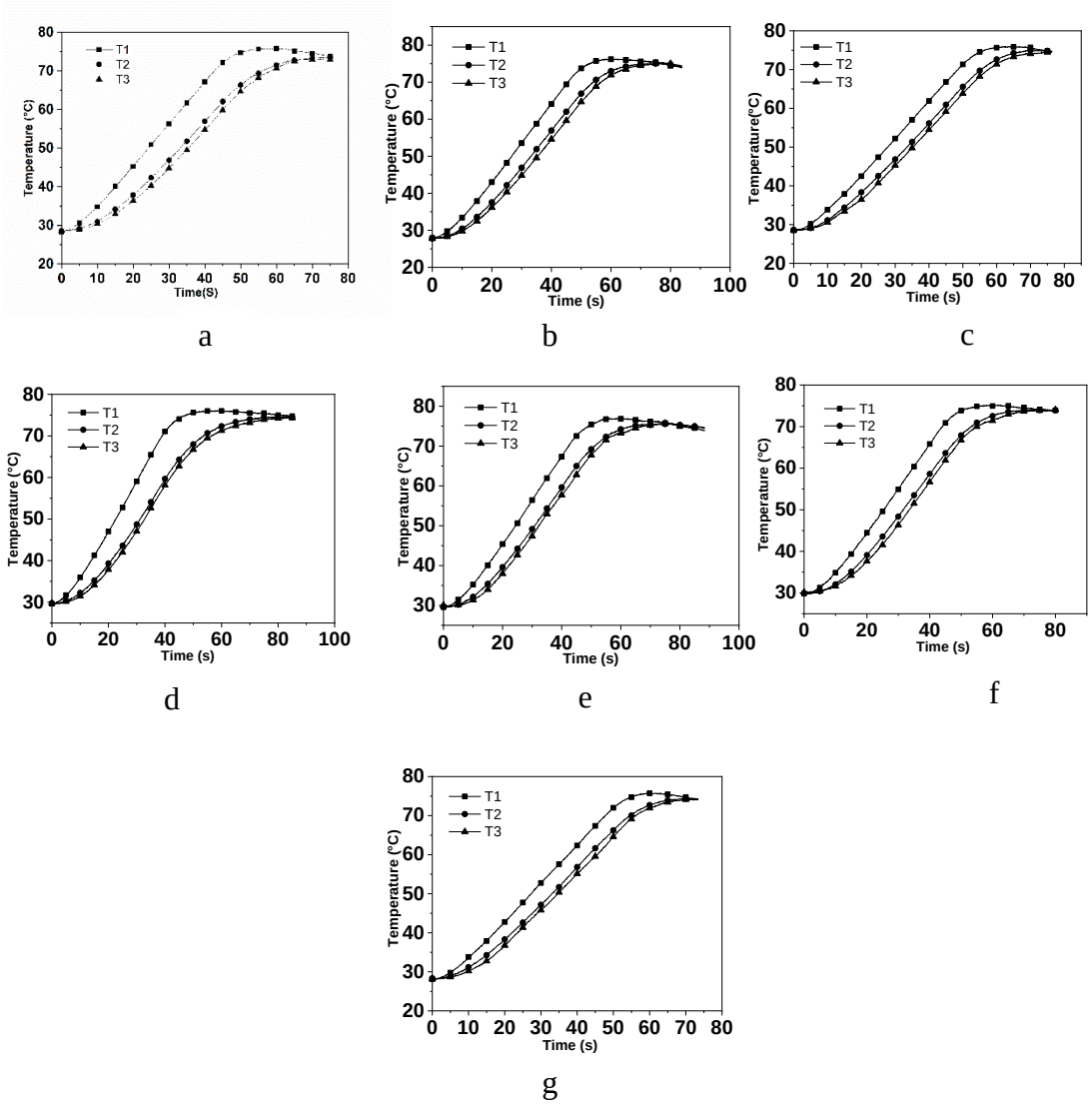

Fig A 3 Variation of temperature with time for a) Al-Cu SG 40kPa b) Al-Cu SG 100kPa c) Al-Cu SG 200kPa d) Al-Cu CTG no load e) Al-Cu CTG 40kPa f) Al-Cu CTG 100kPa g) Al-Cu CTG 200kPa

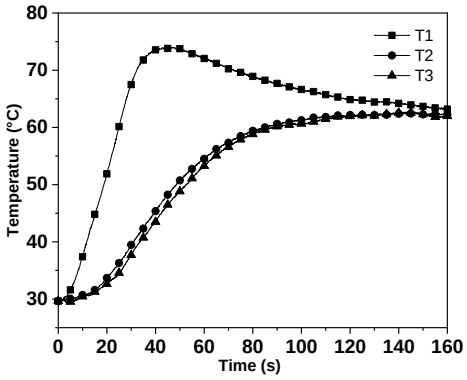

a

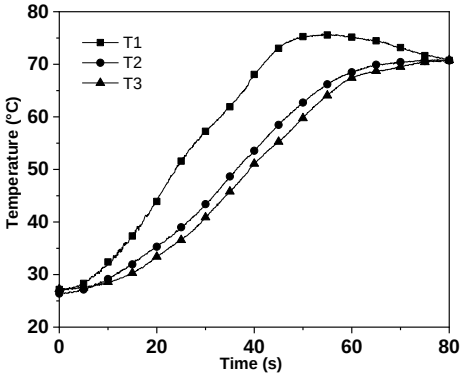

b

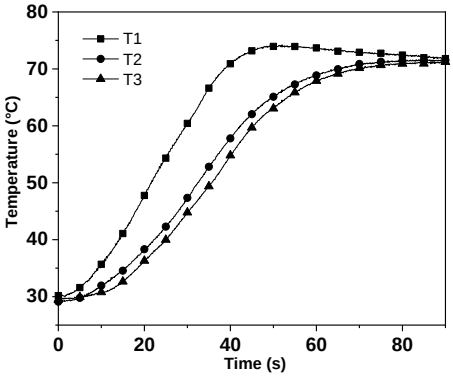

c

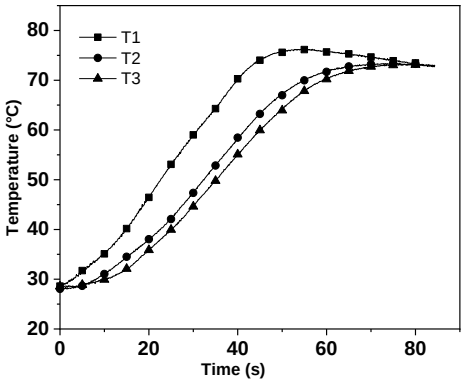

d

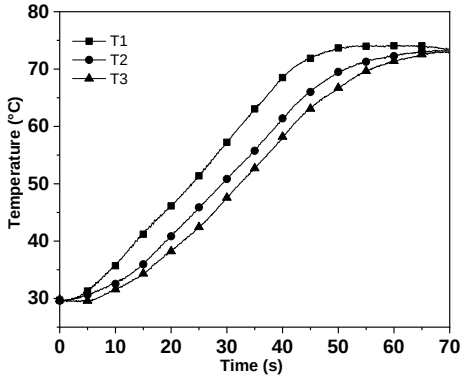

e

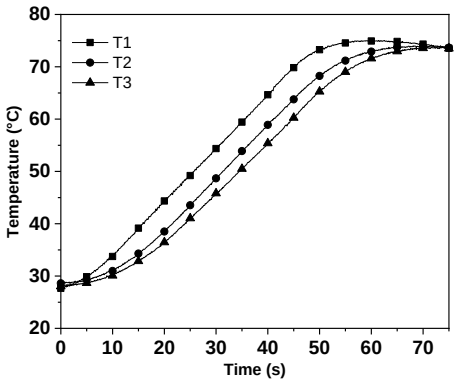

f

Fig A 4 Variation of temperature with time for a) Cu-Al bare NL b) Cu-Al bare 200kPa c) Cu-Al NL-SG TIM d) Cu-Al 40kPa-SG TIM e) Cu-Al 100kPa SG TIM f) Cu-Al 200kPa SG TIM

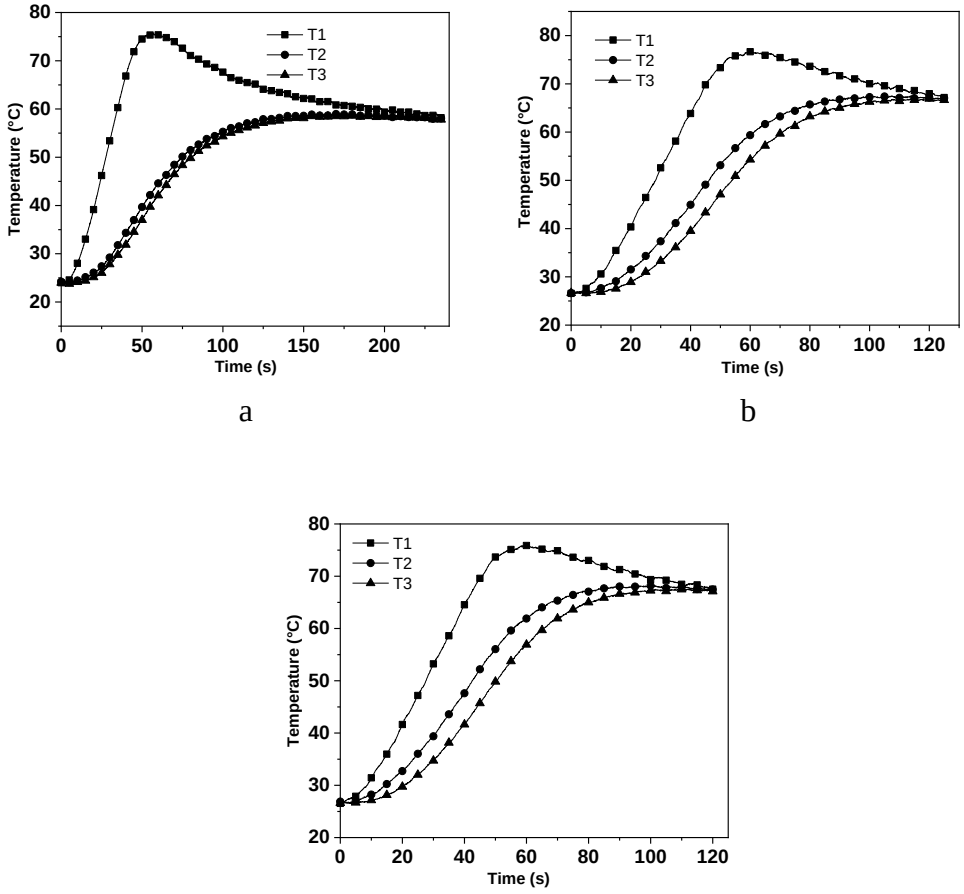

Fig A 5 Variation of temperature with time a) Brass-Brass NL bare interface b) Brass-Brass bare 40kPa c) Brass-Brass bare 100kPa

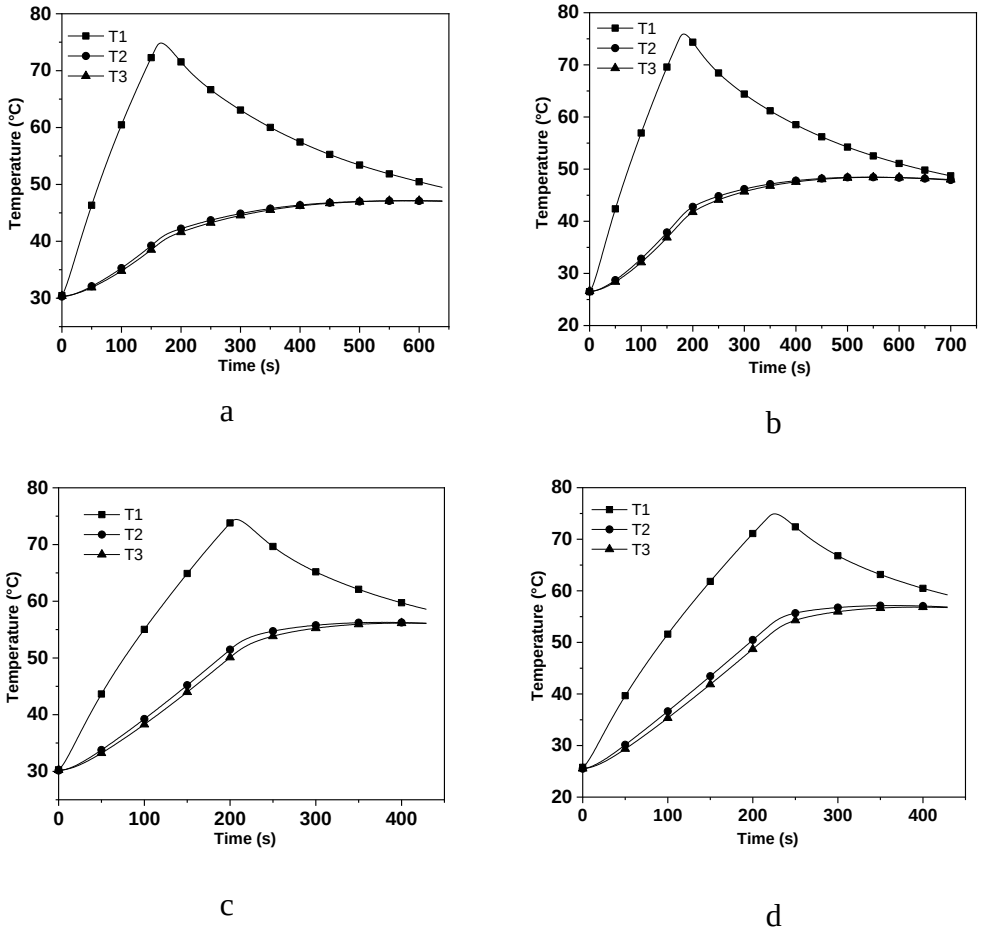

Fig A 6 Variation of temperature with time for Cu-Cu interface with L/D =5
a) 40kPa Bare b) 100kPa Bare c) 40kPa SG TIM D) 100kPa SG TIM

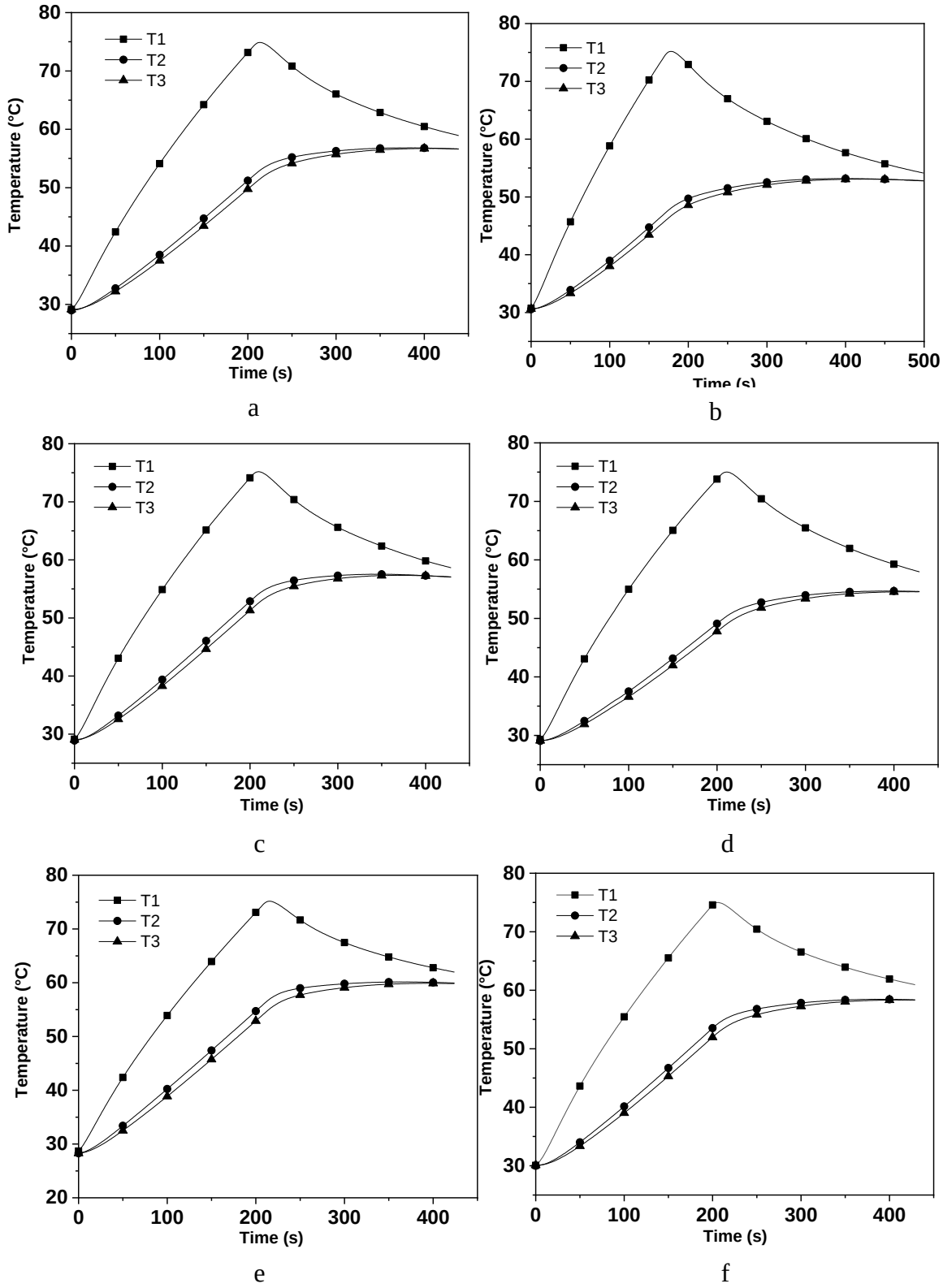

Fig A 7 Variation of temperature with time for Cu-Cu L/D =5 for a) 40kPa-0.1 wt% MWCNT SG b) 40kPa 1wt %MWCNT SG c) 100kPa 0.1 wt% MWCNT SG d) 100kPa 1 wt% MWCNT SG e) 200kPa 0.1 wt%MWCNT SG f) 200kPa 1 wt%MWCNT SG

LIST OF PUBLICATIONS

Journal Publications (Based on PhD work)

1. Ramakrishna Devananda P and K. Narayan Prabhu, "*The effect of load and addition of MWCNTs on silicone based TIMs on thermal contact heat transfer across Cu/Cu interface*" Materials Research Express, 6(11), 1165h9, 2019
2. Ramakrishna Devananda P and K. Narayan Prabhu, "*Thermal interface materials for cooling microelectronic systems: present status and future challenges*" Journal of Materials Science: Materials in Electronics, 32, 11339–11366, 2021
3. Ramakrishna Devananda P, Augustine Samuel, K. Narayan Prabhu, "*Thermal conformance parameters for assessment of heat transfer between similar and dissimilar metal contacts***",** Heat Transfer**,** 53 (5), 2416-2437, 2024

Journal Publications under review

1. Ramakrishna Devananda P**,** and K. Narayan Prabhu, "Enhancing Interfacial Heat Transfer: The Roles of Pressure, TIMs, and NMP" (under review)

BIO DATA

NAME **:** RAMAKRISHNA DEVANAND P

DOB **:** 25/05/1989

Permanent Address : 12-290/B "Chaitra" Near Microwave station, Post Jodumarga, B.C.Road, Bantwal Taluk, D.K. District, Karnataka State, India 574219

Email **:** ramakrishna.devv@gmail.com

Academic Qualification:

B.E. : Bapuji Institute of Engineering and Technology, Davanagere, 2011

M.Tech: National Institute of Technology Karnataka, Surathkal, 2013

Work Experience **:** Assistant Professor (22/7/2013 to till date)

Dept of Mechanical Engineering,
Sahyadri College of Engineering and Management, Adyar, Karnataka, India